DOE/MC/26029 -- 5561

Catalytic Conversion of Light Alkanes

Quarterly Report
January 1 - March 31, 1992

Work Performed Under Contract No.: DE-FC21-90MC26029

For
U.S. Department of Energy
Office of Fossil Energy
Morgantown Energy Technology Center
P.O. Box 880
Morgantown, West Virginia 26507-0880
By
Sun Refining and Marketing Company
2nd and Green Streets
Marcus Hook, Pennsylvania 19061-0835

Disclaimer

ACKNOWLEDGEMENTS

The work contained in this report was performed by the following researchers:

Joseph Biscardi
Paul T. Bowden
Vincent A. Durante
Paul E. Ellis Jr.
Harry B. Gray
Robert G. Gorbey
Robert C. Hayes
Julia Hodge
Maureen Hughes
Wayne A. Langdale
James E. Lyons
Bonnie Marcus
Denise Messick
Ronald A. Merrill
Floyd A. Moore
Harry K. Myers, Jr.
Walter H. Seitzer
Shahid N. Shaikh
Wilbert H. Tsao
Richard W. Wagner
Robert W. Warren
Tilak P. Wijesekera

ABSTRACT

The first Quarterly Report of 1992 on the Catalytic Conversion of Light Alkanes reviews the work done between January 1, 1992 and March 31, 1992 on the Cooperative Agreement. The mission of this work is to devise a new catalyst which can be used in a simple economic process to convert the light alkanes in natural gas to oxygenate products which can either be used as clean-burning, high octane liquid fuels, as fuel components or as precursors to liquid hydrocarbon transportation fuel.

During the past quarter we have continued to design, prepare, characterize and test novel catalysts for the mild selective reaction of light hydrocarbons with air or oxygen to produce alcohols directly. These catalysts are designed to form active metal oxo (MO) species and to be uniquely active for the homolytic cleavage of the carbon-hydrogen bonds in light alkanes producing intermediates which can form alcohols. We continue to investigate three molecular environments for the active catalytic species that we are trying to generate: electron-deficient porphryinic macrocycles (PHASE I), polyoxometallates (PHASE II), and regular oxidic lattices including zeolites and related structures as well as other molecular surface structures having metal oxo groups (PHASE III).

CONTRACT RESULTS TO DATE AND STATUS

We have concieved and reduced to practice new catalytic principles which have encouraged us to design and to synthesize a new family of catalysts that are effective in the conversion of light alkanes to alcohols or other oxygenates. Until now, the chemical reactions needed to produce the desired oxygenates from alkanes could only be accomplished selectively by specialized enzymatic systems operating in vivo. These systems are impractical for commercial fuel production. Aided by computer-assisted molecular design techniques we have created a family of synthetic catalysts which may

operate based on fundamental principles similar to those employed by the biological systems. Our new catalysts, however, can be synthesized in the laboratory from inexpensive raw materials. As mentioned above we have examined catalytically active metals in three molecular environments.

In each of the first two years of the Cooperative Agreement we have synthesized, tested, patented and examined a new electron-deficient porphyrinic macrocycle in detail and many others in a less comprehensive manner. From considering both the electronic and the molecular structure together with the chemical and catalytic activity of metal complexes of the series $M(TPPF_{20})X$, $M(TPPF_{20}\beta\text{-}Cl_8)X$ and $M\ TPPF_{20}\beta\text{-}Br_8)X$; M = Fe,Mn,Cr,Co,Cu,Ru; X = F,Cl,Br,N_3,O,OH we have established a structure-activity correlation which has enabled us to design and begin the synthesis of superior macrocyclic ligand systems. As we have pointed out in past reports, the iron complexes were far and away the best catalysts for light alkane oxidations using molecular oxygen as oxidant. Although these complexes are by far the most active low-temperature liquid phase alkane oxidation catalysts known, we have determined that an increase in activity is still needed to meet the criteria which we have determined for commercial applications. Increased rate can be obtained in many ways including: more electron withdrawal from the macrocycle, better design of molecular (steric) structure, and smaller substituent groups which confer lower molecular weight and a lower per pound cost. Thus we have now embarked on a catalyst synthesis program directed toward complexes which are more active, lower molecular weight and cheaper to make. Included in the new series of complexes which are being constructed are those in which the bulky perhalophenyl groups are being replaced by the even more electron-withdrawing cyano, fluoro, trifluoromethyl, nitro, chloro groups and others. Testing of this new set of complexes will begin in the third quarter of this year.

A polyoxoanionic structure is the second molecular environment into which we have placed the oxidation active transition metals, Fe, Cr, Mn, Co, etc. One of the reasons for our interests in polyoxoanionic complexes of these metals is their high oxidative and thermal stability. We expect that they would hold up well under industrial process conditions. During the past quarter we have made a series of Keggin structures having the formula $(Bu_4N)_{3-7}[MFeM'_{11}O_{37-39}]$ in which the central atom, M, and the framework metals M' are varied in order to enhance the Fe(III)/Fe(II) reduction potential of the complex. One of the major discoveries which has allowed us to make the porphyrin complexes uniquely active, is the finding that catalytic activity increases as M(III)/M(II) reduction potential increases. During the second quarter we will test this series to determine whether a similar structure-activity corelation can be found for polyoxoanionic complexes. Also during the past quarter we have found that a series of heteropolyacid catalysts of the Keggin structure into which iron has been incorporated were uniquely effective for the liquid phase oxidation of ethane. We have seen the highest C_2 oxygenate yields using these catalysts of any catalyst used to date.

The third molecular environment for oxidation active metal centers under investigation is a zeolitic or regular oxidic environment. During the past quarter we have synthesized a number of zeolitic structures which incorporate oxidation active transition metals into their framework. These materials include highly pure Fe[SOD], MnAPO-5, and CoAPSO-5. The latter compounds are aluminophosphate structures into whose framework manganese and cobalt are substituted. As we have reported in the past, Fe[SOD] does not have activity because of the difficulty of incorporating Fe(II) into the sodalite structure. The effective Fe(III)/Fe(II) reduction potential, therefore will be low. When Fe(II) is incorporated into the exchange sites an active catalyst: Fe_xFe[SOD] is prepared. In the case of both MnAPO-5 and CoAPSO-5, the metals may be incorporated in both the (II) and (III) oxidation states. This is important since oxygen will be bound and hopefully activated by Mn(II) and Co(II).

During the past quarter we have tested MnAPO-5 for oxidation of both ethane and methane. This catalyst is more active than Fe_x[Fe]SOD and nearly as selective. Using MnAPO-5 we can homolyze the C-H bond of methane at temperatures fully 35°C lower than when Fe_x[Fe]SOD is used as catalyst. Although selectivity is extremely important, one of our major goals in methane conversion is to lower the temperature at which the C-H bond of methane can be homolyzed under methanol-forming conditions. We will test the cobalt compound in the next quarter.

TABLE OF CONTENTS

TABLE OF CONTENTS (Cont'd)

PAGE

TABLE OF CONTENTS (Cont'd)

PAGE

TABLE OF CONTENTS (Cont'd)

PAGE

TABLES

PAGE

LIST OF FIGURES

LIST OF FIGURES

LIST OF FIGURES

PAGE

1.0 INTRODUCTION

We have found a family of new catalytic materials which, if successfully developed, will be effective in the conversion of light alkanes to alcohols or other oxygenates. Catalysts of this type have the potential to convert natural gas to clean-burning high octane liquid fuels directly without requiring the energy-intensive steam reforming step. In addition they also have the potential to upgrade light hydrocarbons found in natural gas to a variety of high value fuel and chemical products. In order for commerically useful processes to be developed, increases in catalytic life, reaction rate and selectivity are required. Recent progress in the experimental program geared to the further improvement of these catalysts is outlined in Sections 5 and 6.

2.0 PURPOSE

The mission of the work presented in this quarterly report is to generate novel catalytic technology which will permit the development of a simple, efficient and economical process for the direct conversion of natural gas to liquid transportation fuels. This process should be simple enough to liquify natural gas economically even at a remote reservoir site. It is a further mission of this work to find new routes from natural gas or its components to high value oxygenates by direct air-oxidation using these new catalysts.

The technical objective of the research is to design the first effective molecular catalyst for the direct air-oxidation of the hydrocarbons found in natural gas to an alcohol-rich oxidate which can either be used directly or converted into gasoline via known technology. The development of an efficient catalyst for the smooth and selective oxidation of light alkanes to alcohols will not only provide a solution to the problem of liquifying natural gas, but will create new opportunities to utilize the relatively inexpensive and abundant light alkanes for the production of a variety of valuable fuel and chemical products. Processes for converting natural gas or its components (methane, ethane, propane, and the butanes) to alcohols for use as motor fuels, fuel additives or fuel precursors will not only add a valuable alternative to crude oil but will produce a clean-burning, high octane alternative to conventional gasoline.

3.0 TECHNICAL BACKGROUND

The First 1990 Quarterly Report of the Catalytic Conversion of Light alkanes Cooperative Agreement, Section 3.0, can be consulted for details of the technical background relating to this project up until the inception of the research program. Since that time, much progress has been made. A summary of research conducted during Calendar 1991 is presented below. This summary will serve as background for the first quarter, 1992 results presented in this report. We have devised a new catalytic approach to the direct production of alcohols from light alkanes which grew out of the recognition that metal oxo complexes like those that are intermediates of enzymatic alkane hydroxylations might be generated directly from reaction of air or oxygen with metals in certain supportive molecular environments. To date, the enzymatic systems are the only relatively efficient catalysts for the conversion of light alkanes to alcohols. Synthetic systems which mimic the enzymes have also had some limited success in this area. Biological and biomimetic oxidations, however, have the requirement of very specialized and expensive co-reductants which are stoichiometrically consumed during reaction. The catalysts which are the subject of this study are designed to directly activate molecular oxygen and catalyze the oxidation of light alkanes to alcohols using ONLY molecular oxygen without the need for co-reductants which limit the commerical potential of the chemistry. We have used these catalysts to oxidize light alkanes directly by reaction with air or oxygen and find that they are able to convert light alkanes to alcohols under relatively mild conditions.

3.1 PROJECT DESCRIPTION

This project is an experimental approach to the design, synthesis, characterization and testing of oxidation-active transition metal centers for cleaving the dioxygen molecule and producing metal oxo intermediates which react with alkanes to convert them to alcohols. The molecular environment in which the oxidation-active metal center is located is critical in generating active catalysts. It must tune the center electronically to access

appropriate oxidation states and should enable two metal centers to participate in the oxygen splitting process. We are investigating three molecular environments which could be hospitable ones for the active species that we are trying to generate: a) perhaloporphyrin, perhalophthalocyanine or related macrocycles, b) polyoxometallates and c) regular oxidic lattices such as zeolites and related structures. We are testing these three sets of catalysts for activity in the mild oxidation of light alkanes (isobutane, propane, ethane and methane).

3.2 RESULTS AND ACCOMPLISHMENTS

3.2.1 Oxidations Catalyzed By Perhaloporphyrins

Catalytic alkane hydroxylations are accomplished in biological systems by iron in both heme (1) and non-heme (2) environments, Figure 1. These biological systems are monooxygenases and have the stoichiometric requirement of two electrons and two protons for each mole of hydrocarbon oxidized. This requirement is met in vivo by NADH. Biomimetic analogs (3-8) either use oxygen together with a stoichiometric co-reductant, or use a single oxygen atom transfer agent such as iodosylbenzene, a hypochlorite, or a hydroperoxide as the oxidant. In order to meet the needs of the large scale economic conversion of a light alkane to an alcohol for use as a fuel or commodity chemical, one desires a catalyst which uses air or oxygen as the only oxidant and does not rely on costly stoichiometric co-reductants.

We asked (9-11) whether it might be possible to create a synthetic dioxygenase that could operate by a pathway shown schematically in Figure 2, in which the oxygen molecule is not reductively bound between an iron (III) and a proton, Figure 1, but rather is reductively bound between two Fe(III) centers. The oxygen-oxygen bond could then cleave to form the catalytically active ferryl oxo entities. The search for such systems has led to the synthesis and successful application of several new catalysts in which a first-row metal (Cr, Mn, Fe, or Co) is activated by incorporation into an electron-deficient macrocyclic ligand environment. These catalysts are unique in their high activity for selective partial oxidation of light alkanes in the absence of coreductants.

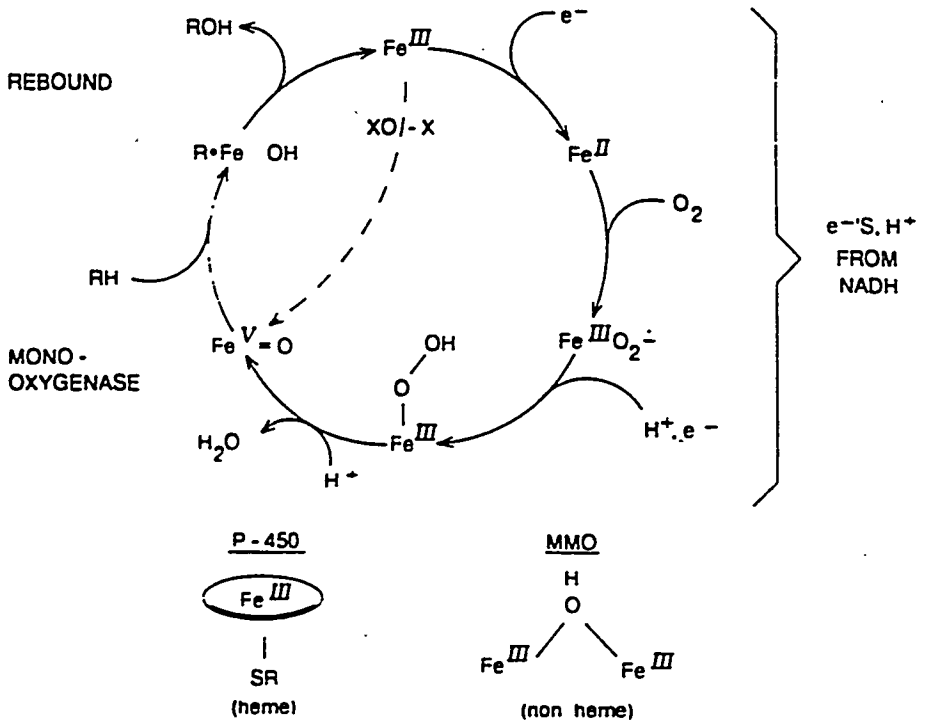

Figure 1. Biological and Biomimetic Alkane Oxidation

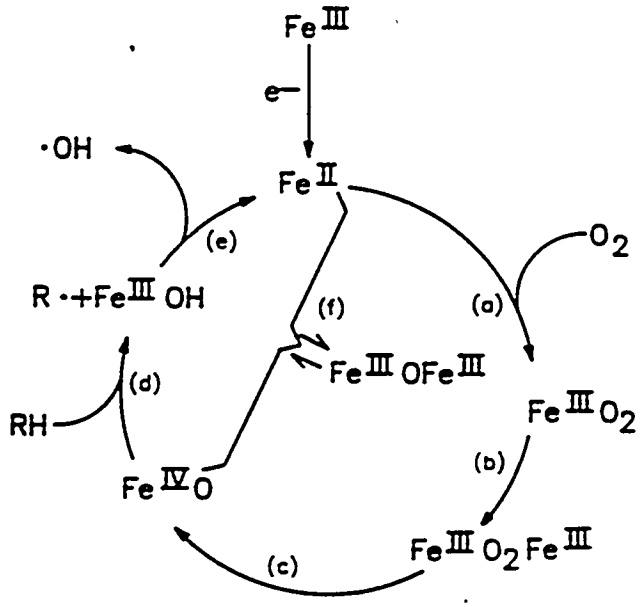

Figure 2. A Hypothetical Synthetic Dioxygenase

3.2.2 Active Catalysts from Metals in Electron Deficient Porphyrins

We have shown that the catalytic activity of tetraphenylporphyrinato complexes of oxidation-active first row transition metals is increased by halogenation of the tetraphenylporphyrin ring system (9-11). As the degree of halogenation is increased, the catalytic activity increases. Iron (III) complexes were shown to be more active than those of chromium, manganese or cobalt in all cases. The iron perhaloporphyrin complex: tetrakis(pentafluorophenyl)β-octachloroporphyrinatoiron(III)chloride, Fe(TPPF$_{20}\beta$-Cl$_8$)Cl, has unprecedented light alkane air-oxidation activity. Using this catalyst, isobutane can be oxidized in neat solution at temperatures ranging from room temperature to 80°C in from 85 to 95% selectivity at isobutane conversion levels over 20%. Over 15,000 moles of tert-butyl alcohol can be produced per mole of iron using this catalyst. Propane can be converted to a mixture of isopropyl alcohol and acetone in a selective manner.

3.2.3 Electron Withdrawal, Reduction Potential and Catalytic Activity

As the C-H bonds around the periphery of the tetraphenylporphyrinato ligand system are changed to C-X bonds (X = F, Cl, Br), the Fe(III)/(II) reduction potential increases. Table 1 shows that the catalytically inactive parent iron porphyrin, Fe(TPP)Cl, exhibits an Fe(III)/(II) half-wave potential at -0.22V whereas the $E_{1/2}$ exhibited by the highly active perhaloporphyrin complex, Fe(TPPF$_{20}\beta$-Cl$_8$)Cl, is fully 0.5V higher. It appears that there is a direct relationship between the extent of electron withdrawal from the porphyrin ring, which causes an increase in the Fe(III)/(II) reduction potential, and the catalytic activity of the iron complex (9-14).

3.2.4 Porphyrin Ring Buckling, Steric Hindrance and Catalytic Activity

What was surprising about Table 1, however, was that the catalytic activity of $Fe(TPPF_{20}\beta\text{-}Br_8)Cl$ was not lower than that of $Fe(TPPF_{20}\beta\text{-}Cl_8)Cl$. Structural information currently being gathered indicates that the steric bulk of the β-bromo substituents may prevent access of large molecules to the central iron atom. This has two possible consequences which could affect reaction rate. Firstly, a sterically hindered porphyrin might bind dioxygen to give a μ-peroxo complex which could cleave to form an active ferryl oxo species. It would be unlikely that a diiron μ-oxo complex, however, would be very stable if it is formed at all. To the extent that ferryl oxo complexes are active intermediates and that diiron μ-oxo species are not, a steric environment which prevents μ-oxo formation could cause an oxidation rate enhancement.

3.2.5 Spectroscopic Structure Determination of the Perhaloporphyrin Macrocycles

Recent work (15) has determined that the greater the steric bulk of hydrocarbon substituents in the β-(pyrrolic) positions of a nickel tetraphenylporphyrin complex, $Ni(TPP\beta\text{-}R_8)$, the greater is the degree of buckling of the porphyrin. This distortion is reflected in the shift of the structure-sensitive resonance Raman bands, ν_2 and ν_4, to lower frequency. We have found a very similar pattern of behavior for nickel tetrakis(pentafluorophenyl)porphyrin complexes, $Ni(TPPF_{20}\beta\text{-}Y_8)$, Y = H, Cl, Br (16). Table 2 indicates that as the β-group becomes bulkier the $TPPF_{20}$ macrocycle goes from a planar geometry when Y = H, to a highly buckled saddle shape when Y = Br, with the octachloro substituent being intermediate in geometry.

Figure 3 shows the structures of $Ni(TPPF_{20}\beta\text{-}Cl_8)$(16). It is clear that the extent of buckling is far more severe in the octabromo complex than in the octachloro compound. Inspection of the structure of the $(TPPF_{20}\beta\text{-}Br_8)$ macrocycle in Figure 3 shows a deep saddle created by severe buckling of the porphyrin ring system. One could imagine the difficulty of making a diiron μ-oxo bridged species from such a severly buckled complex.

TABLE 1. RELATIONSHIP BETWEEN CATALYST REDUCTION POTENTIAL AND ACTIVITY

CATALYST	Fe(III)/(II) $E_{1/2}$ (V)[a]	T.O.[b]
Fe(TPP)Cl	−0.221	0
Fe($TPPF_{20}$)Cl	+0.07	1160
Fe($TPPF_{20}\beta$−Br_8)Cl	+0.19	1890
Fe($TPPF_{20}\beta$−Cl_8)Cl	+0.28	1800

[a] Cyclic voltammetry in CH_2Cl_2, vs. SCE, TBAC− supporting electrolyte, glassy carbon electrode.

[b] Catalyst turnovers for 60°C isobutane oxidations in benzene.

TABLE 2. EFFECT OF β−STERIC BULK IN THE NICKEL TPP−$\beta R_8$15 AND $TPPF_{20}$−βY_8 COMPLEXES ON STRUCTURE−SENSITIVE RR MARKER BANDS.[a]

Compound	Soret (nm)	ν_4 (cm^{-1})	ν_2 (cm^{-1})
Ni($TPPF_{20}$)	406	1375	1586
Ni(TPP)	414	1374	1572
Ni(TPPβ−Me_8)	429	1362	1574
Ni($TPPF_{20}\beta$−Cl_8)	428	1363	1557
Ni(TPPβ−Et_8)	433	1350	1562
Ni(TPPβ−Pr_8)	434	1360	1560
Ni($TPPF_{20}\beta$−Br_8)	438	1354	1542
Ni(TPPβ−Ph_8)	449	1353	1545

[a] CH_2Cl_2(442nm excitation)

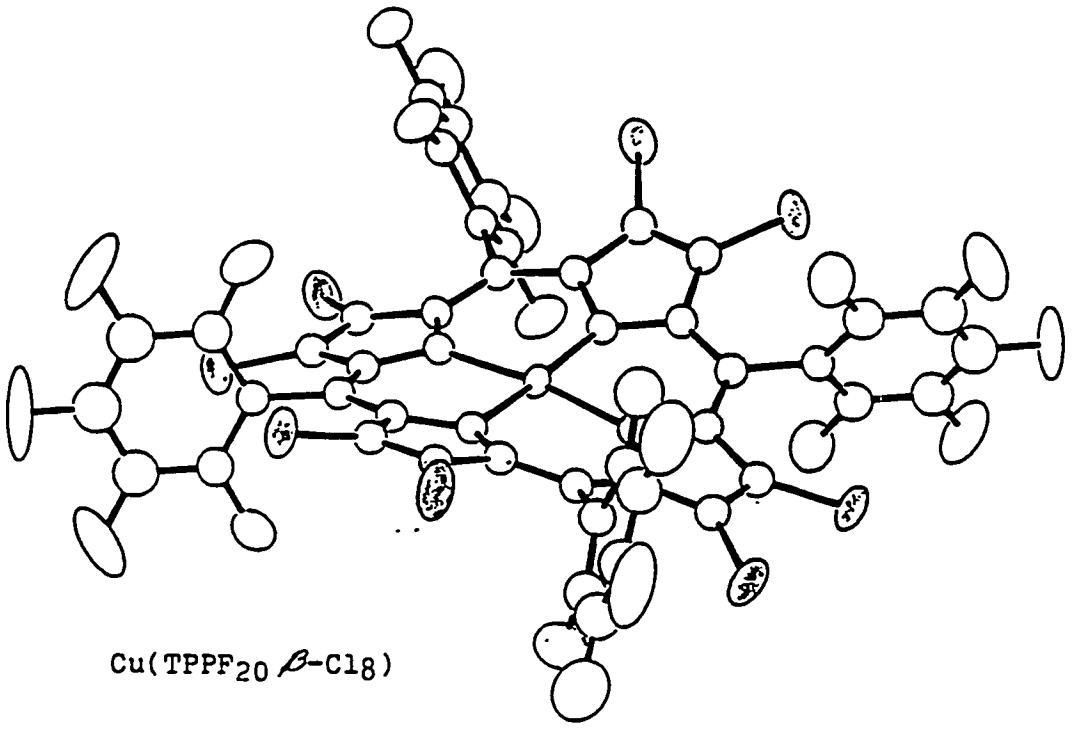

Cu(TPPF$_{20}$$\beta$-Cl$_8$)

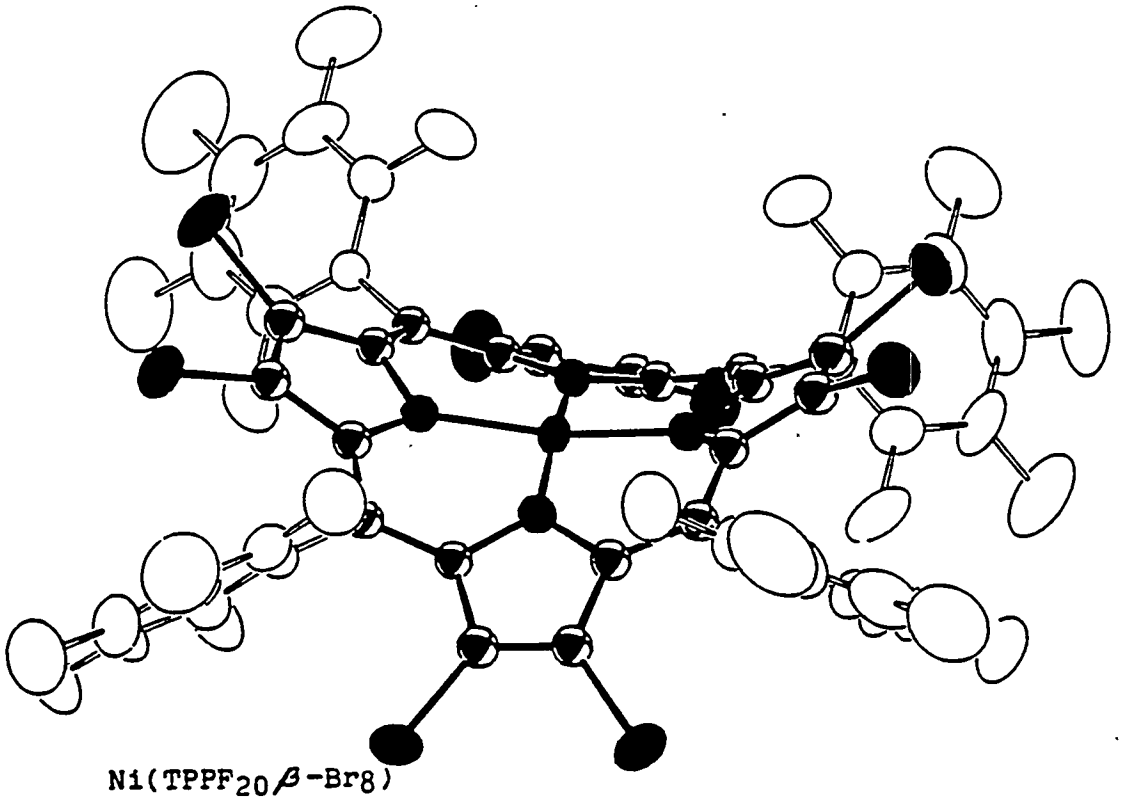

Ni(TPPF$_{20}$$\beta$-Br$_8$)

FIGURE 3

STRUCTURES OF PERHALOPORPHYRIN COMPLEXES

Although we have not as yet generated crystals of the iron $TPPF_{20}\beta\text{-}Y_8$ complexes (Y = Cl, Br) of sufficient quality to obtain a crystal structure, we have obtained resonance Raman data which show that ν_2 and ν_4 have both shifted to lower frequency. The paramagnetic $Fe(TPPF_{20}\beta\text{-}Cl_8)$ complex is converted to a diamagnetic species, probably Fe(II), by treatment with excess pyridine. When a methylene chloride solution of $Fe(TPPF_{20}\beta\text{-}Cl_8)$ is treated with pyridine, and its resonance Raman spectrum obtained, the structure-sensitive marker bands ν_4 and ν_2, respectively, appear at 1353 and 1554 cm^{-1}, in good agreement with the positions of these bands in $Ni(TPPF_{20}\beta\text{-}Cl_8)$.

3.2.6 Azido and Perhalo Phthalocyanine Complexes as Air-Oxidation Catalysts

Transition metal porphyrin complexes do not have good oxidative stability at temperatures of 100°C or more. Phthalocyanine complexes are known to be more robust materials and cobalt phthalocyanine catalysts are used for mercaptan oxidations in the petroleum industry (17). Phthalocyanine complexes, however, are not very hydrocarbon soluble nor very active for low temperature alkane oxidation.

We have found, Tables 3,4 that chromium and manganese phthalocyanine azides catalyze selective oxidation of isobutane to tert-butyl alcohol and that ironperfluorophthalocyanine azides are robust, soluble, active catalysts for the selective oxidation of isobutane and propane under mild conditions of temperature and pressure. Propane is oxidized selectively to C_3 oxygenates with low yields of carbon oxides. Even refractory hydrocarbons such as methane and ethane can be oxidized in the presence of $Fe(\underline{F}Pc)N_3$ but rates, yields and selectivity to alcohols are very low. Methane is oxidized at 285°C and 2000 psig of a 3/1 mixture of methane and air in 1/1 benzene/water to give methanol in 11% selectivity at 60% oxygen conversion using this catalyst. By-products are largely carbon oxides.

TABLE 3

OXIDATION OF ISOBUTANE[a] CATALYZED BY METAL PHTHALOCYANINE AZIDES

Complex	mmoles	T,°C	t,Hrs.	TON[b]	Sel[c]
Mn(Pc)	0.013	80	6	0	-
$Mn(Pc)N_3$	0.013	80	6	400	88
Cr(Pc)	0.013	80	6	0	-
$Cr(Pc)N_3$	0.013	80	7.5	220	91
Fe(Pc)	0.030	80	6	0	-
$[Fe(Pc)]_2N$	0.016	80	6	0	-
Fe(FPc)	0.023	80	6	0	-
$Fe(FPc)N_3$	0.013	80	6	990	82
$Fe(FPc)N_3$	0.013	60	6	156	92

a The catalyst was stirred in 25 ml benzene containing 6 grams isobutane under 100 psig of O_2 at the designated temperature for the time indicated.

b Moles O_2 consumed/mole catalyst used.

c (Moles t-butyl alcohol produced/total moles liquid product) X 100.

TABLE 4

OXIDATION OF PROPANE[a] CATALYZED BY AN IRON PERFLUOROPHTHALOCYANINE AZIDE COMPLEX

Complex	mmoles	Solvent,	T.°C	t,Hrs.	TON[b]	IPA/Acetone[c]
Fe(FPc)	0.023	Benzene	125	3	0	-
$Fe(FPc)N_3$	0.028	Benzene	125	6	48	0.7
Fe(FPc)	0.023	CH_3CN	125	3	57	0.7
Fe(FPc)	0.028	CH_3CN	150	3	460	0.3
$Fe(FPc)N_3$	0.028	CH_3CN	150	3	754	0.7
Fe(FPc)Cl	0.028	CH_3CN	150	3	606	0.7
$Fe(FPc)N_3$	0.028	C_6H_5CN	150	3	1210	0.6

a Propane (1.36 mol) was added to the solvent (48 ml) containing the catalyst. The reactic mixture was stirred at the designated temperature under 1000 psig of air in a glass-lin autoclave. Liquids and gases were analyzed by g.c. Production of carbon oxides nev exceeded 10% of total products. Isopropyl alcohol and acetone exceeded 85 mole % carbon-containing reaction products in all cases.

b Moles of acetone plus isopropyl alcohol formed per mole of catalyst used.

c Molar ratio of isopropyl alcohol to acetone formed.

3.2.7 Oxidations catalyzed by Polyoxoanions

Despite their relatively high stability, the first generation perhalogenated metal catalysts are still not stable enough to survive the higher temperatures required to oxidize propane, ethane, and methane for long periods of time. We have noted that methane monoxygenase has a hydroxo-bridged diiron non-heme active center which, with the help of electrons and protons from NADH, is capable of binding and cleaving the dioxygen molecule and slowly converting methane to methanol even at room temperature (18). For this reason, we are interested in attempting to tune the redox potential of similar small model complexes having bridged diiron in non-porphyrin ligands the same as we have in the porphyrin series. Polyoxoanionic complexes such as Keggin systems, $[MM_{11}O_{37-40}]$, seemed to be a good model. In addition to their electronic properties and the possibility of incorporation of more than one iron into this "ligand" system, these compounds would be expected to have a very high thermal and oxidative stability and, if active, one would expect long catalyst life even at elevated temperatures.

While having interesting high-temperature activity in promoting alkane autoxidation, (19-26), the lower-temperature activity for selective alcohol formation that was observed for the porphyrin complexes was not observed for the polyoxoanionic complexes of oxidation-active transition metals introduced in either their +2 or +3 oxidation states. It is necessary to exceed 100°C to achieve oxidation even of isobutane, and although the entire range of substrates tested: methane, ethane, propane, isobutane, and synthetic natural gas - was oxidized, the selectivity to alcohols was not high. An area in which the use of POA's showed promise was in the liquid phase oxidation of ethane, Table 5. Much higher yields of ethanol were observed using POA's than with classical metal carboxylate-catalyzed autoxidations of ethane.

TABLE 5

LIQUID PHASE OXIDATION OF ETHANE CATALYZED BY METAL-SUBSTITUTED KEGGIN STRUCTURES[a]

Catalyst-mmole	P_{air} psi	Products, mmoles EtOH	MeOH	CH_3CHO	CO/CO_2	T.O.	Ethane Conv. %
None	170	0.51	0	0	0		
$H_7[PW_9Fe_2NiO_{37}]$-0.018	170	3.19	3.49	0.47	2.6	540	2.0
$H_6[PW_9Fe_3O_{37}]$-0.018	170	5.46	2.27	0.75	4.8	660	2.7
$H_6[PW_9Fe_3O_{37}]$-0.018	500	7.73	2.53	0.58	11.8	1130	4.2
Co(II)Naphthenate-0.2	483	0.59	10.67	tr	12.4	120	3.3
	170	0.75	8.12	tr	5.5	72	2.1

[a] Ethane, 40-45g., was oxidized in acetonitrile, 59g., in a glass lined, stirred autoclave for 3 hrs. @ 200°C. under the initial pressures given in the table. Gas and product analysis by g.c.

3.2.8 Oxidations Catalyzed by Zeolites

We have demonstrated that oxidation-active first-row transition metals in the framework of zeolite structures catalyze the oxidation of methane to methanol if certain criteria are met (26-28). We have put high loadings of iron - up to 15% - in the sodalite framework, Figure 4. If no extra framework iron were present, catalytic activity was low, but if, in addition to high framework loadings, iron also occupied exchange sites, Fe_x[Fe]SOD, an active catalyst resulted. This behavior was rationalized on the basis that framework iron could not readily reduce to iron(II) - its Fe(III)/(II) reduction potential was too low. This is due to the constraints of the sodalite system which accepts Fe(III) but not Fe(II). Iron in the exchange site can be reduced to Fe(II) and activate oxygen. Cooperative Fe(II)/Fe(III) sites can bind and cleave dioxygen.

Whether active solid iron, manganese or chromium catalysts are used, we have envisioned the reaction as occurring by homolytic scission of the C-H bond of methane on the surface. Methyl radicals leave the surface and initiate gas phase oxidation to form methanol, Eq. 1 - 4.

$$MO + CH_4 = CH_3\bullet + MOH \quad (1)$$

$$CH_3\bullet + O_2 = CH_3O_2\bullet \quad (2)$$

$$CH_3O_2\bullet = CH_3O\bullet + 1/2O_2 \quad (3)$$

$$CH_3O\bullet + CH_4 = CH_3OH + CH_3\bullet \quad (4)$$

In-depth kinetic analysis of this process indicates that it is unlikely that selectivities as high as 80% to methanol at methane conversions in excess of 20% could be realized by a catalyst that operates exclusively by this mechanism. Figure 5 shows the drop in methanol selectivity predicted to occur for uncatalyzed gas phase methane oxidation under a representative set of conditions as conversion is increased. An hypothetical catalytic reaction which forms methyl radicals in greater abundance than the catalytic reaction will

FIGURE 4

METHANE TO METHANOL

$$CH_4 + {}^1/_2\, O_2 \longrightarrow CH_3OH$$

METHANE (AIR) METHANOL

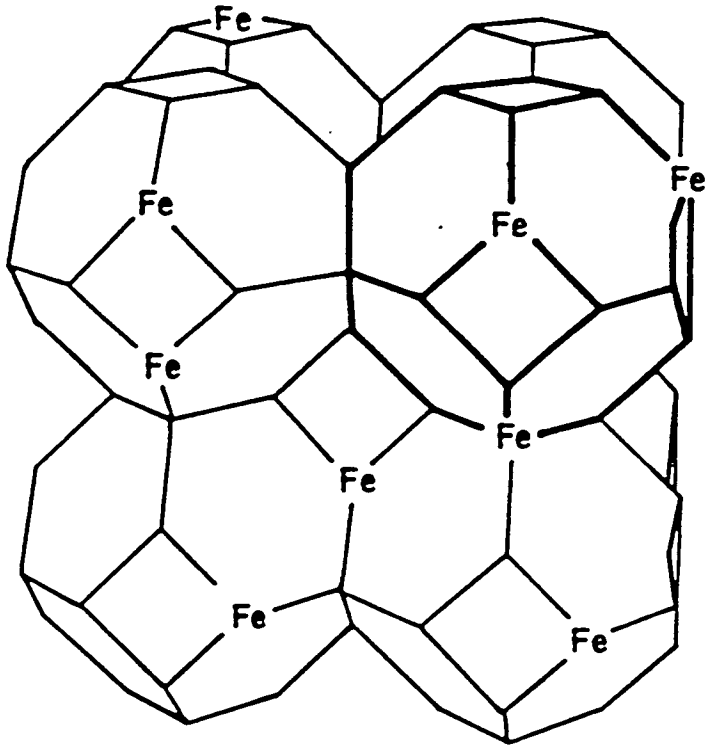

CATALYST = 15% Fe IN SODALITE

CONDITIONS : T = 420°C, G HSV~600, 3/1 METHANE/AIR

	RESULTS	GOAL
O_2 CONVERSION	90%	90%
METHANE CONVERSION	7%	20%
METHANOL SELECTIVITY	70%	80%

give higher selectivity. Figure 6 shows that as methyl radical flux increases, selectivity goes through a maximum. Our kinetic model predicts that this maximum is less than 70% under all conditions which we examined, when methane conversion was 10% or higher. Economic analysis suggests that this performance would not produce a highly attractive commerical process. For this reason, we have now embarked on the synthesis of a series of catalysts which are designed to have oxidation-active metals capable of homolytic scission of C-H bonds but which retain the intermediates on the surface long enough to form methanol. We will place these metals into a hydrophobic environment in order that methanol be expelled from the surface as formed. Such a catalytic process if successfully carried out will not have the yield limitations of the gas phase autoxidations. Ideal temperatures will be in the 250-300°C range which puts demands on the metal centers for higher activity than we have observed to date.

3.3 CONCLUSIONS

Using perhaloporphyrin complexes we may have: a) stabilized active iron-oxygen centers to oxidative decay, b) provided a lipophilic environment to attract the alkane to the active site, c) provided a hydrophilic environment to expel alcohol from the coordination sphere, d) tuned the redox potential of the metal center so that μ-oxo dimer was no longer inactive and so that iron(II) species could be continually regenerated in an oxidizing environment.

We have discussed how the electronic and steric environment about the oxidation-active metal center affects the rate and selectivity of alkane oxidation in both homogeneous liquid phase oxidations as well as heterogeneous catalytic vapor phase reactions. Reaction rate seems to be highly dependent on proper tuning of redox potentials. In the liquid phase, we have achieved unprecedented reaction rates and have electrochemical evidence that much higher rates can still be achieved. In the vapor phase, we have shown the need for proper tuning of reduction potential, but we must synthesize catalysts which have far greater reduction potentials than those which we currently have if we are to achieve the rates that will ultimately be necessary.

FIGURE 5

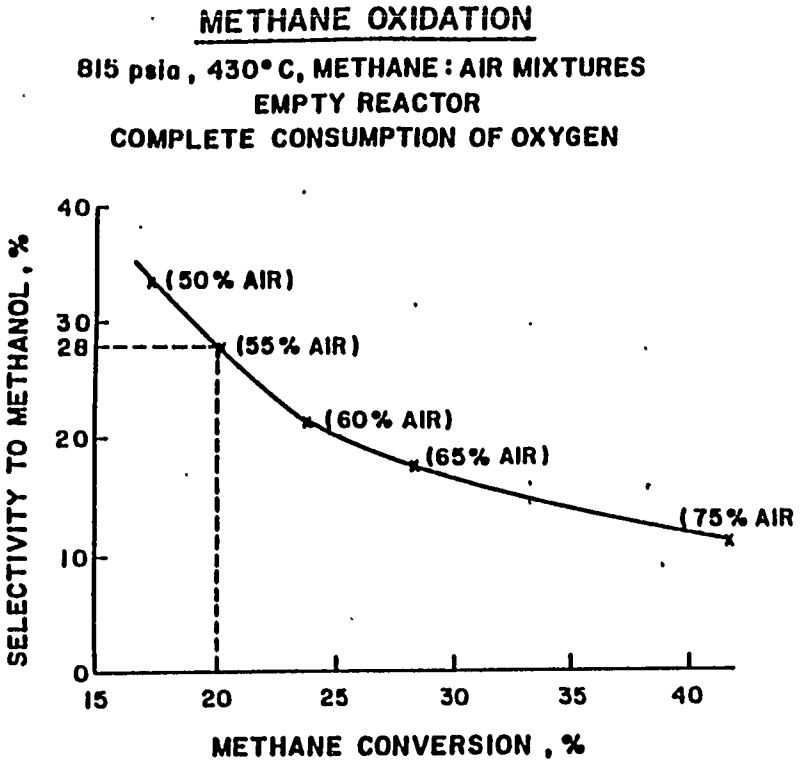

FIGURE 6

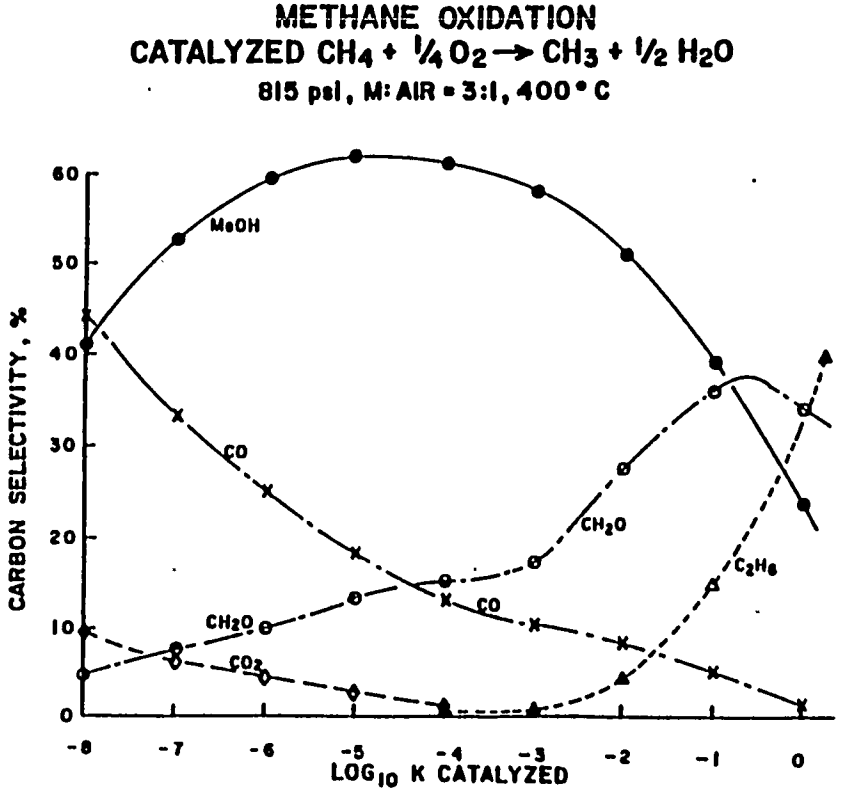

[10] P. E. Ellis, Jr. and J. E. Lyons, Coord. Chem. Rev. 105 (1990) 181.

[11] J. E. Lyons and P. E. Ellis, Jr., Catal. Lett., 8 (1991) 45.

[12] P. E. Ellis, Jr., J. E. Lyons and H. K. Myers, Jr., U.S. Patent 4,900,871, 1990.

[13] P. E. Ellis, Jr., J. E. Lyons and H. K. Myers, Jr., U.S. Patent 4,895,682, 1990.

[14] P. E. Ellis, Jr., J. E. Lyons and H. K. Myers, Jr., U.S. Patent 4,895,680, 1990.

[15] J. A. Shelnutt, C. J. Medforth, M. D. Berber, K. M. Barkigia, and K. M. Smith, J. Am. Chem. Soc. 113 (1991) 4077.

[16] M. E. Hughes, J. A. Hodge, W. P. Schaefer, L. M. Henling, H. B. Gray, J. E. Lyons, P. E. Ellis, Jr., R. W. Wagner, (in preparation).

[17] A. Leitao and A. Rodrigues, Chem. Eng. Sci., 44 (1988) 1245.

[18] H. Dalton and J. Green, J. Biol. Chem., 264, (1989) 17698.

[19] F. Ortega, Doctoral Dissertation, Georgetown University, Page 149, 1982.

[20] R. G. Finke, et.al., J. Am. Chem. Soc., 108, (1980) 2947.

[21] J. E. Lyons, P. E. Ellis, Jr., W. A. Langdale, and H. K. Myers, Jr., U.S. Patent 4,916,101, 1990.

[22] P. E. Ellis, Jr. and J. E. Lyons, U.S. Patent 4,898,989, 1990.

[23] J. E. Lyons, P. E. Ellis, Jr., H. K. Myers, Jr., G. Suld, and W. A. Langdale, U.S. Patent 4,859,798, 1989.

[24] J. E. Lyons, P. E. Ellis, Jr., H. K. Myers, Jr., G. Suld and W. A. Langdale, U.S. Patent 4,803,187, 1989.

[25] P. E. Ellis, Jr. and J. E. Lyons, U.S. Patent 5,091,354, 1992

[26] J. E. Lyons, P. E. Ellis, Jr., and V. A. Durante, Studies in Surface Science and Catalysis, 67, (1991) 99.

[27] V. A. Durante, D. W. Walker, S. M. Gussow, and J. E. Lyons, U.S. Patent 4,918,249, 1990.

[28] V. A. Durante, D. W. Walker, W. A. Seitzer, and J. E. Lyons, Preprints of 3B Symposium on Methane Activation, Conversion and Utilization, at the 1989 International Chem. Congr. of Pacific Basin Societies, December 17-20 (1989).

4.0 METHODOLOGY

Details of the suprabiotic methodology to be used to conduct research on the Catalytic Conversion of Light Alkanes can be found in Section 4.0 of the First Quarterly Report of the Cooperative Agreement.

5.0 RESULTS AND DISCUSSION

The three major thrusts of the research program are catalysis by A) metals in electron deficient macrocycles (PHASE I), B) polyoxometallates (PHASE II), and C, metals in regular oxidic matrices (PHASE III).

5.1 PHASE I - METALS IN ELECTRON-DEFICIENT MACROCYCLES

During the course of the first two years of the Cooperative Agreement we have determined that by increasing the amount of electron withdrawal from either the **meso**- or the **beta**-(pyrrolic) positions of the porphyrinato macrocycle surrounding an oxidation active first row metal center, we are able to greatly increase the M(III)/M(II) reduction potential of the complex. This results in an enormous increase in light alkane oxidation activity and provides us for the first time with a family of metal complexes capable of catalyzing the direct selective air-oxidation of these refractory materials. In a study encompassing porphyrin complexes of the metals: iron, manganese, chromium, cobalt, ruthenium and copper, we have shown that although copper complexes are not active, the activity of all the other metals responds postively to electron withdrawal in both the **meso-** and the **beta**-positions. We have further shown that the light alkane air-oxidation activity of the iron complexes of electron deficient porphyrins are in all cases far superior to that of the other metals.

In this report, we will provide further structural, spectroscopic and chemical documentation on the perhaloporphyrin catalysts that we have discovered. We will also present information synthesis, characterization and testing on new electron-deficient metallomacrocylic complexes.

5.1.1 Spectroscopy of Halogenated Metalloporphyrins

5.1.1.1 Crystal Structures

The X-ray crystal structures of CuLBr and ZnLBr, L = ($TPPF_{20}\beta$-Br_8), have been completed. The ORTEP diagrams (Figure 5-1 and 5-2, respectively). The CuLBr structure is isostructural with the previously solved NiLBr structure. The structure of ZnLBr is different. There is a mirror plane through opposite nitrogen atoms, and four different solvent molecules in the crystal. Several solvents (o-dichlorobenzene, water, carbon tetrachloride and acetone/methanol (50%:50%)) were resolved in

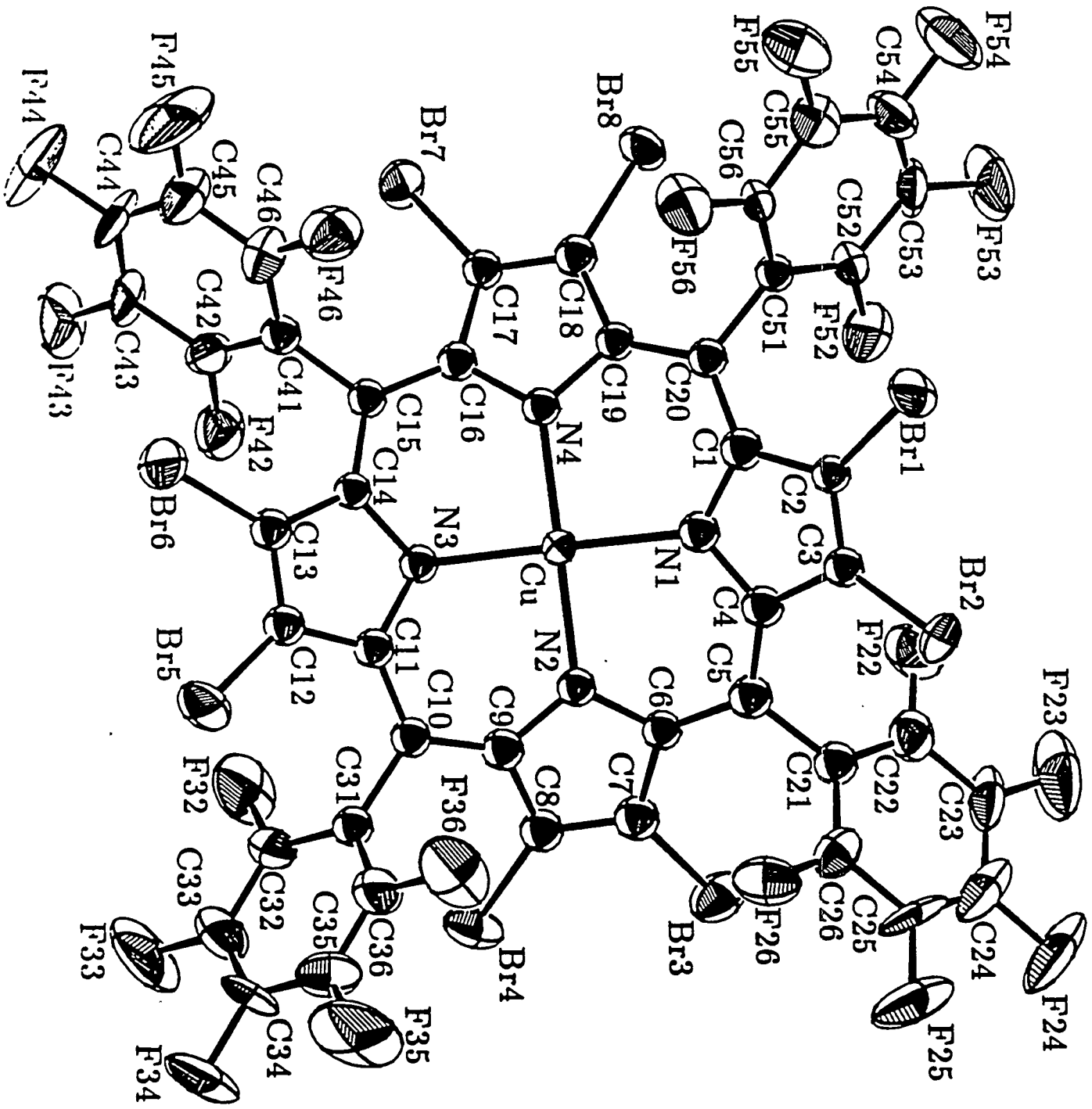

FIGURE 5-1 : $Cu(TPPF_{20}\beta\text{-}Br_8)$

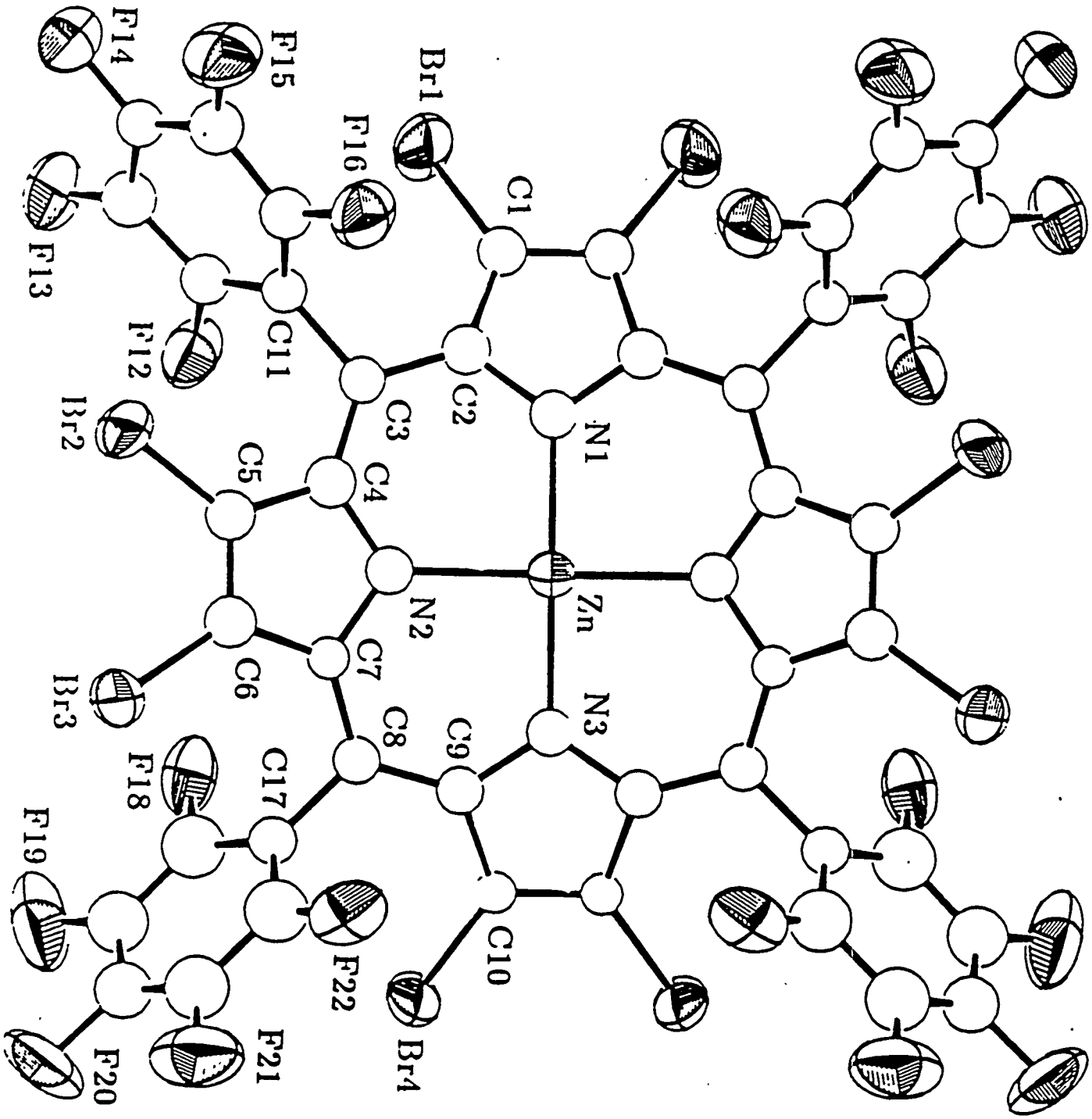

FIGURE 5-2(a):Zn(TPPF$_{20}$$\beta$-Br$_8$)

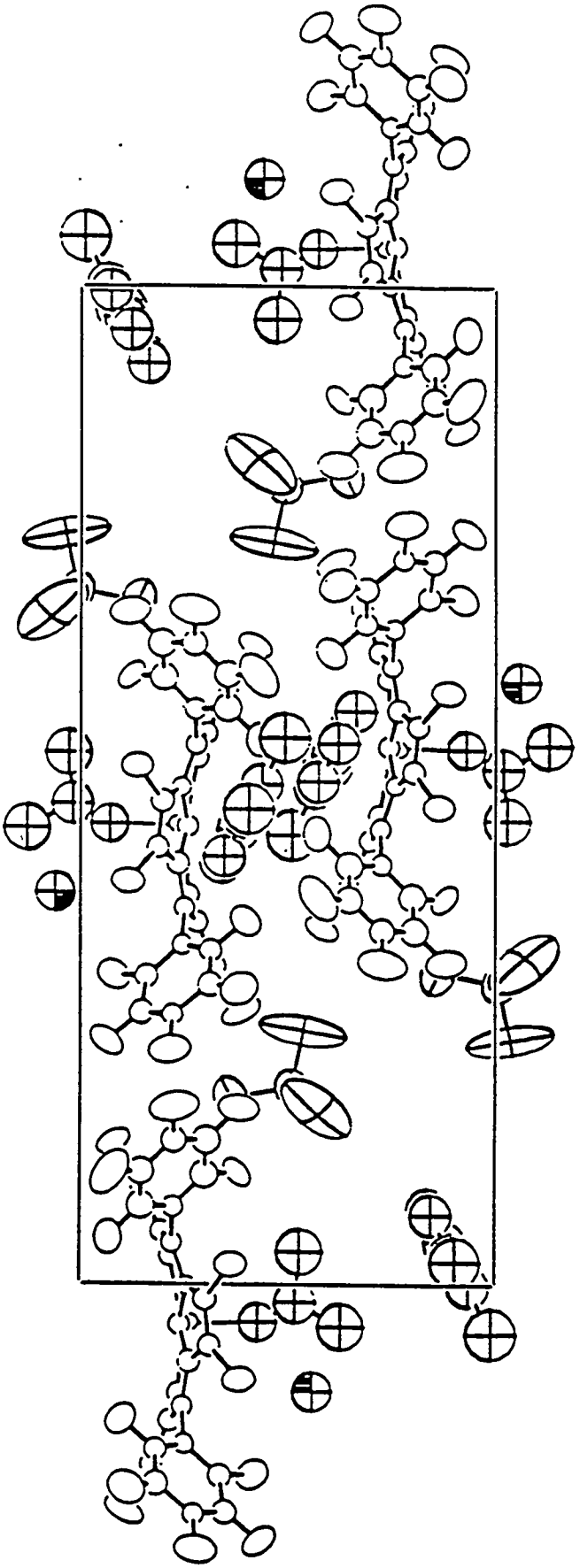

FIGURE 5-2(c):ZnLBr Unit Cell

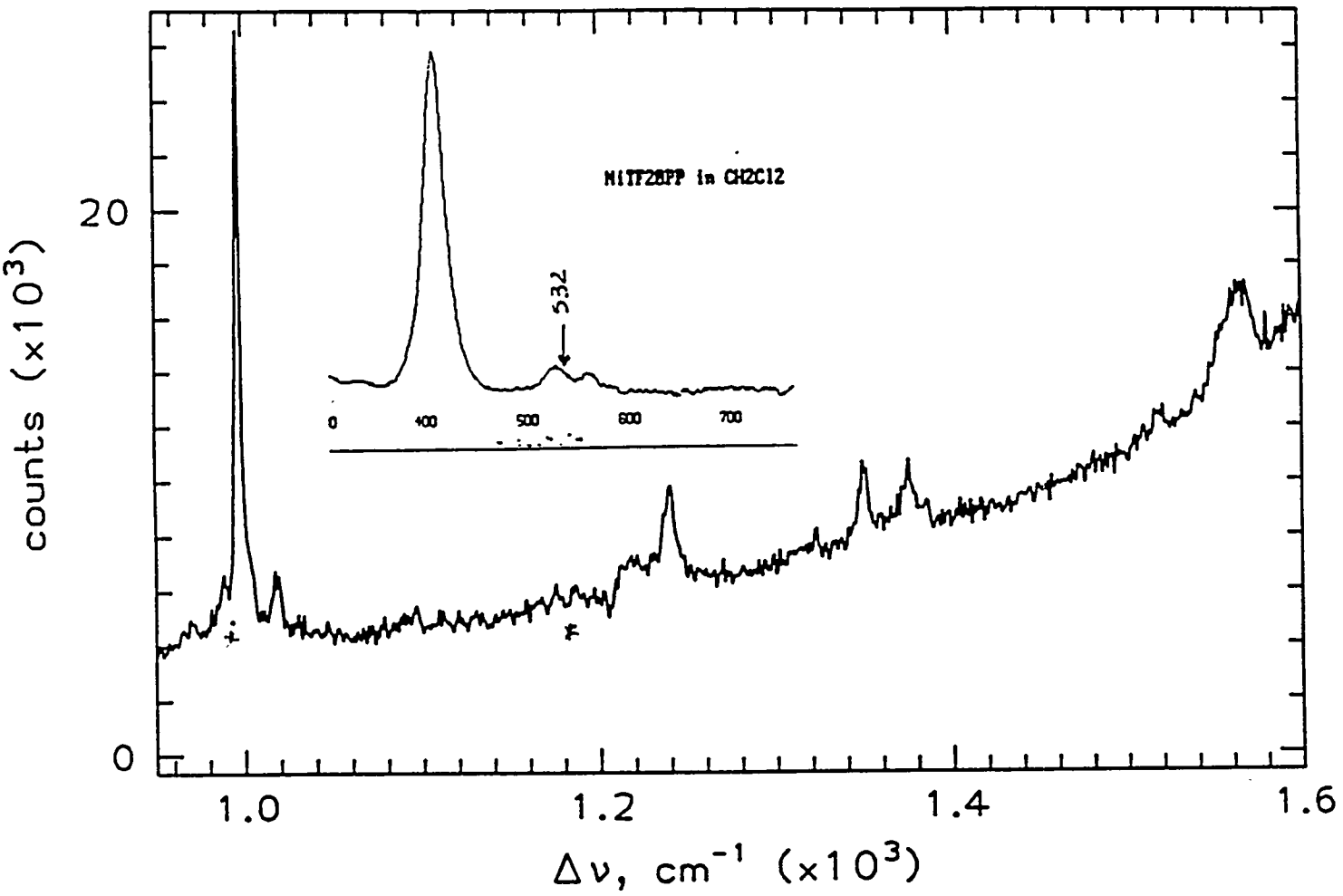

FIGURE 5-3a:$NiTF_{20}$PP RESONANCE RAMAN SPECTRUM
HUGHES 127.000 *C_6H_6

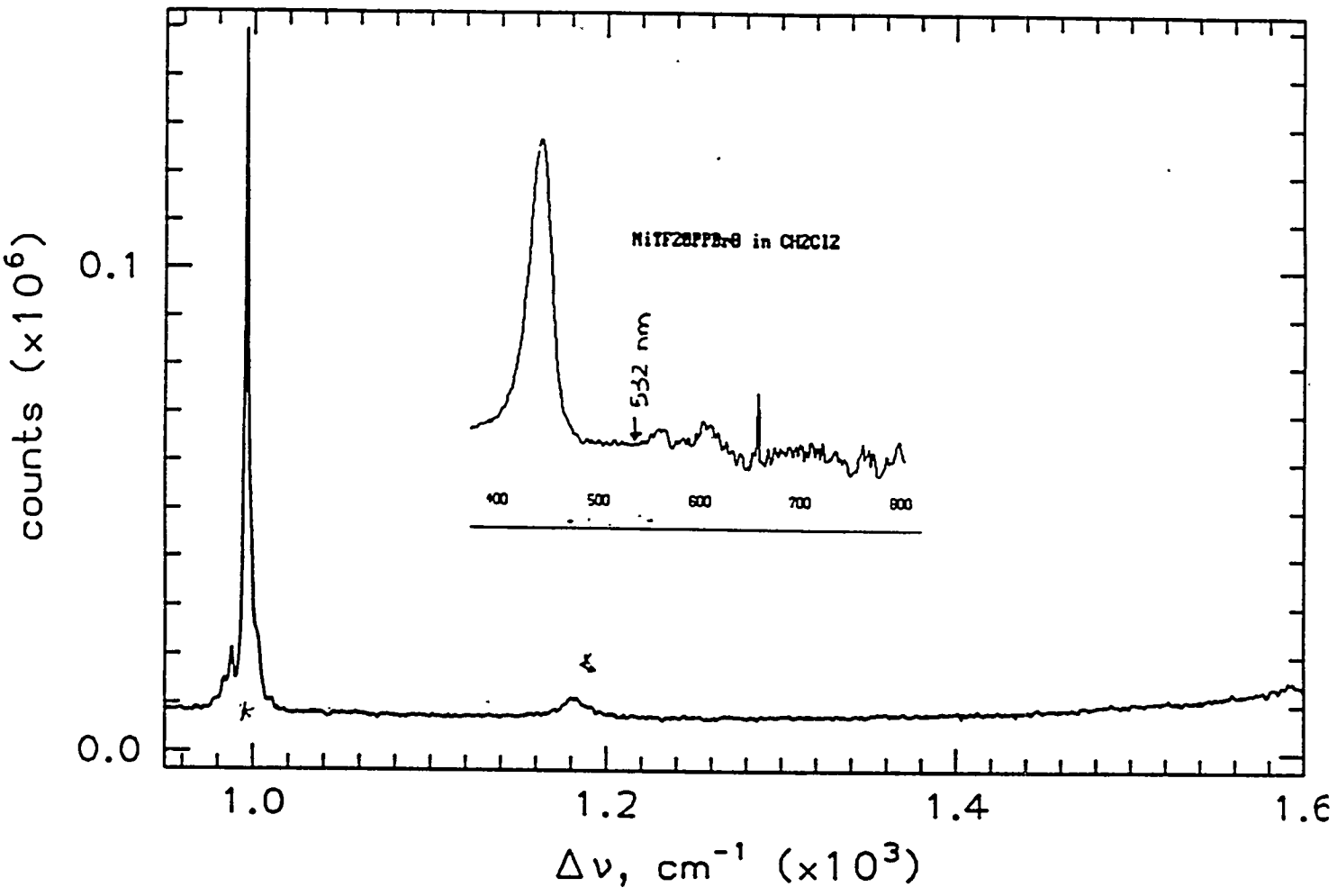

FIGURE 5-3b:$NiTF_{20}PPBr_8$ RESONANCE RAMAN SPECTRUM
HUGHES 128.000 *C_6H_6

FIGURE 5-4

Resonance Raman Spectra of FeLX8 Complexes

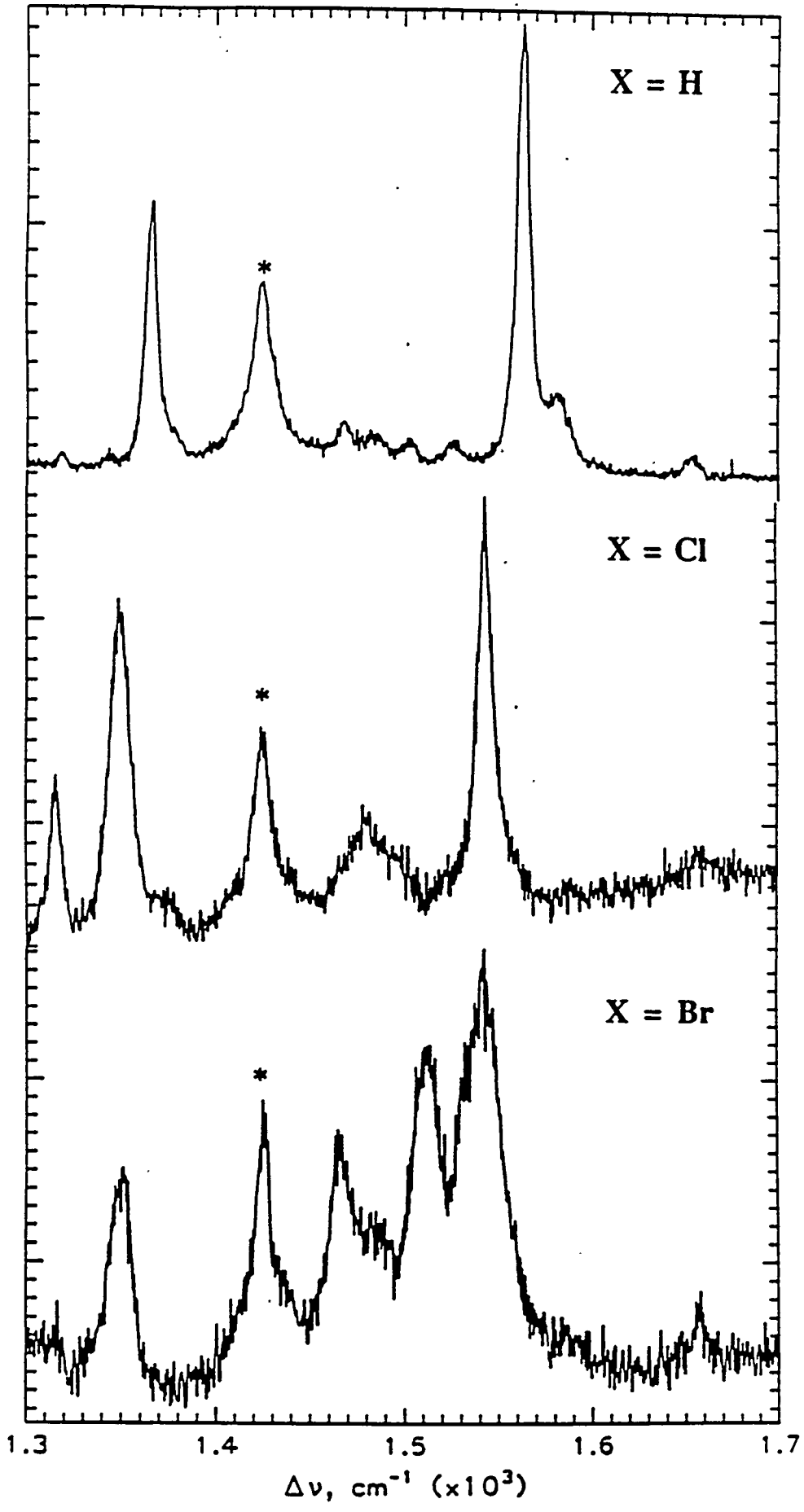

442 nm Excitation; * = CH_2C

Formula: $N_4 F_{20} C_{44} H_8 Zn$?

mw = 1035.972 if ^{64}Zn

NBA/acid

File: EM920314.A06 Spec: 1/1 Scans: 50 Acquired: 03/14/92 15:05:38
Memo: julia's sample Zn [TF$_{20}$PP] Scale: 6.8797

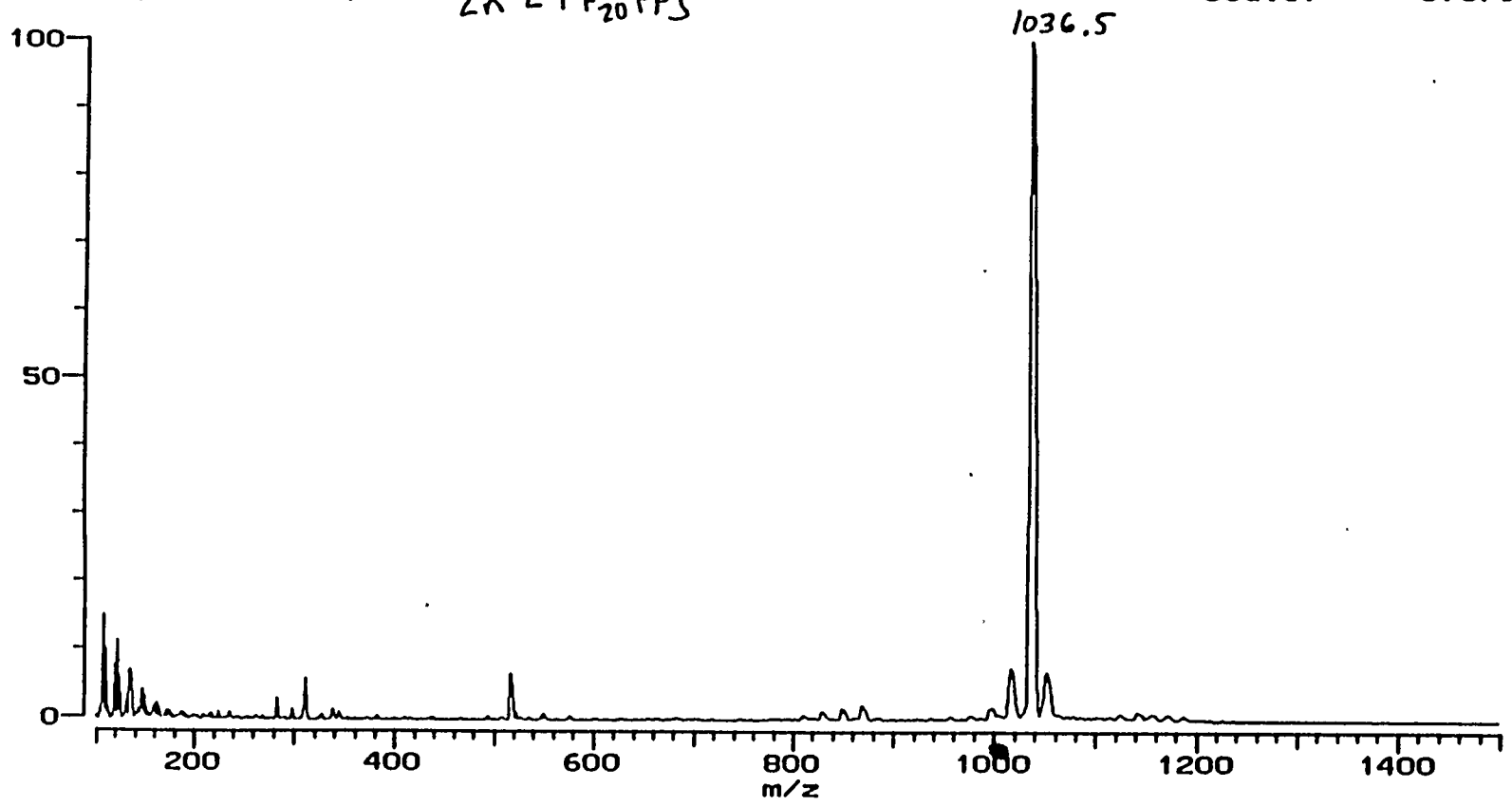

FIGURE 5-5a HIGH RESOLUTION MASS SPECTRUM OF Zn(TPPF$_{20}$)

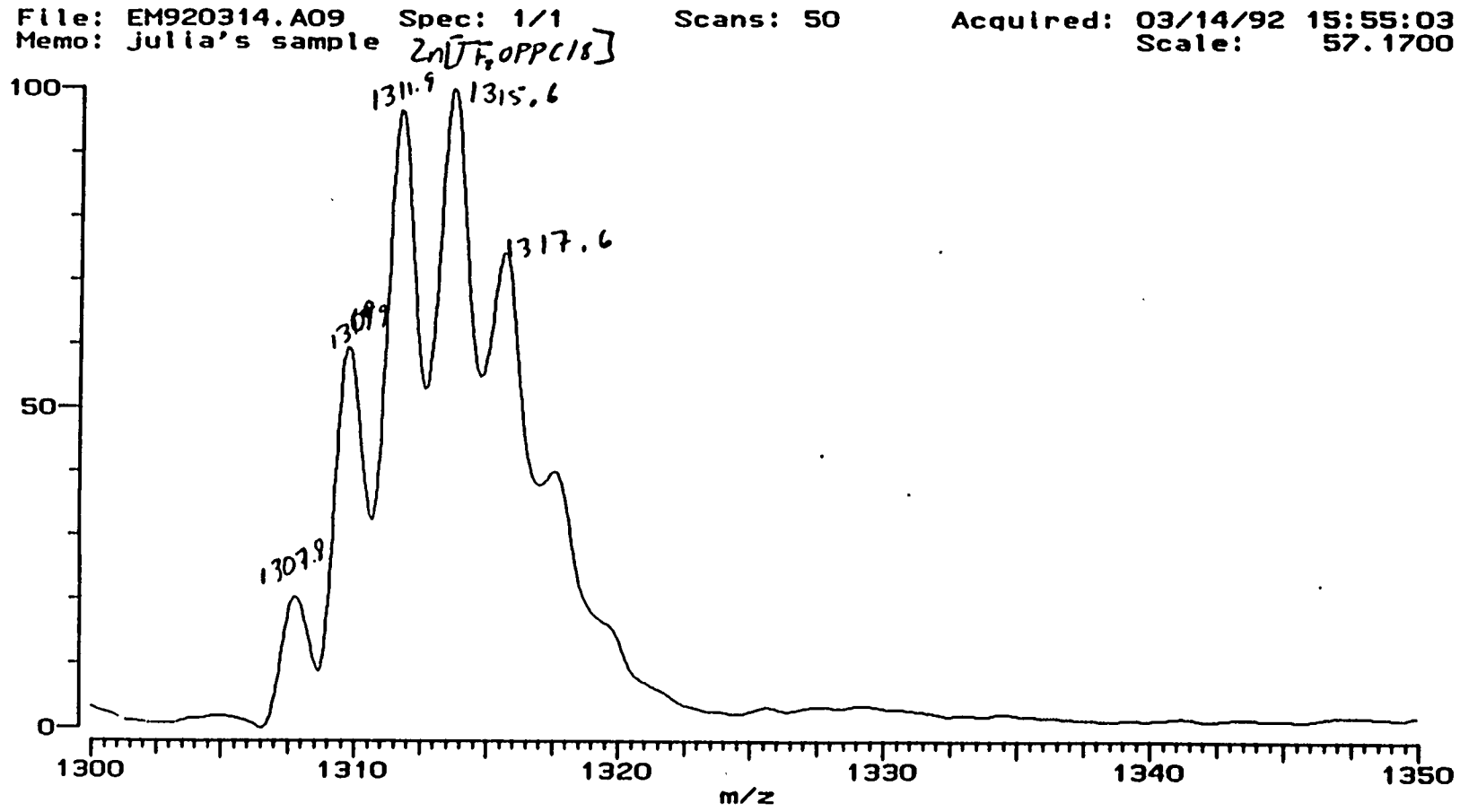

FIGURE 5-5b: MASS SPECTRUM OF $Zn(TPPF_{20}B\text{-}Cl_8)$

Finnigan MAT

Spectrum printed at 10:17 Tue Feb 18 1992

Sample:	FeF20TPPCl8	$\bar{m}$ ~ 1304.0	Low = 1300
Matrix	sinapinic acid standard		
Data File:	FILE NOT SAVED		

Calibration:	Manual Internal	A: -0.040		B/V:	0.634615
No of shots:	1	Laser Aim:	2	Laser Power:	45
Polarity:	Positive	Gain:	31mV	Accelerating Voltage:	20050

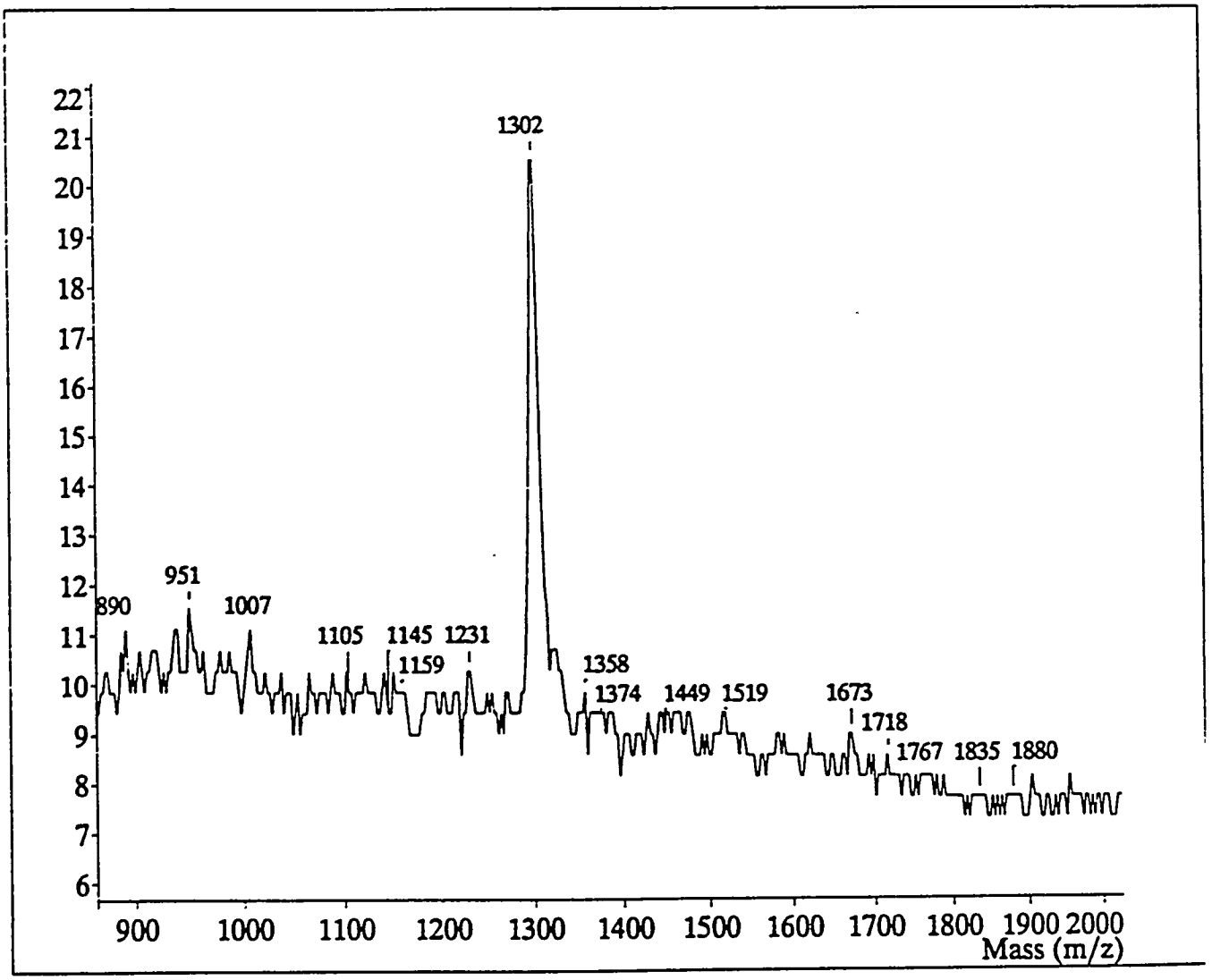

FIGURE 5-6(a): MASS SPECTRUM OF $Fe(TPPF_{20}Cl_8)$

Finnigan MAT

Spectrum printed at 10:11 Tue Feb 18 1992

Sample:	FeF20TPPCl8
Matrix	sinapinic acid standard
Data File:	C:\LASERMAT\DATA\gjc0218.002

Calibration:	External	A: -0.040		B/V:	0.631361
No of shots:	10	Laser Aim:	1	Laser Power:	32
Polarity:	Negative	Gain:	31mV	Accelerating Voltage:	20037

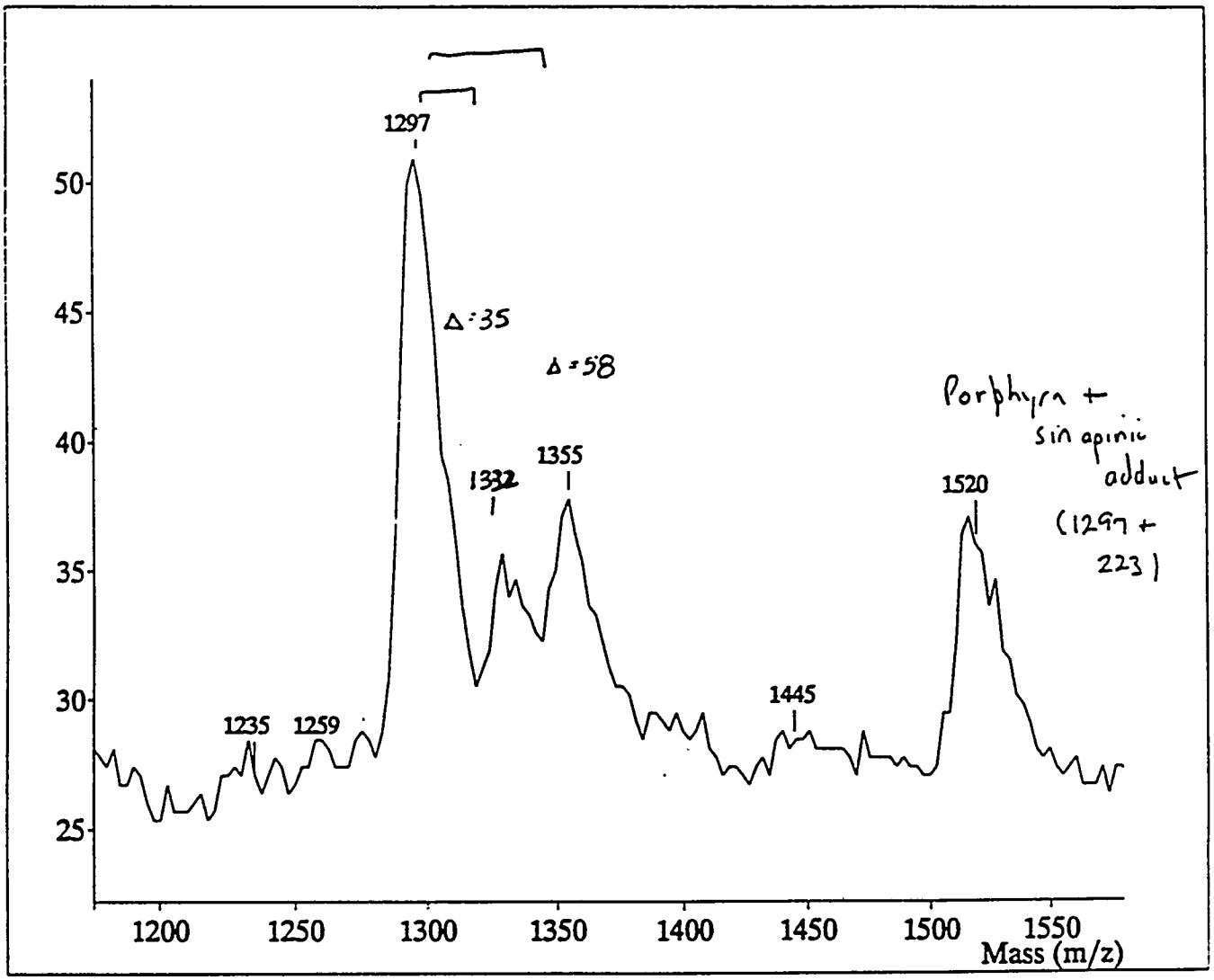

FIGURE 5-6(b): MASS SPECTRUM OF FeLC1

Porphyrin spectra feature an intense band, usually found in the ultraviolet region, known as the B band or the Soret band. The second two bands at lower energy are called Q bands. Figure 5-7 shows how the one electron transitions within the four orbitals mix to give the observed transitions; Figure 5-8 shows the four orbitals.

Previous studies of brominated porphyrins have shown that each bromine at a pyrrole position causes a spectral shift of 6 nm to the red relative to the bands observed for tetraphenylporphyrin (TPP).[4] An attempt has been made to explain these shifts in terms of a parameterized version of the standard four-oribital model.[5] Bhyrappa and Krishnan (BK) only considered electronic effects of the bromine substituents in their analysis of the absorption spectra[5]. Recent crystal structures[6] of these halogenated compounds have shown that significant bending of the porphyrin ring occurs, so it is likely that the BK explanation will require some revision.

5.1.2.1 Calculation Details

In order to assess the changes in spectra with halogenation of the porphyrin, AM1[7] calculations have been performed using MOPAC[8]. These calculations include full CI within Gouterman's four orbitals.

The calculations have been performed upon two series of halogenated porphyrins. The first series includes $TF_{20}PP$, $TF_{20}PPCl_8$, and $TF_{20}PPBr_8$. The second series includes the same porphyrins with Zn in the core rather than two hydrogens.

Crystal structures have been obtained for Cu-$TFPPCl_8$ and Ni$TFPPCl_8$[6]. The calculations on Zn$TFPPCl_8$ used the geometry that was obtained from the crystal structure of Cu$TFPPCl_8$. Similarly, the calculations on Zn$TFPPBr_8$ use the

FIGURE 5-7

Configuration Interaction in the Four Orbital Model

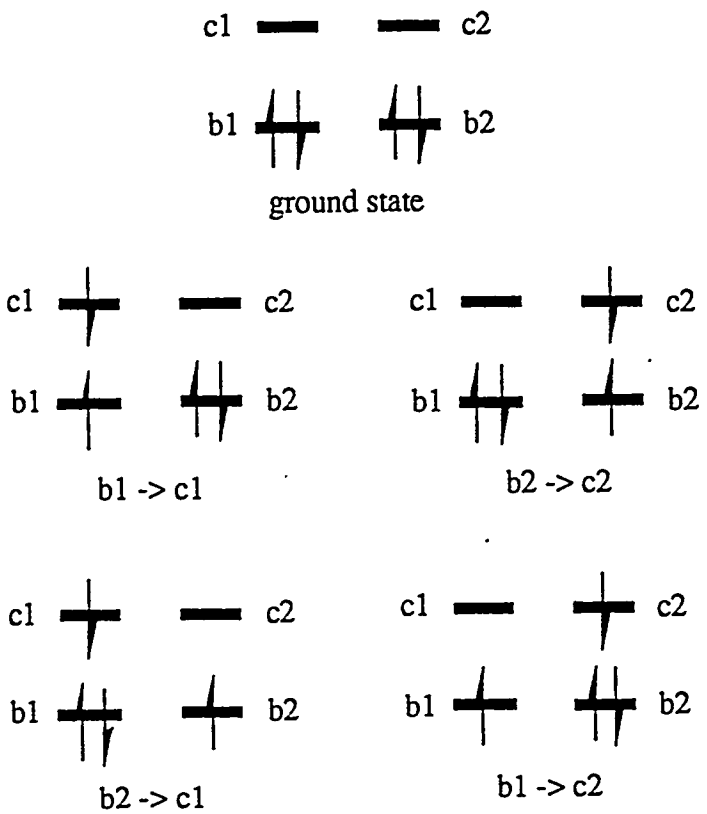

The transitions are defined as:

$$\left.\begin{matrix} Q_x \\ B_x \end{matrix}\right\} = [(b1c2)\pm(b2c1)]$$

$$\left.\begin{matrix} Q_y \\ B_y \end{matrix}\right\} = [(b1c1)\pm(b2c2)]$$

The symmetries of the orbitals are as follows:

$b1=b_{1u}$, $b2=a_u$, $c1=b_{3g}$, $c2=b_{2g}$

see Figure 2 for pictures of the orbitals

geometry that was obtained from the crystal structure of $NiTFPPBr_8$. Since these are first row transition metals, their sizes are roughly equivalent. Thus, it is not a bad approximation to replace Cu and Ni with Zn, while retaining the geometry of the original crystal structure. $TFPPBr_8$[9] and $TFPPCl_8$ have been opitimized using the MOPAC geometry optimization routine[9]. The geometries used for TFPP and ZnTFPP are also Biograf minimized structures using Dreiding force fields. The initial guess for the optimization of $TFPPBr_8$ and $TFPPCl_8$ was based upon the crystallographic data, with the metal replaced by two hydrogens.

5.1.2.2 Experimental Section

TFPP obtained from Aldrich was purified using techniques described earlier[10]. $TFPPCl_8$[11] and $TFPPBr_8$[1] were prepared according to literature procedures. All zinc-metallated species were prepared by refluxing the appropriate porphyrin with $Zn(OAc)_2 \cdot 2H_2O$ in methanol. The zinc acetate was purchased from Aldrich chemicals. All porphyrins were purified on a silica gel column (150 A pore size and 75-150 μparticle size).

Absorption spectra were measured using a Cary 14 spectrophotometer. The porphyrin solutions were prepared by dissolving approximately 1.25 mg of porphyrin in 50 ml of methylcyclohexane and a subsequent 20:1 solvent:solution dilution. Spectra were obtained at 25°C.

5.1.2.3 Results

The experimental data are given in Table 5-1; corresponding calculational data are set out in Table 5-2.

FIGURE 5-8

The four orbitals

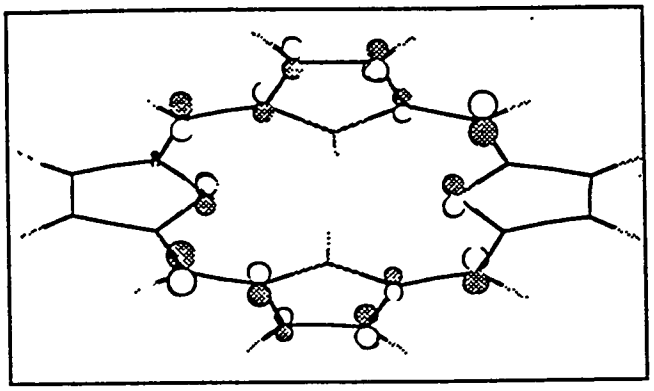

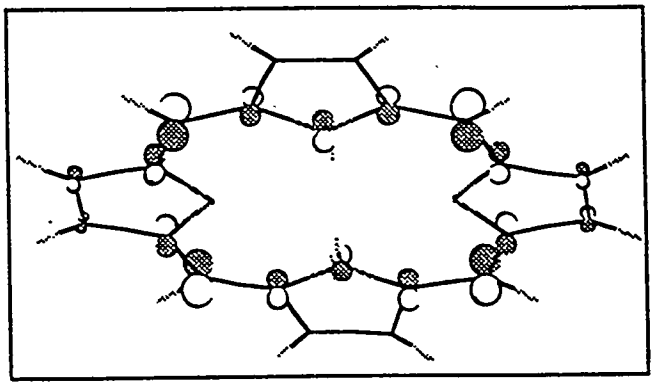

B_{2g} unoccupied B_{3g}

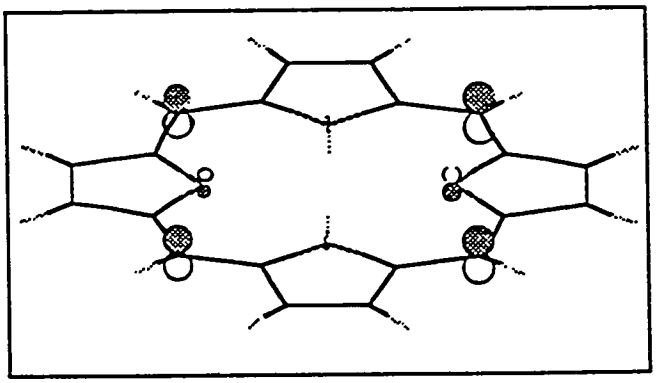

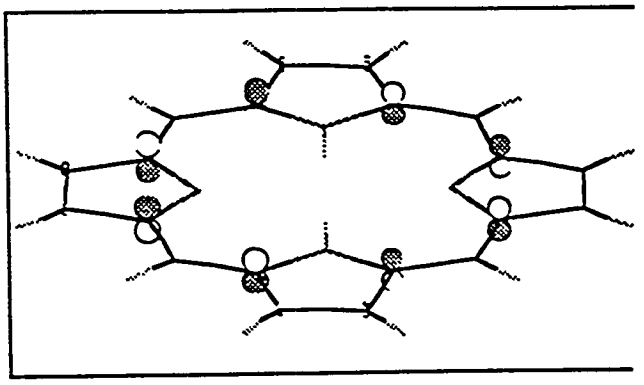

B_{1u} occupied A_u

Table 5-1: **Absorption data**

Compound	Q_x	Q_y	Soret
ZnTFPP	544 nm		412 nm
$ZnTFPPCl_8$	575 nm		442 nm
$ZnTFPPBr_8$	596 nm		464 nm
TFPP	584 nm	506 nm	412 nm
$TFPPCl_8$	624 nm	536 nm	436 nm
$TFPPBr_8$	640 nm	553 nm	452 nm

Table 5-2: **Calculated band positions**

Compound	Q_x	Q_y	$Soret_x$	$Soret_y$
ZnTFPP	508 nm	508 nm	319 nm	317 nm
$ZnTFPPCl_8$	535 nm	533 nm	329 nm	328 nm
$ZnTFPPBr_8$	545 nm	543 nm	339 nm	338 nm
TFPP	585 nm	515 nm	332 nm	330 nm
$TFPPCl_8$	626 nm	611 nm	384 nm	382 nm
$TFPPBr_8$	652 nm	636 nm	401 nm	399 nm

5.1.2.4 Discussion

Examination of Tables 5-1 and 5-2 shows that the calculations reproduce the experimental trends. As the size of the substitutents increases, the red shift in the absorption spectrum increases. Thus, porphyrins with hydrogen at the beta (pyrrolic) positions exhibit the highest energy transitions, whereas those compounds with bromine in the pyrrolic positions have the lowest energy transitions. In order to ascertain the source of this red shifting, the four-orbital transition energies were examined. The data are displayed in Figure 5-9. The orbital energies are given in table 5-3. It seems clear that the red shifting is caused by sterically induced distortion; if electronegativity of the ligands were the key factor, chlorine would red shift more than bromine. Figure 5-9 shows that as the ligands get bulkier, the four-orbital transition energies decrease. This decrease in transition energies causes the red shifting of the bands. Table 5-3 shows that the energies of the filled orbitals decrease with increasing electronegativity of substituents. However, the unfilled orbitals are stabilized to a greater extent than filled orbitals. Thus the energy gap between the occupied and the unoccupied orbitals decreases, thereby shifting the absorption bands to lower energy.

In order to unambiguously determine the effect of bending of the porphyrin ring, the following calculation was performed: the bromines of $TFPPBr_8$ were removed and replaced with hydrogens, while the geometry of $TFPPBr_8$ was retained. Since steric factors were not changed, the only variable examined is the electronegativity of the ring substituent. The results of this calculation are given in Table 5-4.

It is clear that if the electronic effects of bromine caused the red shifting, then replacement of the bromines with hydrogens should have reduced the red shifting of the bands by a significant amount. However, the bands of the bent TFPP are still significantly red shifted compared with the transition energies of the planar TFPP. The data in Table 5-4 also show that the absolute energies of the orbitals are much lower when bromine is the ring substituent rather than hydrogen. Thus, the electronic effect of bromine is to lower the overall orbital energies.

FIGURE 5-9: Four Orbital Trends

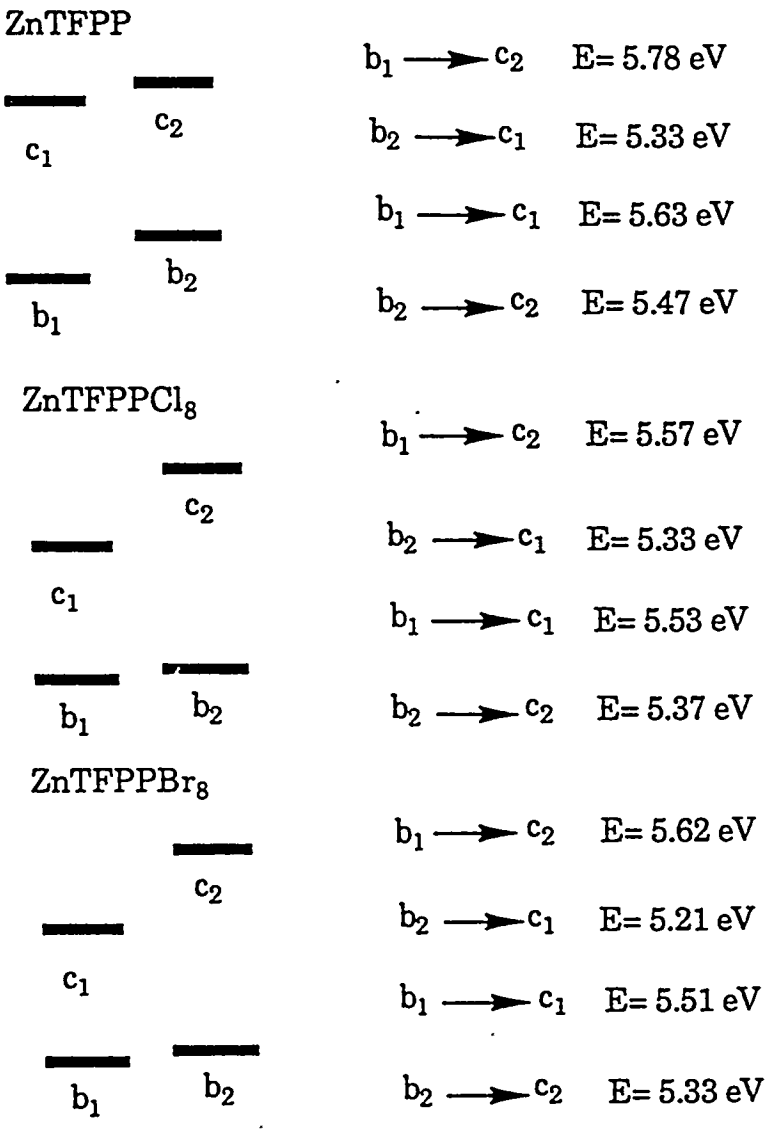

Table 5-3: Orbital Energies

Compound	b_1	b_2	c_1	c_2
TFPP	-8.66 eV	-8.43 eV	-2.27 eV	-2.15 eV
$TFPPCl_8$	-9.73 eV	-9.65 eV	-3.56 eV	-2.99 eV
$TFPPBr_8$	-9.13 eV	-9.02 eV	-2.91 eV	-2.69 eV
ZnTFPP	-8.60 eV	-8.29 eV	-2.97 eV	-2.82 eV
$ZnTFPPCl_8$	-8.87 eV	-8.67 eV	-3.34 eV	-3.30 eV
$ZnTFPPBr_8$	-8.88 eV	-8.60 eV	-3.38 eV	-3.26 eV

Table 5-4: Test of steric effects

Compound	Q_x	Q_y	$Soret_x$	$Soret_y$
TFPP no bending	585 nm	515 nm	332 nm	330 nm
$TFPPBr_8$	652 nm	636 nm	401 nm	399 nm
TFPP bent structure	643 nm	624 nm	391 nm	389 nm
Orbital Energies	b_1	b_2	c_1	c_2
TFPP bent structure	-8.63 eV	-8.57 eV	-2.34 eV	-2.08 eV
$TFPPBr_8$	-9.13 eV	-9.02 eV	-2.91 eV	-2.69 eV

The red shift in spectra with increased bending of the porphyrin ring can be attributed to a loss in orbital overlap within the porphyrin ring. As the porphyrin ring buckles, the p_z type molecular orbitals cannot overlap as efficiently. Thus, the antibonding interactions decrease, lowering the energy of the orbitals. Upon examination of Figure 2, it is clear that the antibonding interactions are much more significant in the unoccupied orbitals; hence the energy reduction is much greater in these orbitals compared with the filled orbitals, decreasing the overall transition energy.

5.1.2.5 Conclusions

1. The red shifting in the absorption spectrum is due to the contraction of the energy gap between the HOMOs and LUMOs, which is a result of the distortion of the porphyrin ring.

2. The electronic effect of the halogens is to lower the absolute energies of the orbitals, thereby explaining the increased stability of the porphyrin to ring oxidation.

5.1.2.6 References

[1] Ellis, P. E.; Lyons, J. E.; Coord. Chem. Rev. 1990, 105, 181.

[2] Bartoli, J. F.; Brigaud, O.; Battioni, P.; Mansuy, D.; J. Chem. Soc. Chem. Commun., 1991, 440.

[3] Gouterman, M.; J. Mol. Spectrosc., 1961, 6, 138.

[4] Callot, H. J.; Bull. Soc. Chim. Fr. 1974, 8, 1492.

[5] Bhyrappa, P.; Krishnan, V; Inorg. Chem. 1991, 30, 239.

[6] Structure analyses done at the Beckman Institute.

[7] Dewar, M. J. S.; Healy, E. F.; Stewart, J. J. P.; Zoebisch, E. G.; J. Am. Chem. Soc. 1985, 107, 3902.

[8] Stewart, J. J. P.; QCPE581.

[9] Cummins, P. L.; Gready, J. E.; Comp. Chem. 1989, 10, 393 and references therein

[10] Kaizu, Y.; Misu, N.; Tsuji, K.; Kaneko, Y.; Kobayashi, H.; Bull. Chem. Soc. Japan 103, 58, 103.

[11] Wijesekera, T.; Matsumoto, A.; Dolphin, D.; Lexa, D.; Angew. Chem.Int. Ed. Engl. 1990, 39, 12028.

5.1.3 Fe(TPPF$_{20}$$\beta$-Br$_8$)Cl Characterization by NMR

During the third quarter of 1991 we developed a ^{19}F NMR method for the characterization of Fe(TPPF$_{20}$$\beta$-Cl$_8$)Cl. We recently used ^{19}F NMR spectroscopy to characterize H_2TPPF$_{20}$$\beta$-Br$_8$ and Fe(TPPF$_{20}$$\beta$-Br$_8$)Cl. The ^{19}F NMR spectrum of H_2TPPF$_{20}$$\beta$-Br$_8$ in $CDCl_3$ is shown in Figure 5-10. The additional resonances in the spectrum (Figure 5-10) are probably due to protonated porphyrin species. The mono- or dication results because the $CDCl_3$ used is acidic. Addition of triethylamine to the NMR tube eliminates the protonated species and the spectrum exhibits (Figure 5-11) three sets of resonances as expected. The lack of beta-hydrogen resonances in the ^{1}H NMR spectrum (Figure 5-12) is indicative of a fully beta-halogenated H_2TPPF$_{20}$ macrocycle. The ^{19}F NMR spectrum of Fe(TPPF$_{20}$$\beta$-Br$_8$)Cl in $CDCl_3$ is shown in Figure 5-13. The broadened resonances, shift of the ortho fluorines to low field, and the splitting of the ortho and meta flourines are indicative of a paramagnetic Fe^{III} porphyrin axially ligated

Figure 5-10

282 MHz ^{19}F NMR $H_2TPPF_{20}\beta\text{-}Br_8$

#977913A in $CDCl_3$

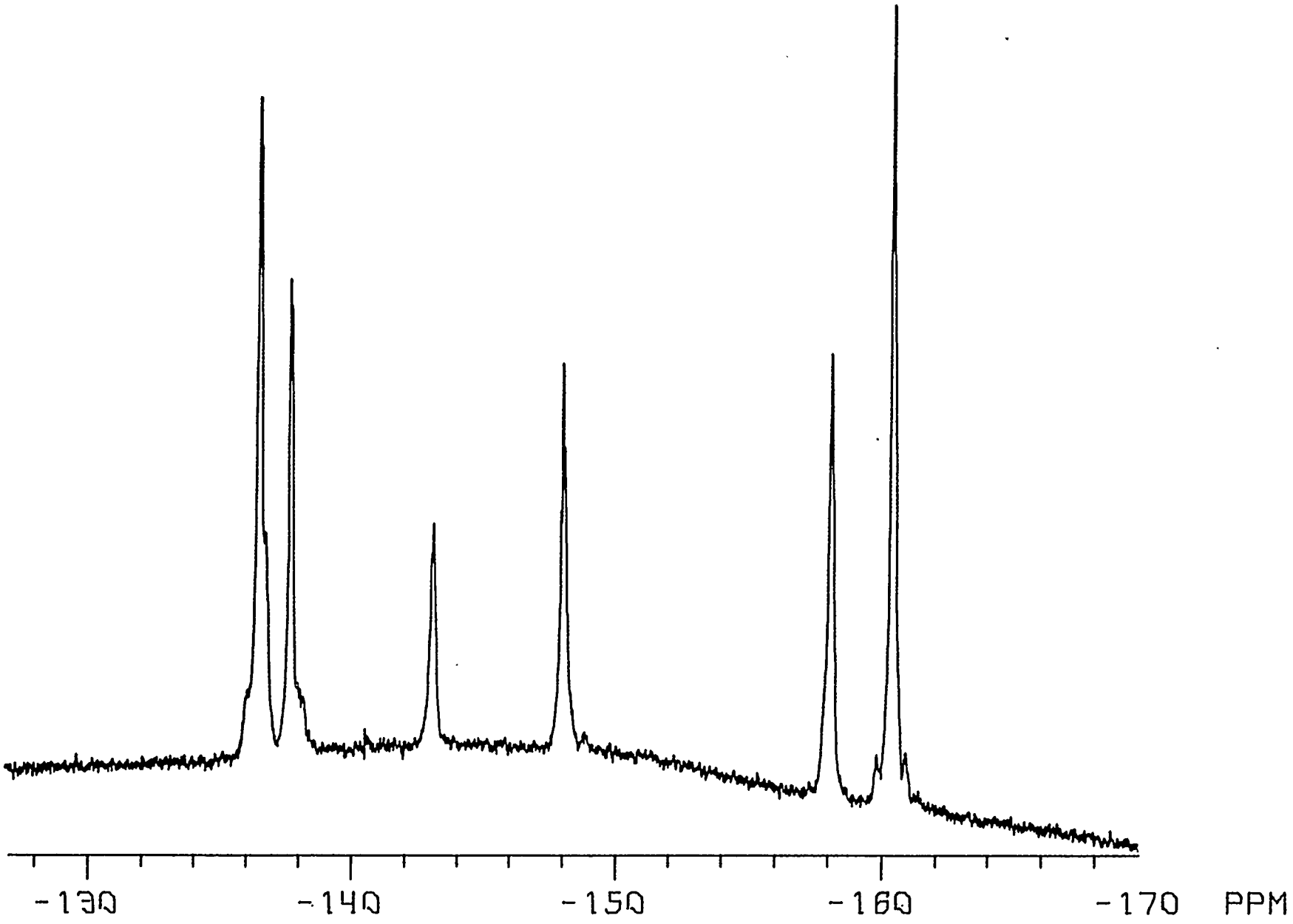

Figure 5-11

282 MHz ^{19}F NMR $H_2TPPF_{20}\beta$-Br_8

#977913A in $CDCl_3$ + TEA

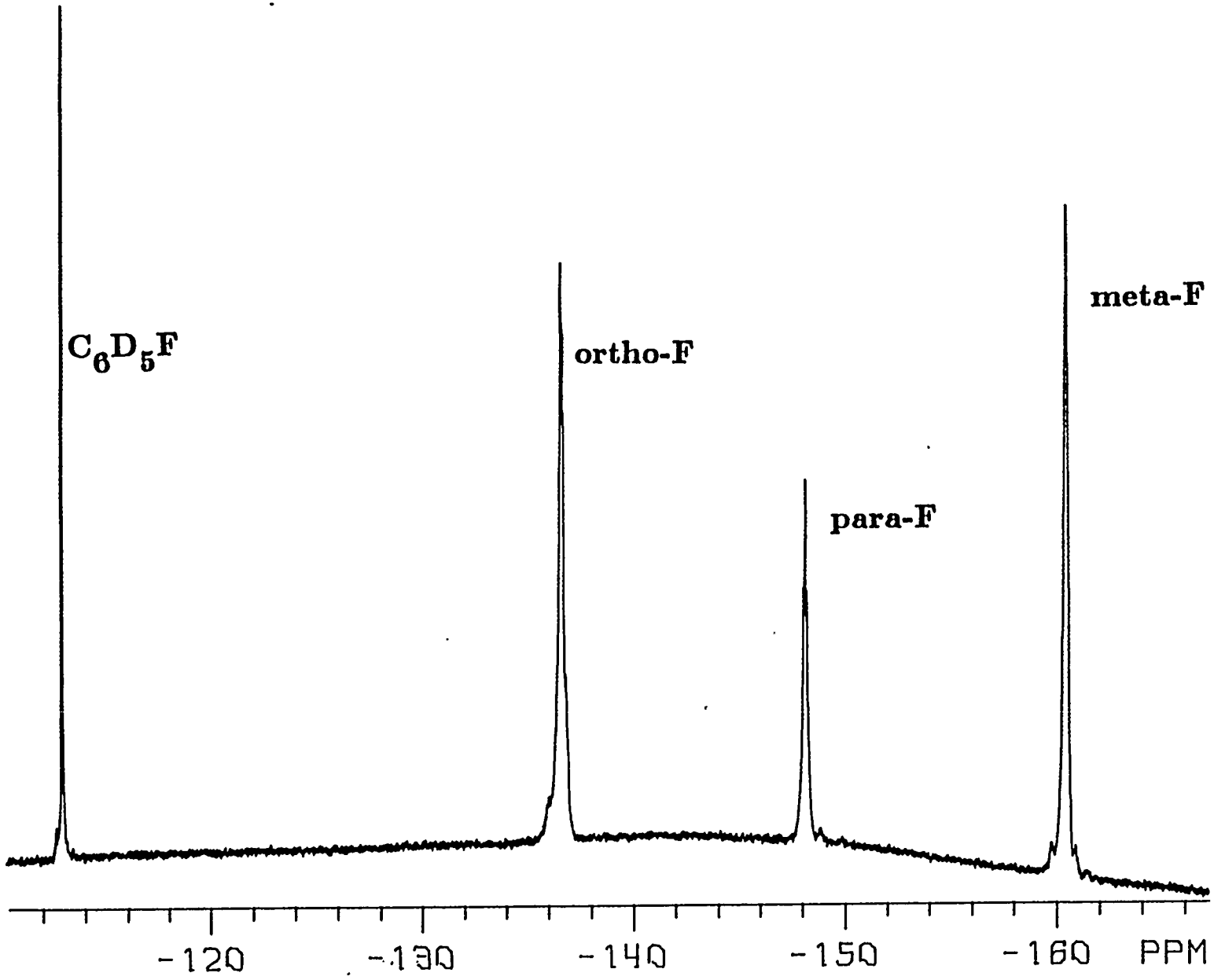

Figure 5-12

300 MHz ^{1}H NMR $H_2TPPF_{20}\beta\text{-}Br_8$

#977913A in $CDCl_3$

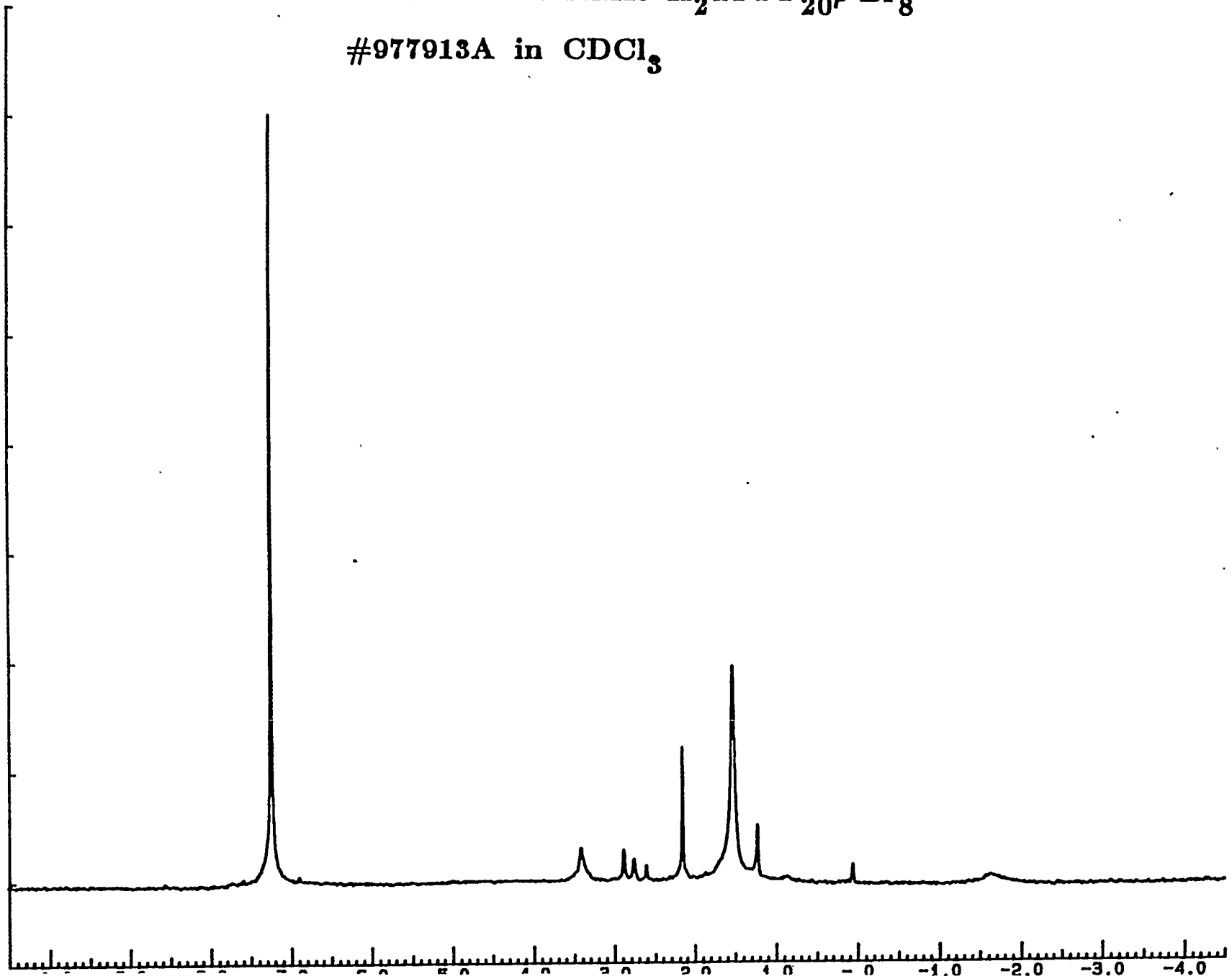

Figure 5-13

282 MHz ^{19}F NMR $Fe(TPPF_{20}\beta\text{-}Br_8)Cl$

#977913B in $CDCl_3$

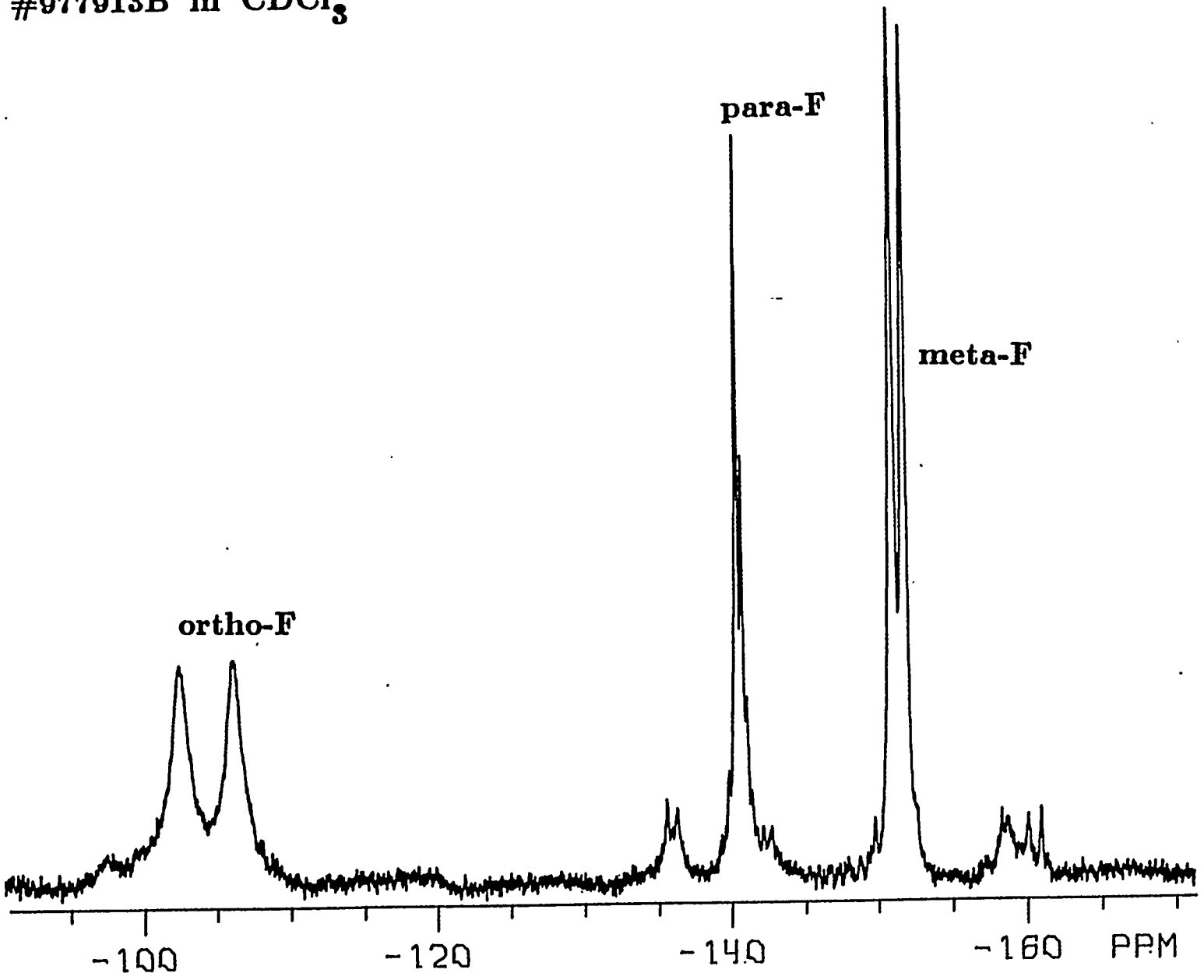

Figure 5 -14

282 MHz ^{19}F NMR $Fe(TPPF_{20}\beta\text{-}Br_8)Cl$

#977913C in pyridine-d_5

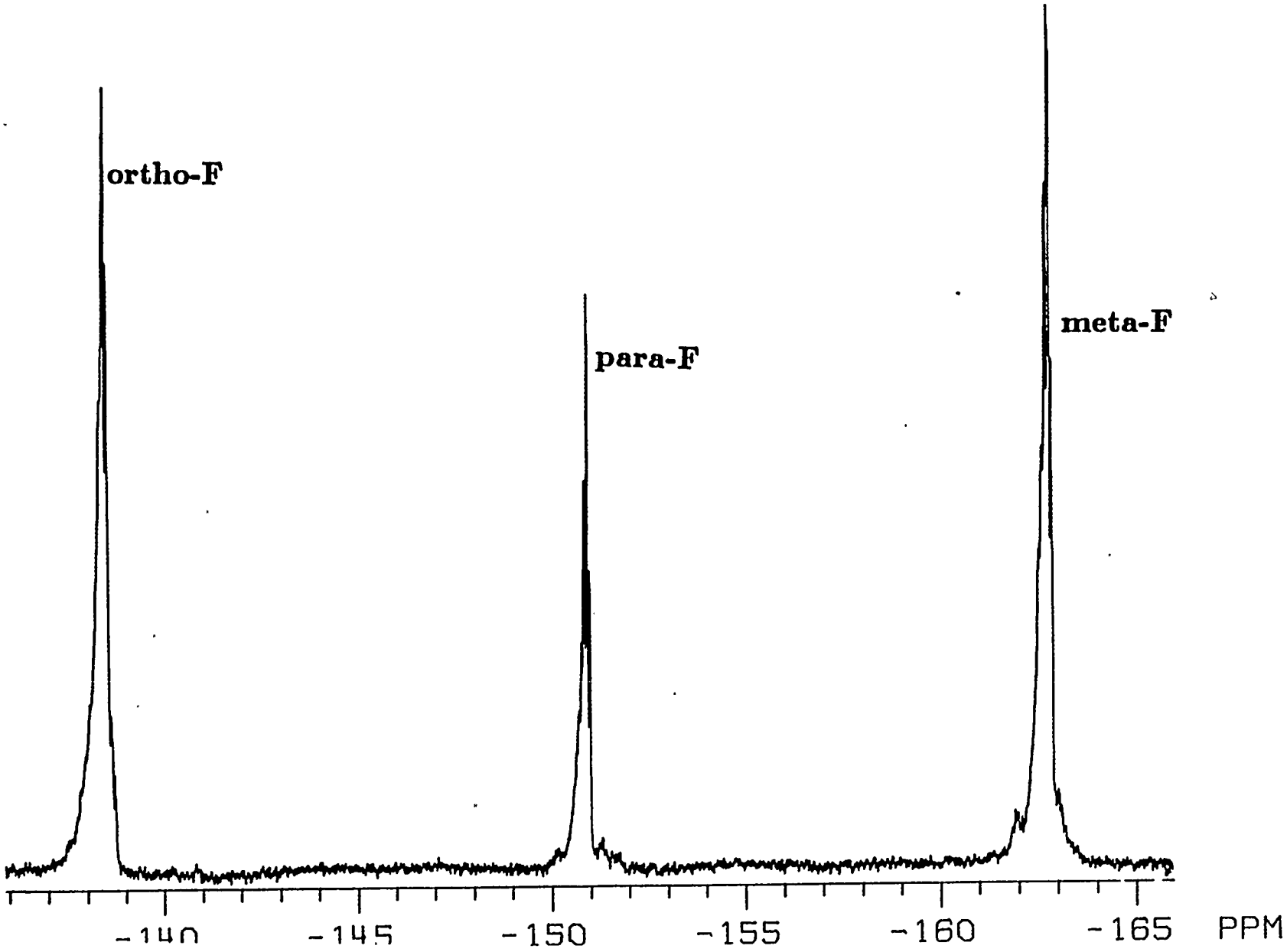

Figure 5-15

282 MHz ^{19}F NMR $H_2TPPF_{20}\beta$-Br_8

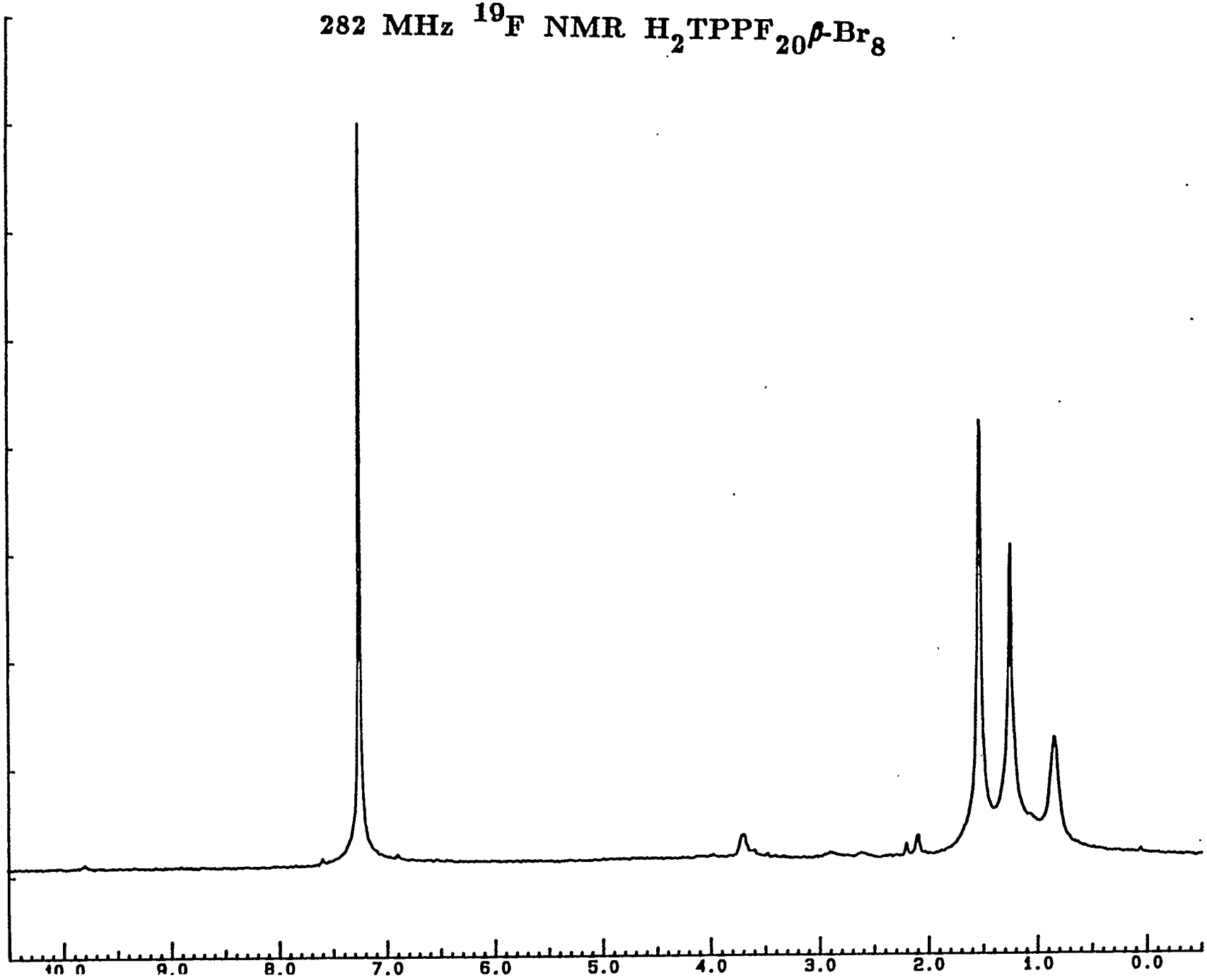

Complexation of TBA can deactivate the catalyst toward oxygen binding and could slow the rate. The more hindered the binding site the more poorly TBA will coordinate. Interestingly, $Fe(TPPF_{20}\beta\text{-}Br_8)Cl$ appears to bind the alcohol less strongly since it is more highly buckled and may suffer less inhibition of rate than the beta-chloro analog. In addition, the more electron defficient the porphyrin ring system, the more tightly an alcohol might bind. Inhibition, therefore, may be highly dependent on the structure of the catalyst and the degree of inhibition may be influenced greatly by design of catalyst structure. Figures 5-16, 5-17, 5-18, show the hindrance to docking of TBA to an iron as a function of macrocycle structure.

5.1.5 Design of New Electron Deficient Porphyrin Complexes

5.1.5.1 Electronic Effects

We have shown that there is a direct correlation between Fe(III)/Fe(II) reduction potential and catalytic activity for light alkane oxidation. Figure 5-19 demonstrates this correlation for the 6 hour oxidation of isobutane at 80°C and propane at 125°C. Thus, the higher the Fe(III)/Fe(II) reduction potential, the greater is the expected catalytic air-oxidation activity of an iron porphyrin complex. We have presented evidence that cyano, nitro and trifluoromethyl groups on the periphery of a porphyrin macrocycle are expected to have greater effects than halo (Br, Cl, F) groups on the reduction potentials of metals in their coordination sphere. We would predict therefore that iron porphyrins having large numbers of cyano, nitro or trifluoromethyl groups would have higher Fe(III)/II reduction potentials than their halo counterparts and therefore greater oxidation activity. For these reasons we are embarking on a program geared to the synthesis of complexes of this type during the last three quarters of the Cooperative Agreement.

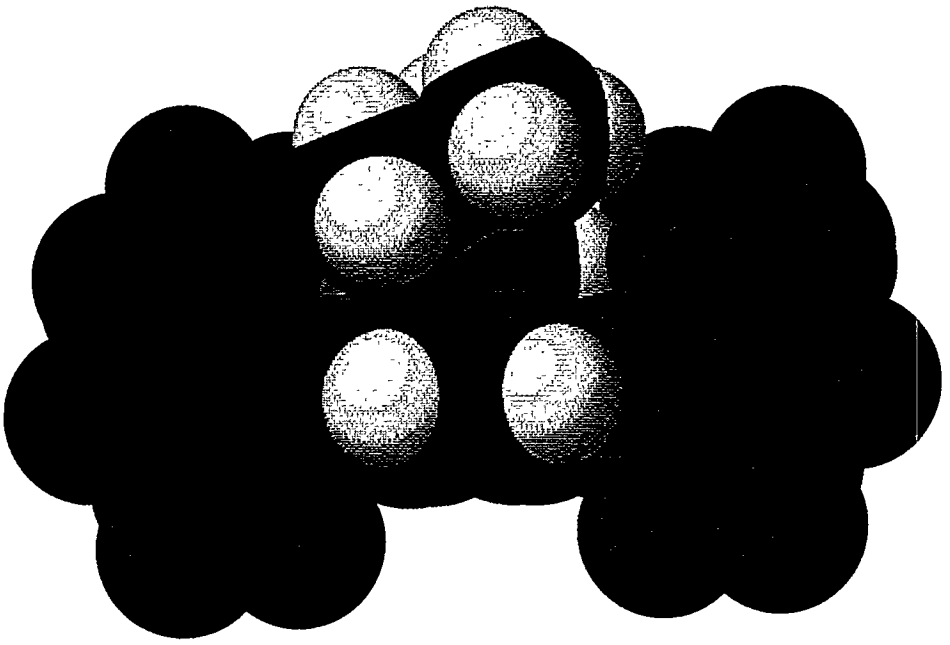

FIGURE 5-16: $Fe(TPPF_{20})(TBA)$

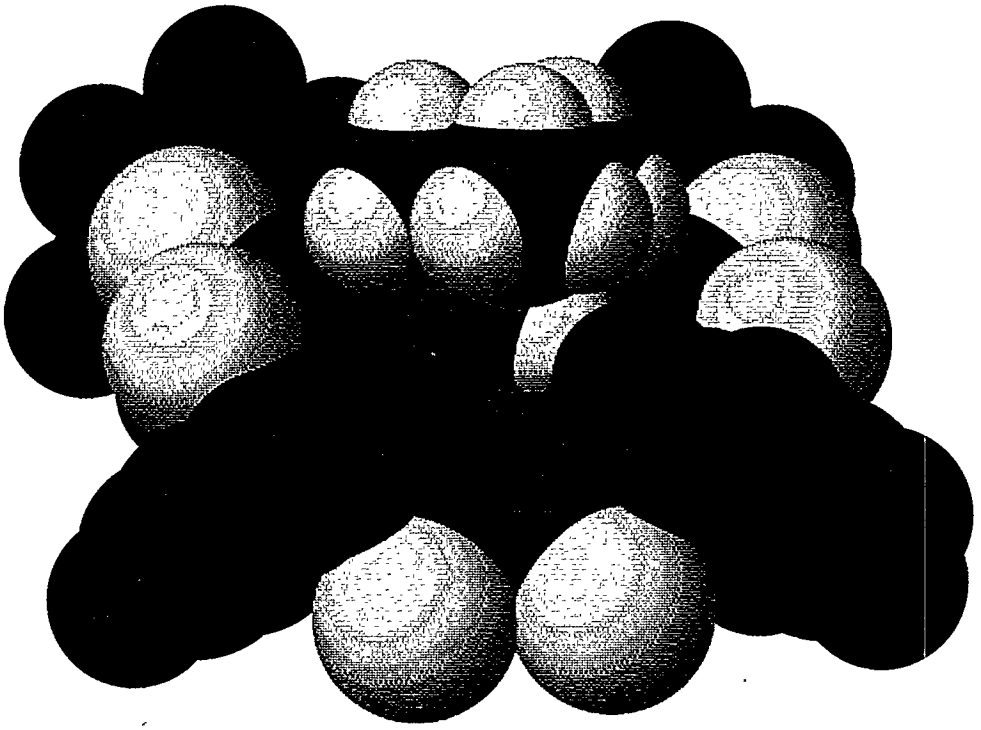

FIGURE 5-17: $Fe(TPPF_{20}\beta\text{-}Cl_8)(TBA)Cl$

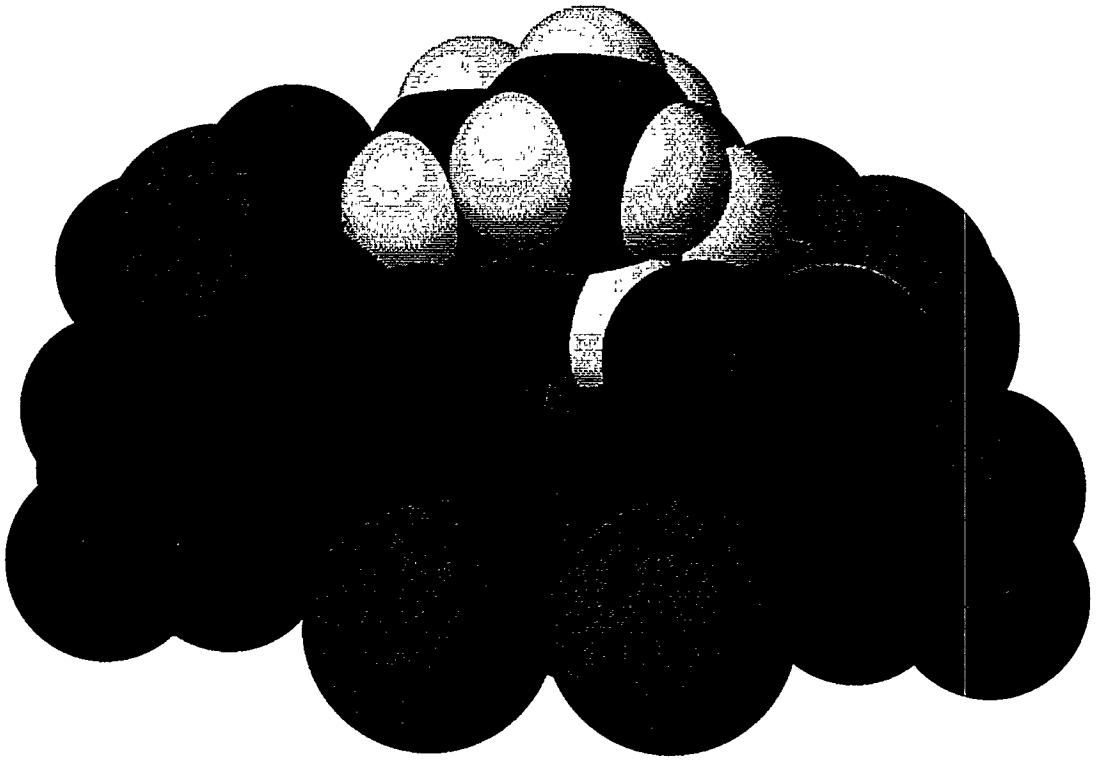

FIGURE 5-18: $Fe(TPPF_{20}\beta\text{-}Br_8)(TBA)(Cl)$

FIGURE 5-19
CATALYST ACTIVITY vs. REDOX POTENTIAL

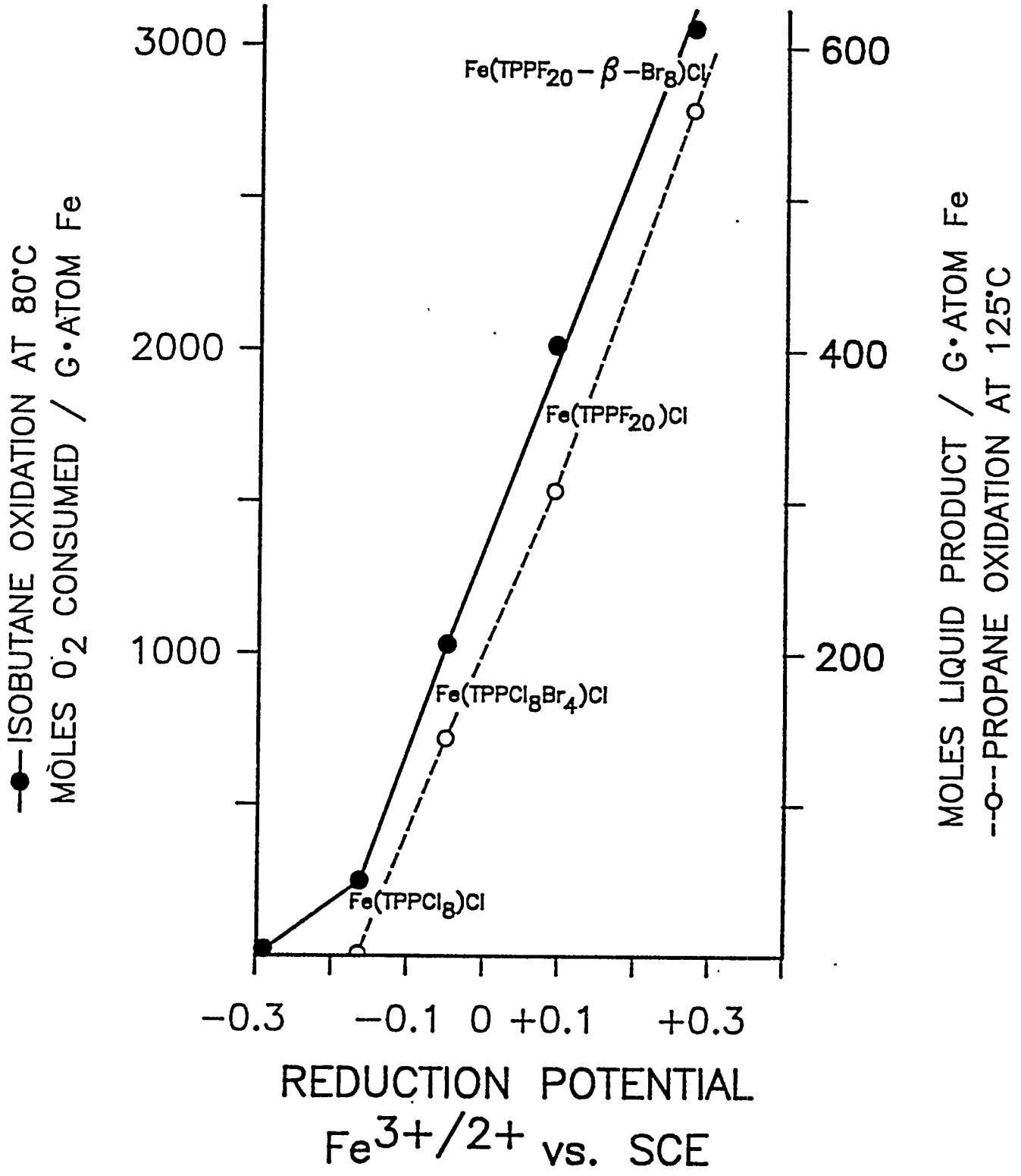

5.1.5.2 Structural Effects

Structural features of electron deficient porphyrin complexes also appear to play an important role in catalytic air-oxidation reactions. In particular, steric interactions which could limit or prevent μ-oxo dimer formation, Figure 2f, may be important for high catalytic activity. We have identified two different types of steric interactions which may be important. One way in which μ-oxo dimer formation could be suppressed is through severe buckling of the porphyrin macrocycle due to steric bulk in the beta-positions. It can be seen that as the bulk of the β-substitutent increases from H to Cl to Br, the extent of buckling increases. It does not seem possible to make the μ-oxo species when the beta-positions bear eight bulky bromines.

Secondly, large electron withdrawing groups such as chloro- in the ortho-position of the phenyl rings of tetraphenylporphyrinato complexes make μ-oxo dimer formation impossible. For this reason we have prepared the perhaloporphyrinato complex, $Fe(TPPCl_{28})Cl$. Wijesekera, et al., Angewandte Chemie, 1990, and have shown that the Fe(III)/(II) reduction potential of this complex is nearly as high (0.27v) as that of $(Fe(TPPF_{20}\beta\text{-}Cl_8)Cl$. It is possible that $Fe(TPPF_{20}\beta\text{-}Cl_8)Cl$ could form a μ-oxo dimer. On the other hand $Fe(TPPCl_{28})Cl$ could not form a μ-oxo dimer because of the huge non-bonded interactions resulting from the eight ortho-chloro substituents on each macrocycle cause significant buckling of the macrocycle, Figures 5-20, 5-21.

5.1.5.3 Synthesis of Chloro meso-Tetrakis(Pentachlorophenyl)-β-Octachloroporphinatoiron(III) $TPPCl_{28}FeCl$

Synthesis of the above compound involved four steps:

1. Synthesis of pentachlorobenzaldehyde

2. Condensation of pyrrole and pentachlorobenzaldehyde to give meso-tetrakis(pentachlorophenyl)porphyrin H_2TPPCl_{20}

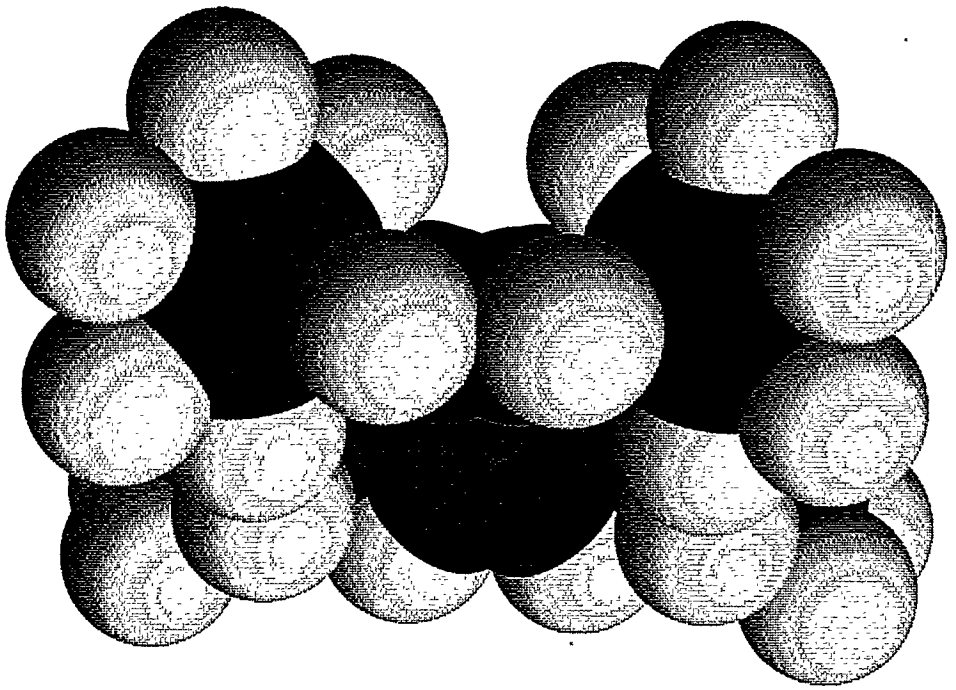

FIGURE 5-20: $Fe(TPPCl_{28})$

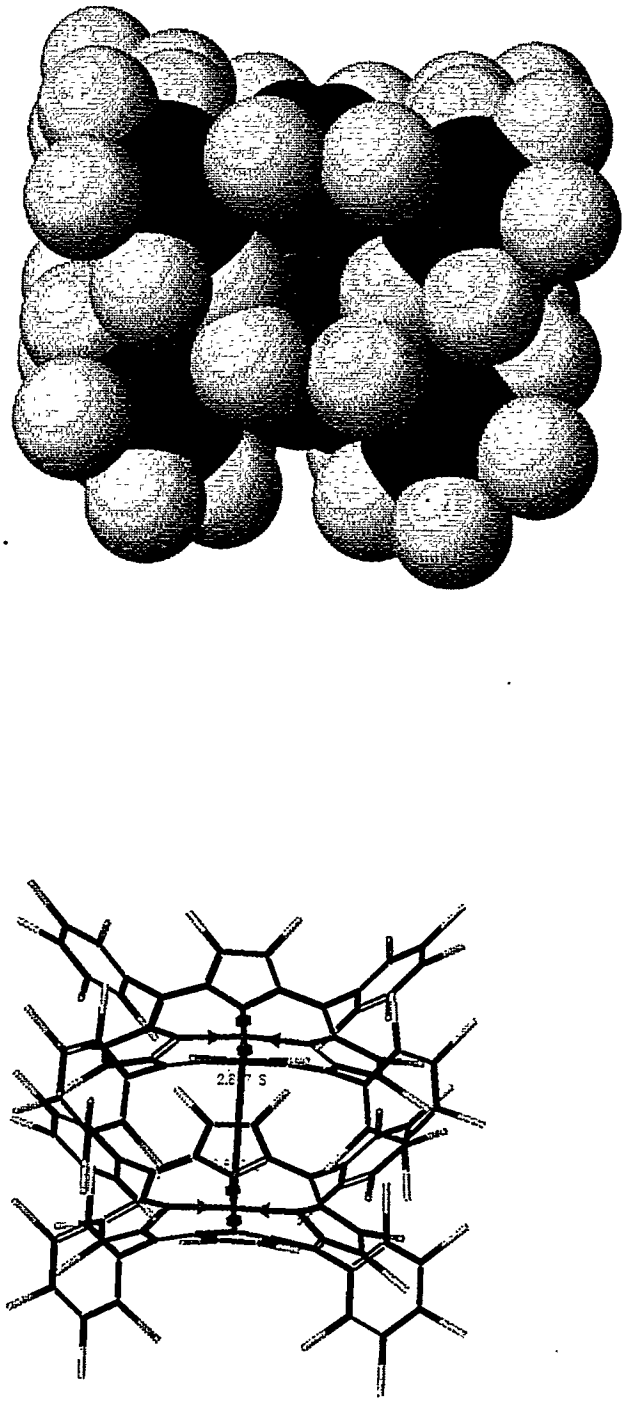

FIGURE 5-21: $[Fe(TPPCl_{28})]_2O$

3. Insertion of iron into 2 to give the iron(III) chloride $TPPCl_{20}FeCl$

4. β-Chlorination of 3 to give $TPPCl_{28}FeCl$

Pentachlorobenzaldehyde was prepared from hexachlorobenzene using a procedure adapted from that used for the preparation of pentachlorobenzoic acid (D.E.Pearson and D. Cowan, Org. Synthesis, 44 78 1964). Condensation of pyrrole and pentachlorobenzaldehyde to give porphyrin 2 has previously been carried out using modified Rothmund zinc-template based procedures (1. G.M. Badger, R. A. Jones and R. L. Laslett, Aust. J. Chem., **17**, 1028 1964; 2. P.S. Traylor, D. Dolphin and T. G. Traylor, J. Chem. Soc. Chem. Commun. 1984 279) but the product yields have been low (2-4%). By using an adaptation of the condensation method developed by Lindsey for the synthesis of meso-tetraphenylporphyrins (J. S. Lindsey and R. W. Wagner, J. Org. Chem., **54** 828 1989), a procedure hitherto not been used to prepare the porphyrin **2**, it was possible to obtain yields of up to 40%. Iron insertion to porphyrin **2** was carried out using a standard procedure (A.D. Adler, F. R. Longo, F. Kampas and J. Kim, J. Inorg. Nucl. Chem., **32** 2443 1970) and the resulting metal complex **3** was chlorinated using chlorine gas/anhydrous ferric chloride according to a literature procedure.

5.1.5.3.1 Synthesis of Pentachlorobenzaldehyde

This synthesis involved two steps carried out in a single pot. In the first step, a Grignard reagent was prepared from the commercially available hexachlorobenzene which was in turn reacted with a formylating agent N,N-dimethylformamide (DMF). Since the inert hexachlorobenzene does not form the Grignard reagent directly, an entrainment reaction was carried out using the active halide 1,2-dibromoethane. An excess of both magnesium and the dihalide are used to improve the yield of the Grignard reagent which was reacted with DMF without isolation.

5.1.5.3.2 Synthesis of meso-Tetrakis(Pentachlorophenyl)Porphyrin

Pentachlorobenzaldehyde (2.785g; 10 mmmoles) and chloroform (1L; stabilized with amylenes, distilled from K_2CO_3) were placed in a 2-liter 3-neck round-bottom flask fitted with an argon inlet tube and a reflux condenser, the third neck carrying a septum. Degassed the solution for 30 min., introduced pyrrole (695μL; 10mmoles; redistilled prior to use), closed the system in argon and heated to gentle reflux. Protected the flask from ambient light, syringed in boron trifluoride etherate (1.32mL of a 2.5M stock solution) and continued reflux for 1h. The reaction mixture was cooled to room temperature, added a solution of DDQ (2g) in benzene (100mL), allowed to stir for 30 min. and heated at reflux for 30 min. Triethylamine (2mL) was added to the solution, evaporated the solvent under reduced pressure and removed the residual solvent at high-vacuum. The crude product was scraped off the flask, transferred to a 60°F sinter funnel and washed with small portions of methanol until the washings were nearly colorless. The solid was dried in a vacuum-dessicator, dissolved in 300 mL chloroform and chromatographed on neutral alumina (Activity I; 400g) using dichloromethane for elution. The porphyrin product eluted out as an orange-purple fraction, which was concentrated and crystallized from methanol. Filtered and washed with methanol to give 1.06g (32.5%). The yield varied between 25-38% in several trials carried out on 1/10 scale, depending primarily on the freshness of the catalyst solution used.

5.1.5.3.3 Synthesis of meso-Tetrakis(Pentachlorophenyl) porphinatoiron(III)chloride $TPPCl_{20}FeCl$

Insertion of Iron into H_2TPPCl_{20}

---> WAVELENGTH SCAN REPORT <---

Date : 02-27-1992
Time : 14:49:05
Operator : Not Entered

Sample Name : 996774-1
Solvent Name : CHCL3
Concentration : 1.0000
Units :

Function : Absorbance
Wavelength Range : 300 to 700 nanometer
Integration Time : 1 seconds
Std Deviation : OFF

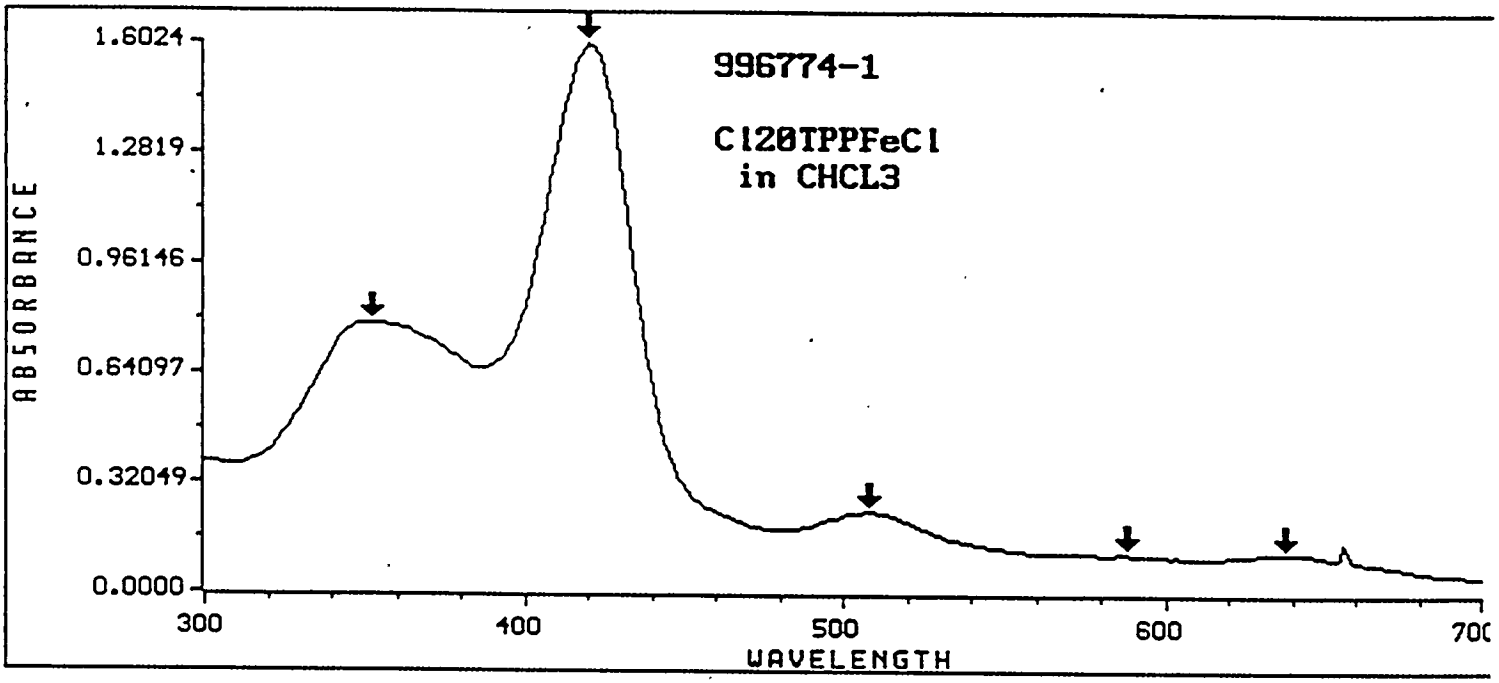

Annotated Wavelengths:

1	Wavelength =	352	Result =	0.788361
2	Wavelength =	420	Result =	1.602432
3	Wavelength =	508	Result =	0.233765
4	Wavelength =	588	Result =	0.111588
5	Wavelength =	638	Result =	0.114319

FIGURE 5-22 UV/VISIBLE SPECTRUM OF $Fe(TPPCl_{20})Cl$

Figure 1

5.1.5.3.4 Synthesis of meso-Tetrakis (pentachlorophenyl)-β-Octachloroporphinatoiron III Chloride $TPPCl_{28}FeCl$ 4

Anhydrous ferric chloride (400mg), $TPPCl_{20}FeCl$ (100mg) and ortho-dichlorobenzene (25mL) were placed in a 100mL 3-neck round-bottom flask fitted with a gas inlet tube, reflux condenser (surmounted by a drying tube) with the third neck closed. The flask was heated to 140°C, protected from ambient light and bubbled chlorine gas for 5 min. Continued heating at 140°C and monitored the reaction by UV-spectroscopy. The split Soret of the starting material 352/420 moved to 394/442nm on completion of the reaction (usually 30 min.; if incomplete, chlorine gas should be bubbled for another 3 min. and heating continued for a total of 1 hour). The solvent was removed under reduced pressure (high vacuum), the residue redissolved in chloroform (stabilized with amylenes: 100mL) and extracted with 3N hydrochloric acid (100mL). Washed the organic layer with water (100mL) and evaporated to dryness.

Purification

The crude solid dissolved in chloroform (stabilized with amylenes), was chromatographed on dry silica (100g; Fisher, Act. I 230-400 mesh). With dichloromethane, the demetallated perchloroporphyrin eluted out first and on changing the solvent to 5% methanol-dichloromethane the metalloporphyrin eluted out. Evaporated the product fraction to dryness, redissolved in chloroform (150mL) and extracted once with conc. hydrochloric acid (100mL). The organic layer was separated, washed with water (3x100mL), dried (Na_2SO_4) and the perchlorometalloporphyrin 4 was isolated; yield 107mg (85%); UV:Figure 5-23.

---> WAVELENGTH SCAN REPORT <---

Date : 03-03-1992
Time : 19:53:46
Operator : Not Entered

Sample Name : 996784
Solvent Name : CHCL3
Concentration : 1.0000
Units :

Function : Absorbance
Wavelength Range : 300 to 700 nanometers
Integration Time : 1 seconds
Std Deviation : OFF

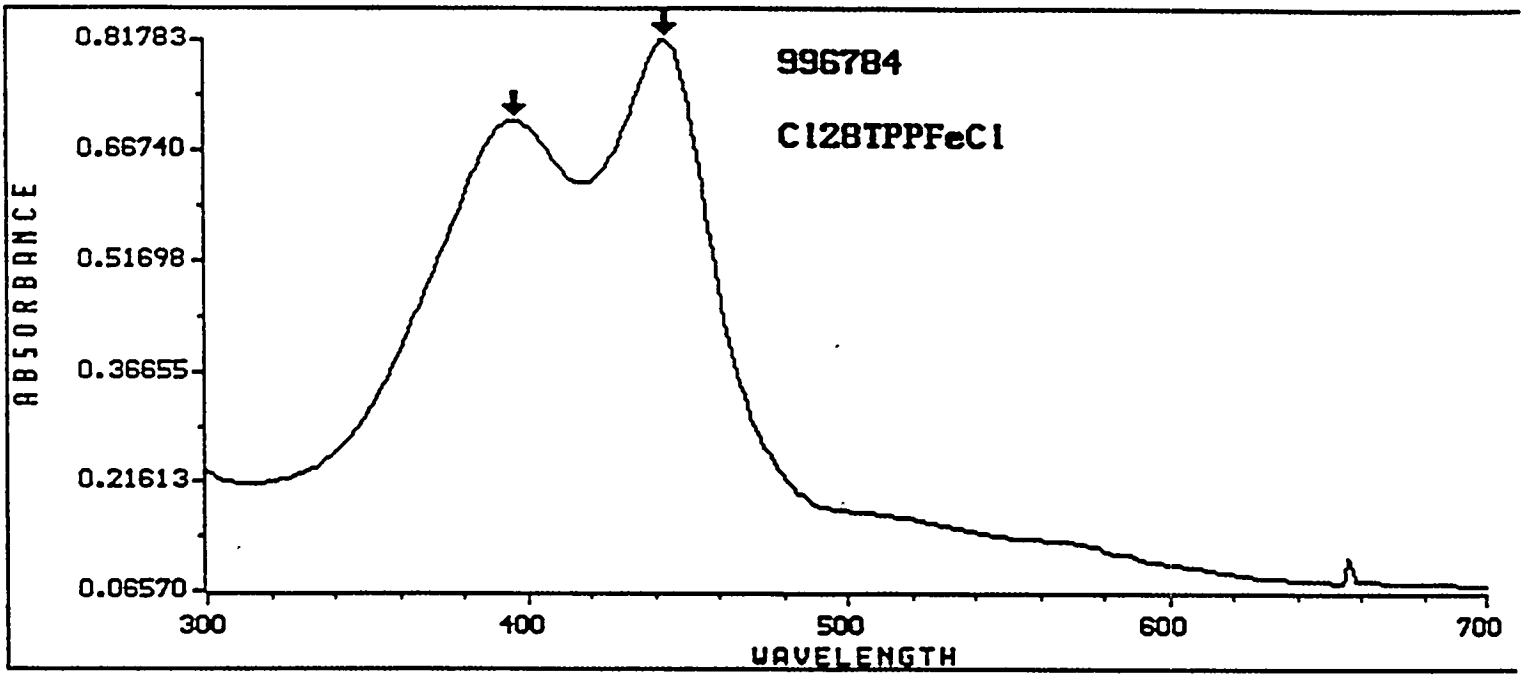

Annotated Wavelengths:
1 : Wavelength = 396 Result = 0.708115
2 : Wavelength = 444 Result = 0.817825

FIGURE 5-23 UV/VISIBLE SPECTRUM OF $Fe(TPPFCl_{28})Cl$

Figure 2

5.1.5.4 Oxidation of Alkanes Using $Fe(TPPCl_{28})Cl$ as Catalyst

We attempted the oxidation of isobutane (20%) in benzene under standard test conditions (100psig 0_2, 6 hours) at 40, 60, and 80°C using $Fe(TPPCl_{28})Cl$ as the catalyst. No reaction occurred. Under these conditons nearly 2,000 turnovers would have been observed at 60°C using $Fe(TPPF_{20}\beta\text{-}Cl_8)Cl$ as the catalyst. One interpretation of these results is that not only is the μ-oxo dimer, $[Fe(TPPCl_{28})]_2O$, unable to form, but even the μ-peroxo dimer, $[Fe(TPPCl_{28})]_2O_2$ cannot be made. Inspection of the molecular model of the monomeric Fe(II) complex, Figure 5-20 shows that the iron is surrounded by a nearly symmetrical barrier of chlorine atoms. Thus, it is possible that steric hindrance about the iron centers is so great that this complex may not be able to reductively bind dioxygen, Figure 4(b).

If this explanation is correct then small single oxygen atom transfer reagents should still be able to oxidize the iron center to a ferryl which will oxidize hydrocarbons. It has been found that $Fe(TPPCl_{28})Cl$ oxidizes cyclohexane to the alcohol and the ketone and oxidizes cyclohexene to the epoxide when iodosyl benzene is the oxidant.

Thus, when a small oxygen donor having oxygen in the reductively bound state is used, oxidations presumably occurring through an active ferryl intermediate are possible. When it is necessary to reductively bind a dioxygen molecule in order to get the active catalytic intermediate, steric bulk prevents this reaction from occurring.

Thus we may now have spanned the range of steric requirements for both μ-oxo and μ-peroxo complex formation. It would appear that a properly tuned iron complex which can readily form a μ-peroxo dimer but which cannot form μ-oxo dimer should give the greatest concentration of active ferryl, and thus should be the best catalyst. We are currently studying other complexes with varying steric requirements to test this hypothesis.

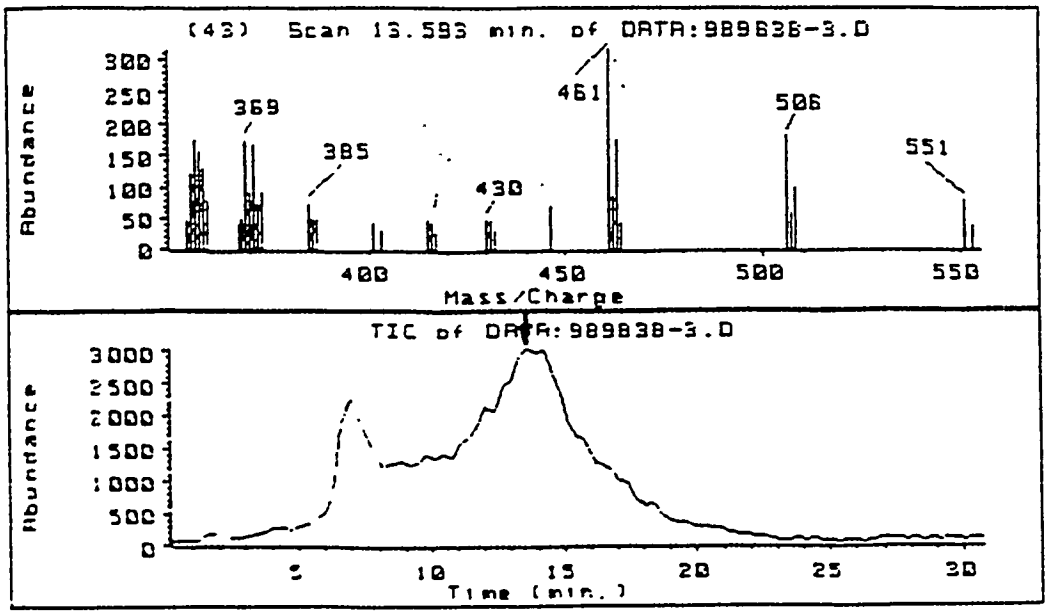

T: ----------
Z: TIC of DATA:989838-3.D
Y: Scan 6.938 min. of DATA:98
X: Scan 13.593 min. of DATA:9

[MS3]

Scan 13.593 min. of DATA:989838-3.D

AMU.	Abundance	AMU.	Abundance	AMU.	Abundance
353.95	47.00	373.00	92.00	446.05	68.00
355.05	122.00	385.00	75.00	460.90	317.00
355.95	173.00	386.00	46.00	461.80	87.00
356.95	156.00	386.90	49.00	462.90	176.00
358.00	133.00	400.90	44.00	463.90	43.00
359.00	80.00	403.00	32.00	505.95	182.00
367.10	39.00	414.85	46.00	506.95	56.00
368.10	50.00	415.95	43.00	507.95	97.00
369.00	176.00	416.25	25.00	551.00	76.00
370.00	93.00	429.65	47.00	553.00	35.00
371.00	168.00	430.95	46.00		
372.00	71.00	431.65	30.00		

FIGURE 5-24 MASS SPECTRUM OF Cu (T-$(NO_2)_4$)P,MW=551.8

5.1.5.5.3 Demetallation of CuP - Preparation of H_2P

Since we could not remove the Cu from Cu(T-NO_2)P we decided to make FePCl and attempt its nitration.

200 mg of CuP mass spectrum shown in Figure 5-24a, IR in Figure 5-25 is stirred into 30 mL of FSO_3H for 5 minutes. The color goes from greenish-brown to the bright green of the H_4CuP^{2+} cation. This solution is added to 500 mL of H_2O/CH_3OH and neutralized by adding solid sodium bicarbonate. The H_2P is extracted with $CHCl_3$ then evaporated to dryness UV/VIS ($CHCl_3$) 393, 491, 516, 550 nm. IR's of the CuP and product H_2P are included. Preparation of FePCl (Iron porphine chloride): 100 mg of H_2P is dissolved in 350 ml of DMF with 10 ml of glacial acetic acid. The solution is heated to reflux with stirring then 700 mg of $FeCl_2.4H_2O$ is added. After 1 hour the reaction is cooled and the contents added to 350 ml of saturated NaCl solution which precipitates the product. The solids are washed, dried and chromatographed on Alumina (Fisher A-540) eluting with $CHCl_3$. The first red to red-brown band elutes with $CHCl_3$ and is collected. (Soret = 406 nm). This material may be the μ-oxo dimer. No IR was taken.

5.1.5.5.4 Nitration of FePCl

The FePCl or PFeOFeP from the previous work above was reacted with excess NO_2 in $CHCl_3$. The final UV/VIS spectrum showed a Soret band at 426 nm. The $CHCl_3$ solution was evaporated to dryness and put on an alumina column elution with $CHCl_3$. Two bands were obtained: the first green band with Soret = 423 nm and the later green band needing methanol to remove it with Soret = 417 nm. Much more work was performed on these two materials but the reaction has proven to be complex and the yields of tractable material is small. IR analysis shows that little NO_2 has been incorporated into the products with red-shifted UV/VIS bands.

5.1.5.5.5 Preparation of ZnP

Because of the difficulty in preparing pure FePCl and even greater difficulty

FIGURE 5-25: 2500, 989829, Cu Porphine, PEE, FRC, KBr, 3/13/92

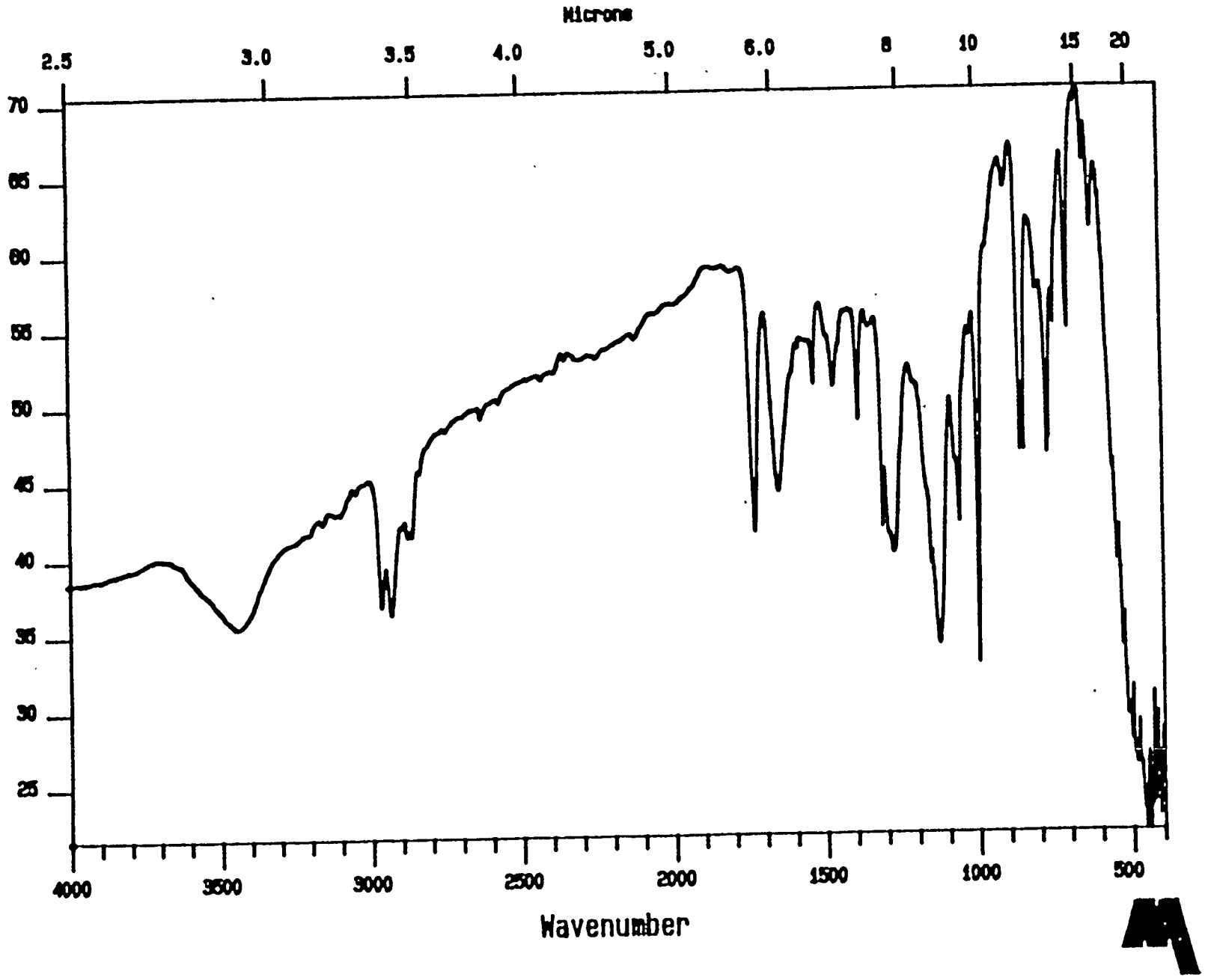

tmp.res

5.1.5.5.3 Demetallation of CuP - Preparation of H_2P

Since we could not remove the Cu from Cu(T-NO_2)P we decided to make FePCl and attempt its nitration.

200 mg of CuP mass spectrum shown in Figure 5-24a, IR in Figure 5-25 is stirred into 30 mL of FSO_3H for 5 minutes. The color goes from greenish-brown to the bright green of the H_4CuP^{2+} cation. This solution is added to 500 mL of H_2O/CH_3OH and neutralized by adding solid sodium bicarbonate. The H_2P is extracted with $CHCl_3$ then evaporated to dryness UV/VIS ($CHCl_3$) 393, 491, 516, 550 nm. IR's of the CuP and product H_2P are included. Preparation of FePCl (Iron porphine chloride): 100 mg of H_2P is dissolved in 350 ml of DMF with 10 ml of glacial acetic acid. The solution is heated to reflux with stirring then 700 mg of $FeCl_2.4H_2O$ is added. After 1 hour the reaction is cooled and the contents added to 350 ml of saturated NaCl solution which precipitates the product. The solids are washed, dried and chromatographed on Alumina (Fisher A-540) eluting with $CHCl_3$. The first red to red-brown band elutes with $CHCl_3$ and is collected. (Soret = 406 nm). This material may be the μ-oxo dimer. No IR was taken.

5.1.5.5.4 Nitration of FePCl

The FePCl or PFeOFeP from the previous work above was reacted with excess NO_2 in $CHCl_3$. The final UV/VIS spectrum showed a Soret band at 426 nm. The $CHCl_3$ solution was evaporated to dryness and put on an alumina column elution with $CHCl_3$. Two bands were obtained: the first green band with Soret = 423 nm and the later green band needing methanol to remove it with Soret = 417 nm. Much more work was performed on these two materials but the reaction has proven to be complex and the yields of tractable material is small. IR analysis shows that little NO_2 has been incorporated into the products with red-shifted UV/VIS bands.

5.1.5.5.5 Preparation of ZnP

Because of the difficulty in preparing pure FePCl and even greater difficulty

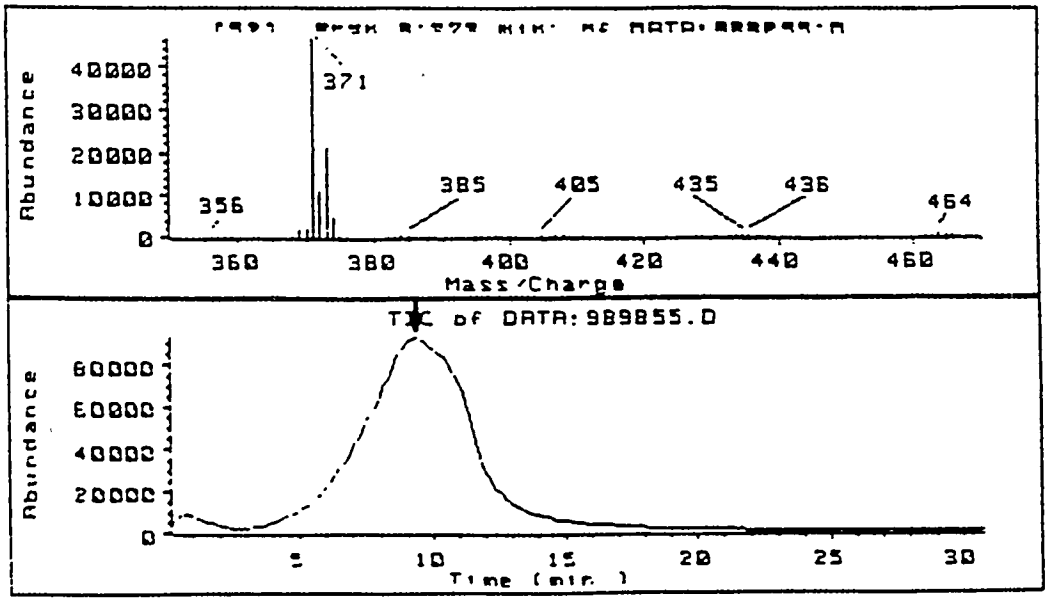

T: Scan 18.867 min. of DATA:9
Z: TIC of DATA:989855.D
Y: Scan 18.122 min. of DATA:9
X: Scan 9.373 min. of DATA:98

[E]

Scan 9.373 min. of DATA:989855.D

AMU.	Abundance	AMU.	Abundance	AMU.	Abundance
355.85	128.00	382.00	27.00	399.90	52.00
356.85	54.00	383.00	27.00	400.90	79.00
358.00	86.00	383.90	206.00	404.80	403.00
359.00	61.00	384.90	184.00	405.95	144.00
366.00	112.00	385.90	143.00	406.95	349.00
368.90	1846.00	386.90	91.00	407.95	291.00
370.00	1848.00	388.00	70.00	408.95	152.00
370.90	46480.00	389.00	26.00	409.95	131.00
371.90	11004.00	395.00	37.00	410.95	49.00
372.90	21126.00	395.90	50.00	427.65	41.00
373.90	4615.00	396.90	58.00	430.85	37.00
374.90	526.00	397.90	54.00	432.85	172.00
376.00	51.00	398.90	164.00	433.75	236.00

Scan 9.373 min. of DATA:989855.D

AMU.	Abundance	AMU.	Abundance	AMU.	Abundance
434.85	240.00	440.75	59.00	462.90	66.00
435.75	274.00	442.75	38.00	463.80	750.00
436.85	117.00	446.85	26.00	464.90	253.00
437.75	85.00	448.75	32.00	465.80	349.00
438.75	55.00	461.90	21.00	466.90	106.00

FIGURE 5-24a:MASS SPECTRUM OF CuP,M.W.=371.8

in nitration of FePCl, we decided to nitrate the Zn and proceed in that way to the nitrated iron porphyrin.

200 mg of H_2P IR spectrum: Figure 5-26 is dissolved in 200 mL of DMF and heated to reflux. 350 mg of $Zn(OAc)_2$ is added with stirring at reflux for 15 min. TLC showed the reaction to be complete. The DMF solution is added to H_2O to precipitate the product which is washed thoroughly with H_2O and dried. TLC shows a single spot so no chromatography was needed. UV/VIS ($CHCl_3$): 397, 518, 549. This is comparable to CuP with UV/VIS ($CHCl_3$): 392, 516, 550, IR spectra-Figures 5-27, 5-28.

5.1.5.5.6 Nitration of ZnP to Zn(T-NO_2)P

20 mg of ZnP is dissolved in 100 ml of $CHCl_3$ and reacted with 2 drops of liquid NO_2 (large excess). After 10-15 minutes, the Soret has shifted to 424 nm. The solution, now green, is washed with H_2O then evaporated to dryness UV/VIS ($CHCl_3$) 424, 521, 571 nm. This is similar to Cu(T-NO_2)P with absorptions at 427, 546 and 596 nm and Zn (OEP)$(NO_2)_4$ with absorptions at 426, 520 (sh.), 561 and 580 nm. IR (KBr) spectrum shows two new stretches not found in H_2P or ZnP at 1356cm^{-1} (strong) and 1541cm^{-1} (medium). These are comparable to those found in trinitro-octaethylporphine at 1375 and 1534cm^{-1} [R. Bonnett and G. F. Stephenson, J. Org. chem. **30**, 2791 (1965]

5.1.5.5.7 Removal of Zinc Preparation of H_2(T-NO_2)P

HCl gas bubbled through a solution of Zn(T-NO_2)P in $CHCl_3$ was not sufficient to remove the Zn as monitored by UV/VIS and TLC. 100 mg of Zn(T-NO_2)P is dissolved in 100 mL of CH_2Cl_3 containing 10 ml of 70% $HClO_4$. This solution is stirred at room temperature for 1 hour then washed with H_2O, two times and neutralized with saturated sodium bicarbonate solution. The $CHCl_3$ is reduced to dryness. Characterization of this material is continuing.

FIGURE 5-27: 2537, 1000909, Zn (P) Nitro, PEE, FRC, KBr, 4/15/92

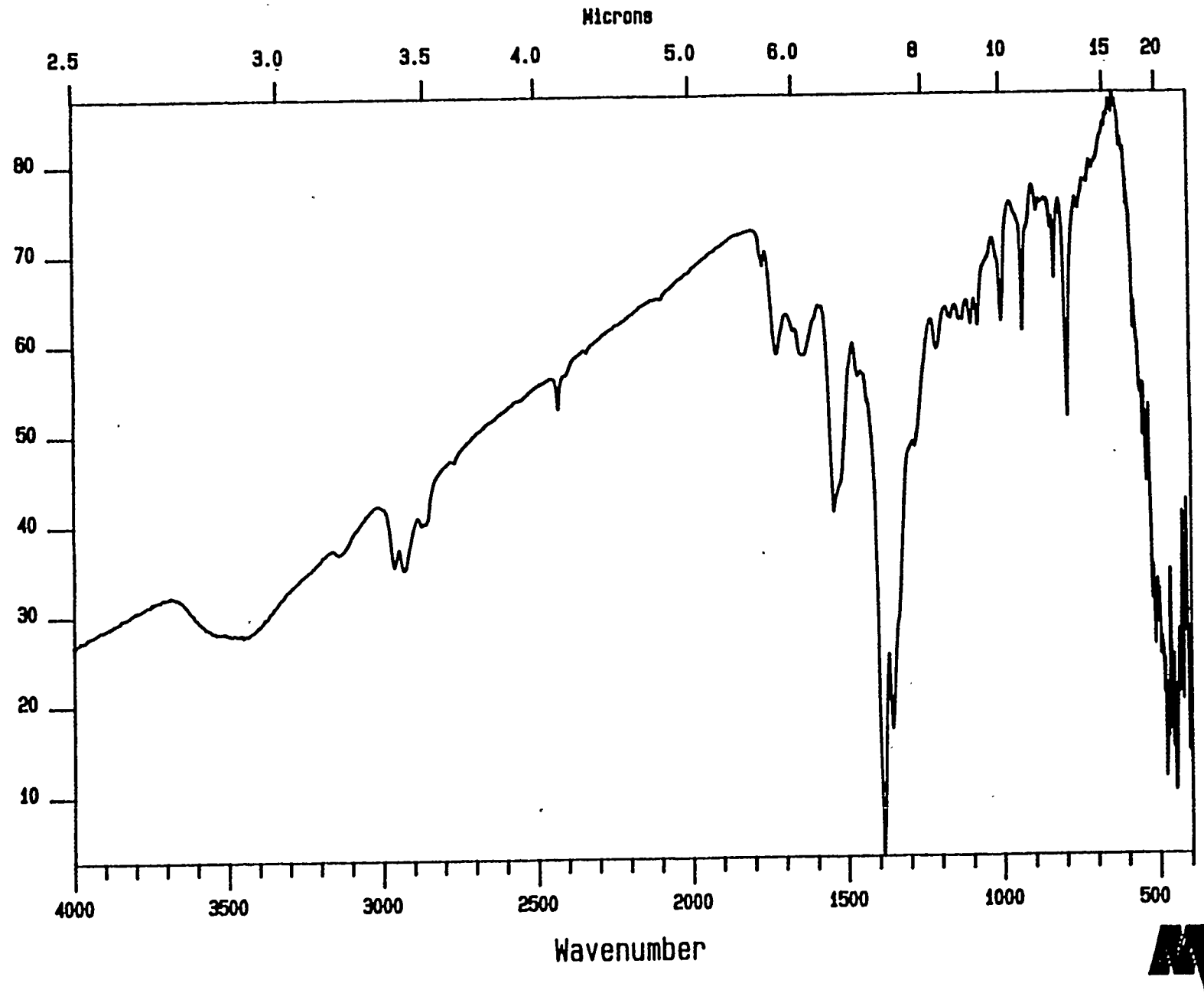

tmp.ras

FIGURE 5-26: 2507, H2 (P) Ref. Sample, Wayne L., FRC, KBr, 3/20/92

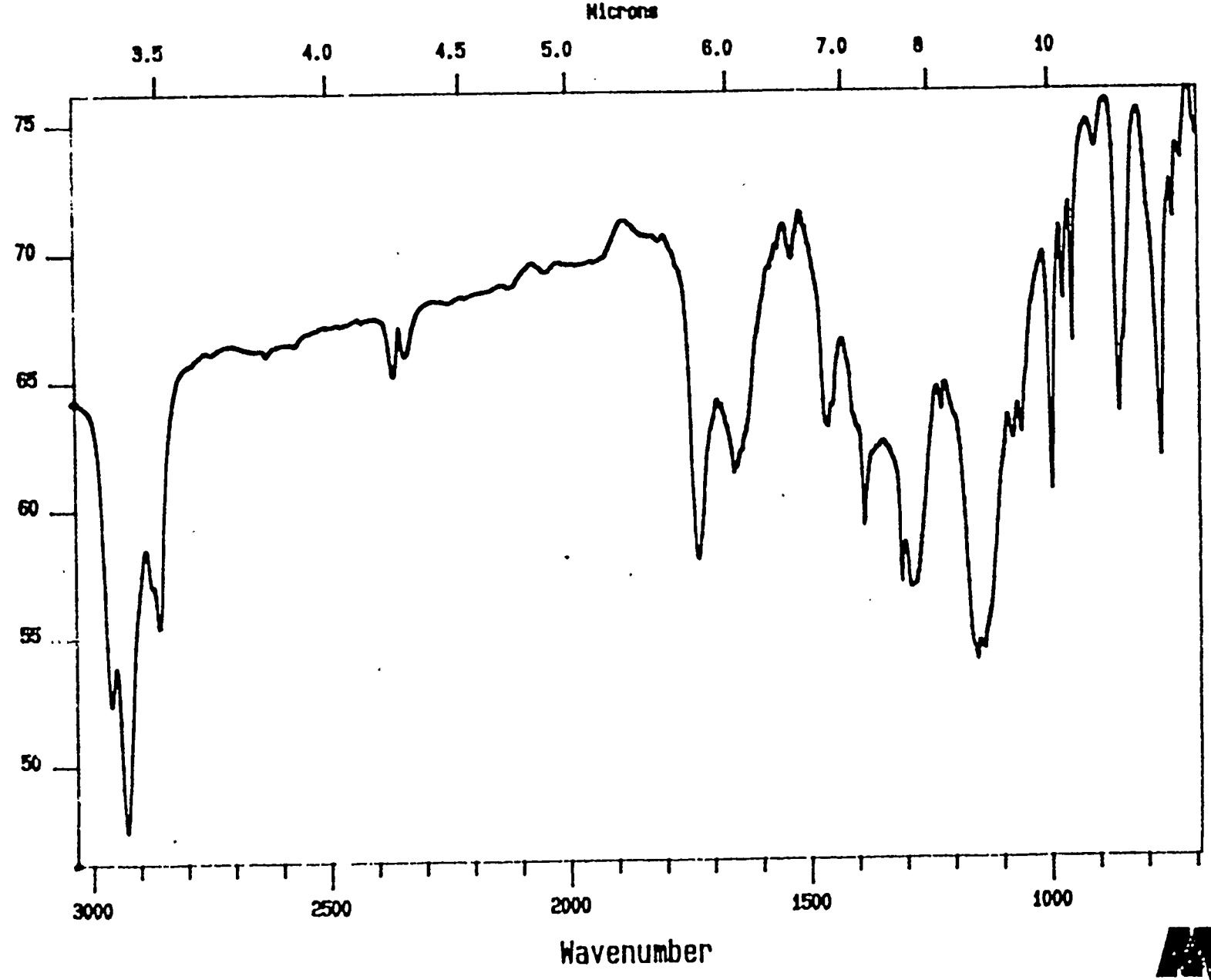

tmp.ras

FIGURE 5-28: 2537, 1000909, Zn (P) Nitro, PEE, FRC, KBr, 4/15/92

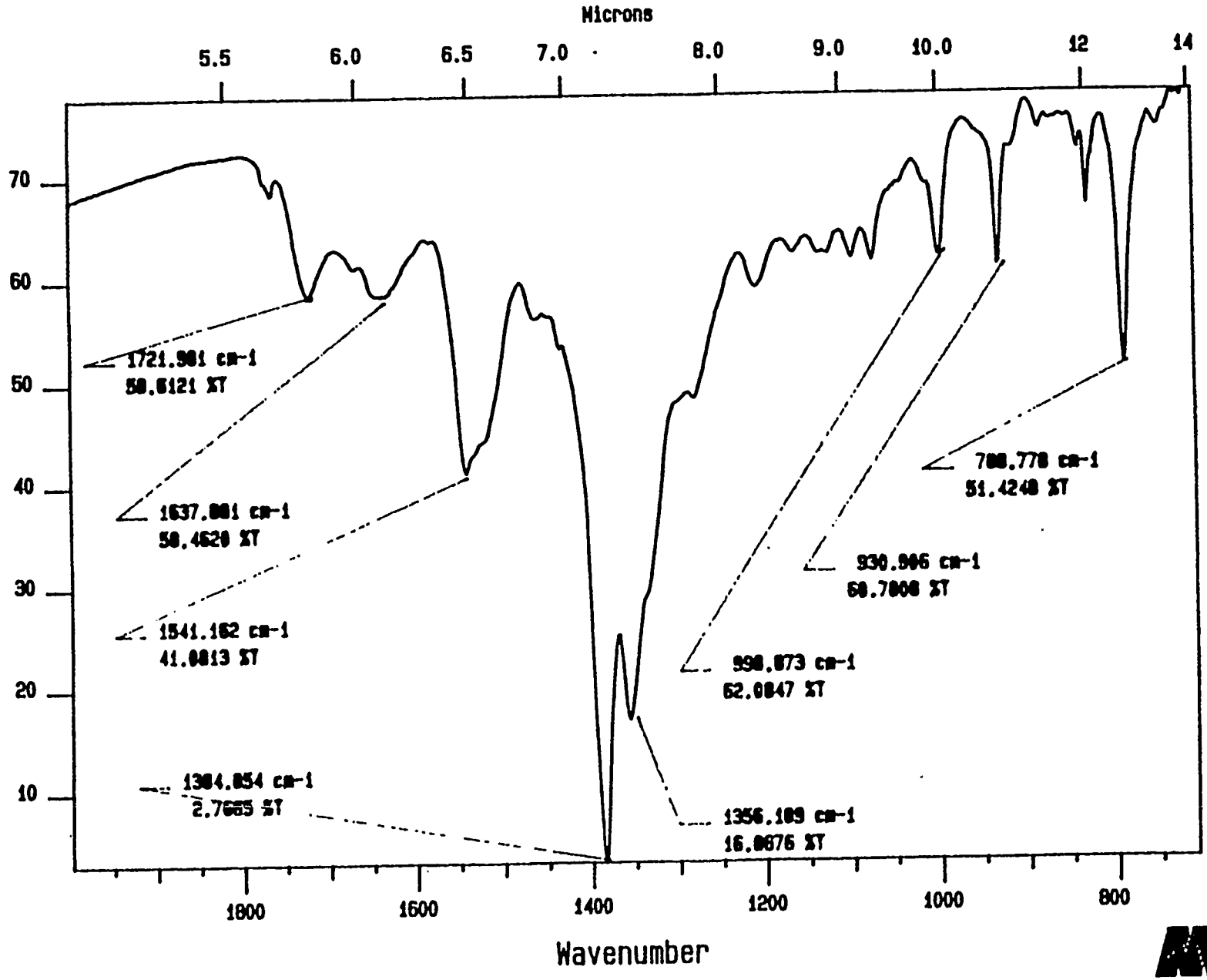

% Transmission

tmp.ras

5.1.5.6 Synthesis of Electron Deficient Porphines

Two routes to electron deficient porphines were examined this past quarter. Scheme 5-1 outlines the first route that was pursued. The pathway shown in Scheme 5-1 was abandoned when difficulties were encountered with the carbonyl reduction. The classic diborane reduction gave only alcohol and the zinc/HCl reaction (referred to as the Clemmenson reduction) gave only 10-20% yields of the desired product.

The second route explored for porphine synthesis is shown in Scheme 5-2. We have prepared three different nitroalcohols and the corresponding nitroacetates. We have focused on the formation of ethyl 3-trifluoromethyl-4-ethylpyrrole-2- carboxylate so that the total synthesis of one electron-deficient porphine would be completed this quarter. The nitro aldol condensation of trifluoroacetaldehyde methyl hemiacetal with nitropropane gave the nitroalcohol. Acetylation with acetic anhydride gave the nitroacetate in 63% overall yield. Treatment of the nitroacetate with two equivalents 1,8-diazabicyclo[5.4.0]undec-7-ene (DBU) in the presence of ethyl isocyanoacetate gave the desired pyrrole in 50% yield after chromatography. Reduction of the carboxylate group with lithium aluminum hydride followed by acid catalyzed condensation has given the porphine 10-30% yields, 1R-Figure 5-29.

5.2 POLYOXOMETALLATES

During the past quarter we have been synthesizing Keggin structures with first row oxidation-active metals in the framework. Our goal has been to synthesize complexes with high M(III)/M(II) reduction potentials. In particular we have synthesized compounds in which we could vary the Fe(III)/Fe(II) reduction potential by changing the central atom, the pH of the medium, the ligand, and the counter ion. It is our goal to find out whether a relationsip between reduction potential and catalytic activity exists in Keggin ions similar to what we have observed in the iron porphyrin systems. If active metal complexes of polyoxoanions can be synthesized, these materials will have the advantages of high thermal and oxidative stability and the ability to incorporate proximate iron centers for dioxygen binding.

Scheme 5-1

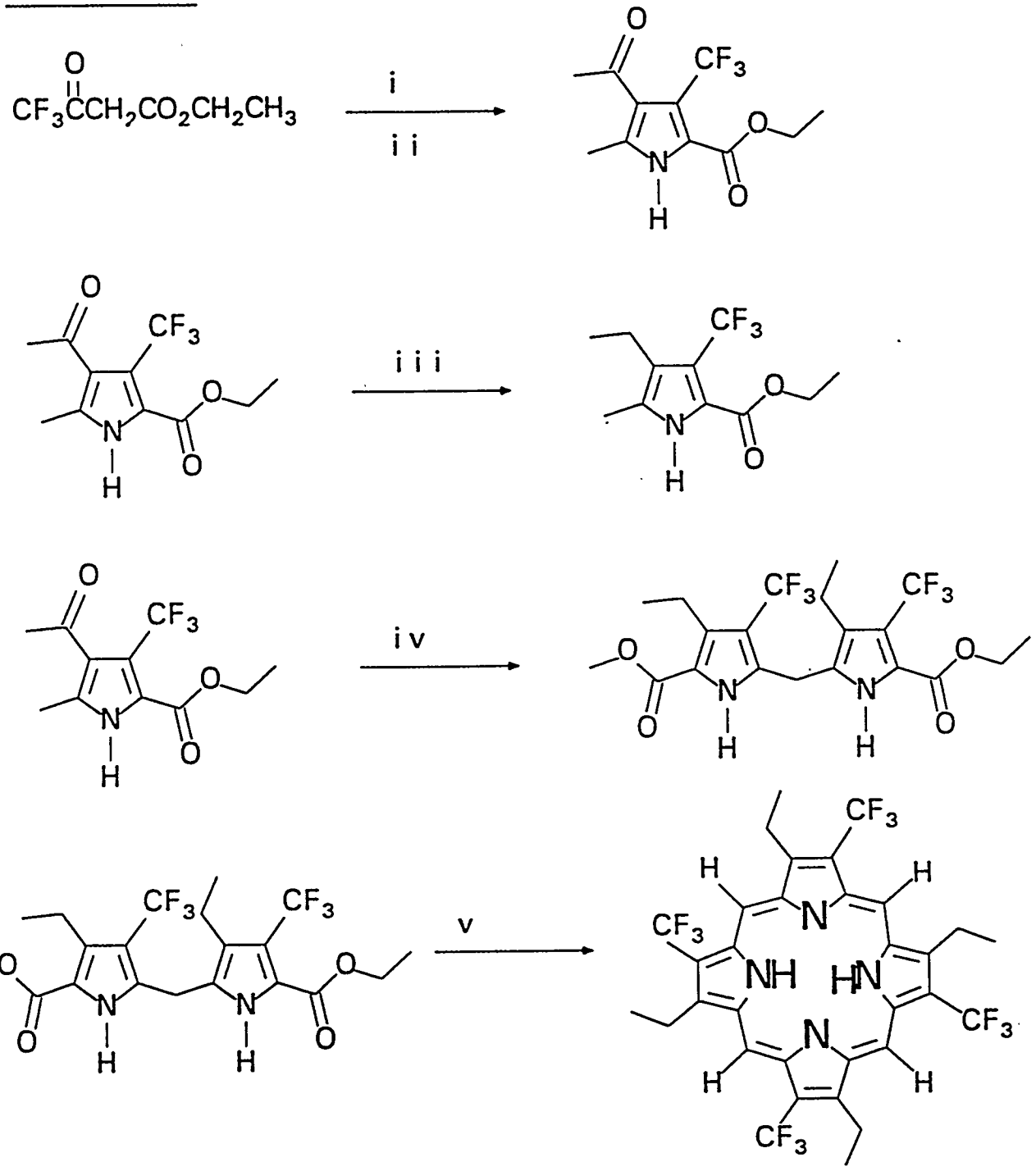

Scheme III. Reagents and conditions: i, $NaNO_2/H^+$, room temperature, 1h; ii, 2,4,-pentanedione/ Zn/H^+, room temperature, overnight (50%); iii, Zn(activated)/HCl (30%) [diborane and $NaBH_4/BF_3$:etherate gave only alchohol]; iv, lead tetraacetate/acetic anhydride; v, lithium aluminum hydride/H^+

Scheme 5-2

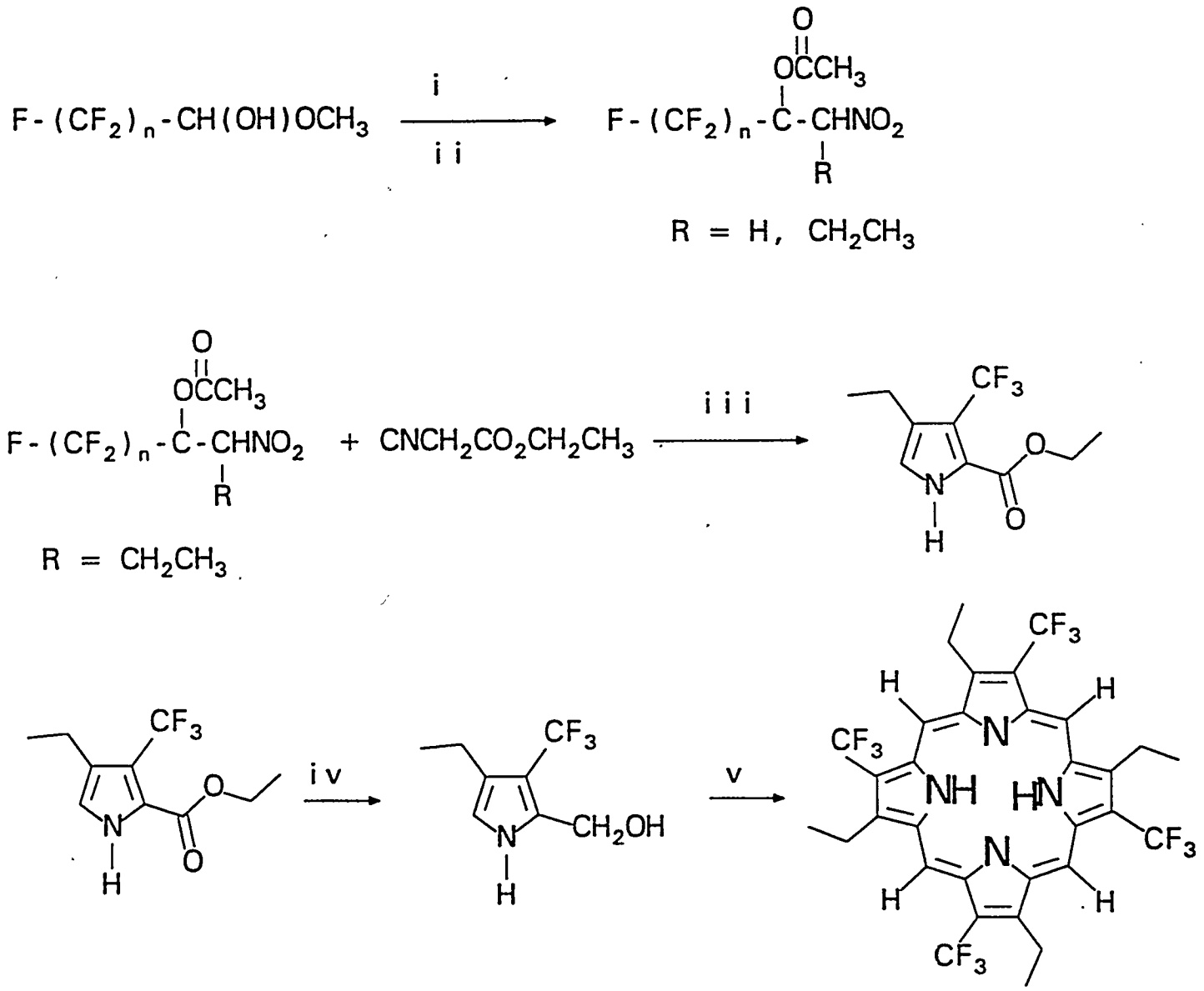

Scheme IV. Reagents and conditions: i, nitromethane or nitropropane 40-50 °C, 4h, room temperature overnight; ii, acetic anhydride, dimethylaminopyridine, room temperature, overnight (70% yield); iii, 1,8-diazabicyclo[5.4.0]undec-7-ene (DBU), room temperature overnight (50% yield); iv, lithium aluminum hydride, tetrahydrofuran, 0 °C, the product is not isolated; v, p-toluenesulphonic acid monohydrate (10% yield) or trifluoroacetic acid (28% yield), 2,3-dichloro-5,6-dicyano-1,6-benzoquinone (DDQ).

FIGURE 5-29

H_2Porphine-β-$(CF_3)_4$-β-$(Et)_4$ Absorption Spectrum in CH_2Cl_2/ethanol 3:1

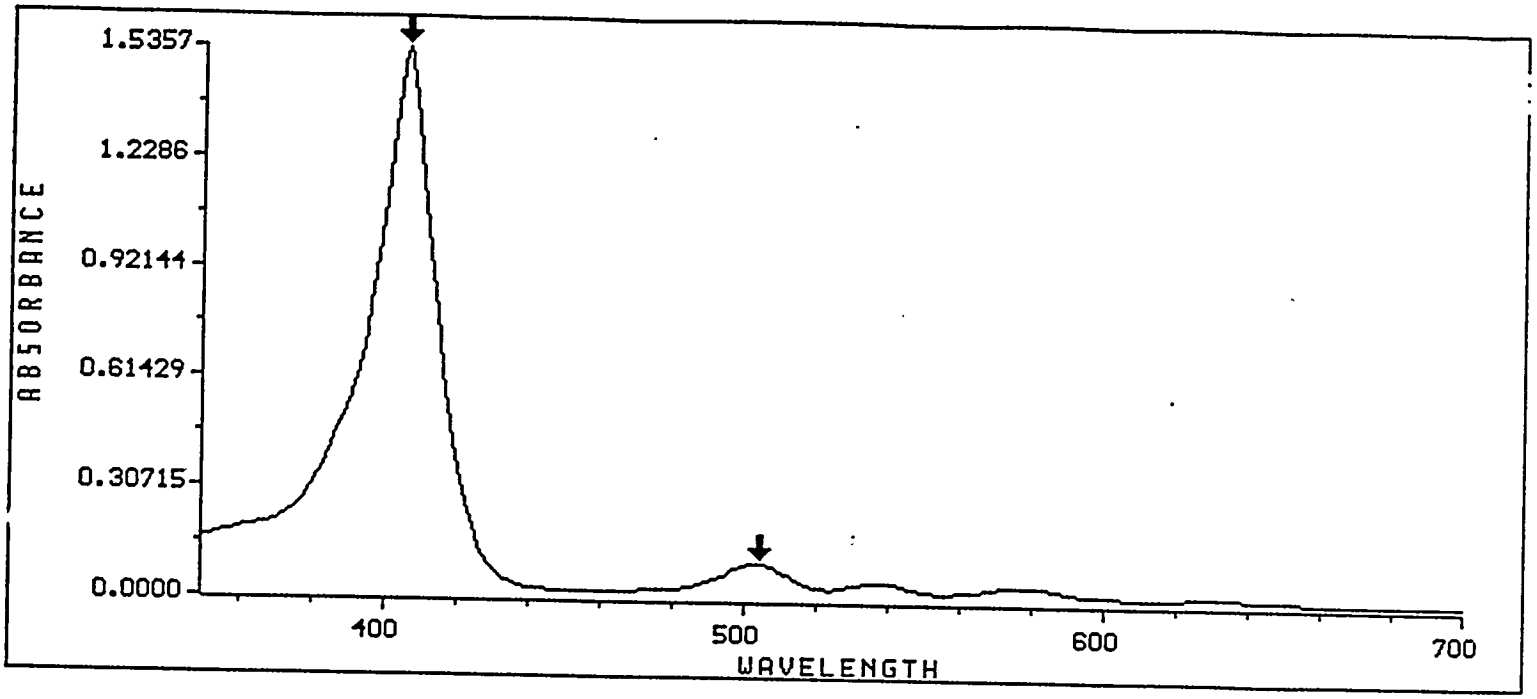

Annotated Wavelengths:

1 :	Wavelength =	406	Result =	1.535736
2 :	Wavelength =	504	Result =	0.101944

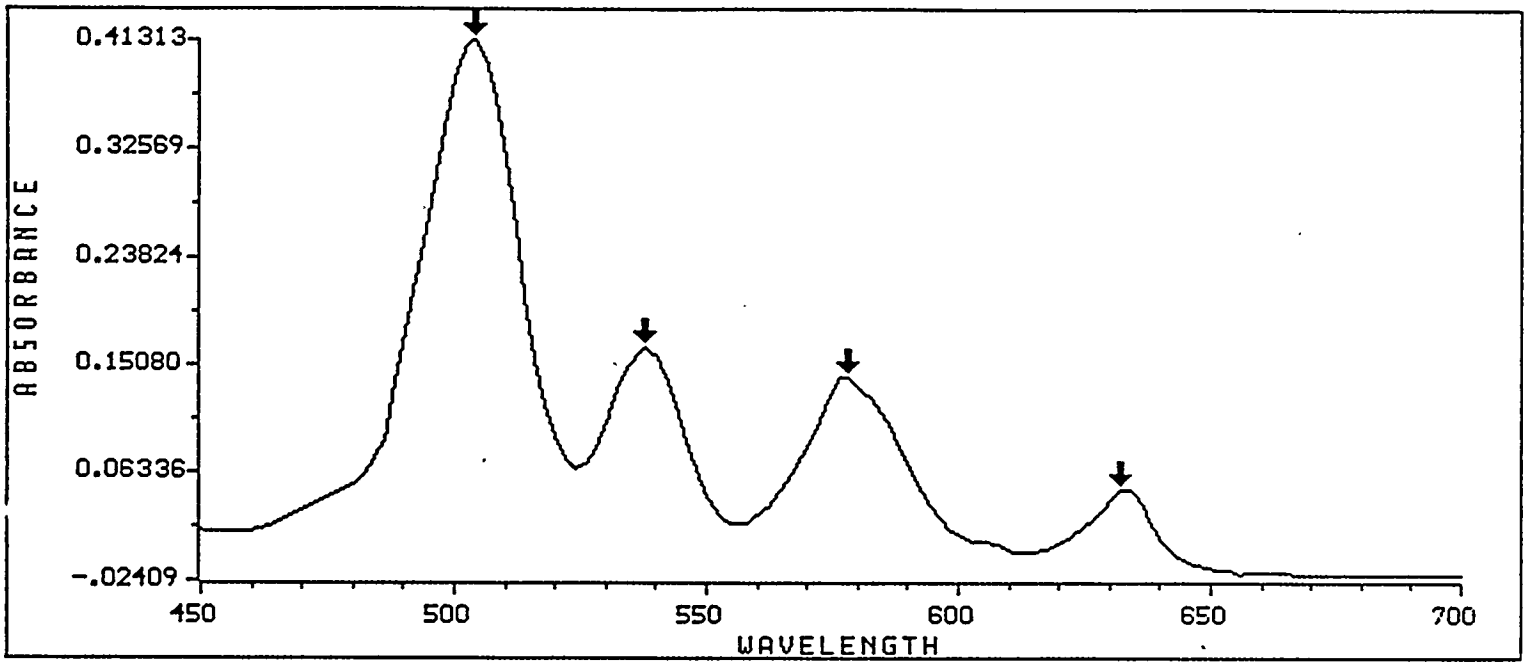

Annotated Wavelengths:

1 :	Wavelength =	504	Result =	0.413132
2 :	Wavelength =	538	Result =	0.164658
3 :	Wavelength =	578	Result =	0.140884
4 :	Wavelength =	632	Result =	0.048752

TABLE 5.5

Formal potentials of the three redox couples exhibited by $FeXW_{11}O_{39}^{z-}$ heteropolyanions. a,b

X	Z	One-electron wave (Fe(III)/Fe(II))	Z	First two-electron wave	Z	Second two-electron wave
Si(V)	-5	-0.145	-6	-0.580	-8	-0.720
Ge(IV)	-5	-0.065	-6	-0.557	-8	-0.666
P(V)	-4	0.039	-5	-0.560	-7	-0.706
As(V)	-4	0.123	-5	-0.537	-7	-0.655

a. Entries are in volts vs. SSCE.

b. Supporting electrolyte: 0.1 M $NaClO_4$ + 0.01 M $HClO_4$. $T = 22 \pm 2°C$.

TABLE 5.6

Formal Potentials of the Fe^{III}/Fe^{II} couple of $H_2OFeGeW_{11}O_{39}^{5-}$ in various supporting electrolytes

A. Fixed pH (5)

Counter-ion	Counter-ion conc., M	E^f, mV	ΔE^f, mV
Na^+	0.001	-171	-34
Na^+	0.1	-137	0
Na^+	1.1	-86	+51
Li^+	1.1	-95	+42
K^+	1.1	-77	+60
Rb^+	1.1	-62	+75

B. Fixed counter-ion (Na^+)

pH	E^f, mV $[Na^+] = 0.1$ M	E^f, mV $[Na^+] = 1.1$ M	ΔE^f, mV
2.0	-50	-18	+32
3.0	-102	-60	+42
4.0	-135	-92	+43
5.0	-137	-86	+51
6.0	-149	-117	+32
7.0	-172	-190	+18
8.0	-247	-220	+27

minimum vol of slightly warmed HPLC grade CH_3CN and filtered to remove any turbidity to get a yellow solution. Enough anhydrous Et_2O was added to the above solution to the point of incipient precipitation and then refrigerated at 5°C overnight to get a yellow microcrystalline product. Repeated the above procedure once more to obtain homogeneous crystalline material. The final product was dried under vacuum at 60°C for 4-5 hrs. yield: 60%. Infrared (KBr, cm^{-1}): 1000 (w), 960 (s), 910 (vs), 880 (m), 790 (vs), 750 (shoulder).

Analysis calculated for $C_{64}H_{147}N_4SiW_{11}O_{40}$: C, 20.67; H, 3.99; N, 1.50; Fe, 1.50; Si, 0.76; W, 54.39. Found: C, 19.97; H, 3.79; N, 1.45; Fe, 1.56; Si, 0.68; W, 54.19.

TGA (weight loss at 550°C under N_2). Calculated for 4 n-Bu_4N^+: 26.08%. Actual: 23.42%.

5.2.2.2 Synthesis of $(n\text{-}Bu_4N)_4[PFe(H_2O)W_{11}O_{39}]$

$K_7PW_{11}O_{39}$ was prepared in-situ by following the literature procedure: $K_3PW_{12}O_{40}.xH_2O$ (18.8 g, 6.28 mmol) was suspended in hot deionized water (95°C). 25mL of 1.0 M of $KHCO_3$ solution was added slowly with vigorous stirring as to keep the pH of solution below 5. The white suspension dissolved upon complete addition of base to give clear solution and pH was maintained at 4.8 0.1 at 85°C. The temperature was raised to 95°C over hot-plate and $Fe(NO_3)_3.9H_2O$ (2.57g, 6.4 mmol) was added slowly under stirring. The solution became yellow and after complete addition of iron nitrate, a brown turbidity persisted. The solution was cooled down to room temperature and filtered to get yellow solution. The yellow ppt was formed by the addition of solid n-Bu_4NBr (10.0 g. 31 mmol) to the solution with vigorous stirring. The crude product was collected on medium frit, washed with 50°C warm water until washings were free of Br ions ($AgNO_3$ test), followed by ethanol, aspirated to dryness, and finally allowed to air dry overnight at room temperature to obtain 14.9 gm of product. This product contained water (IR Spectrum). The crystallization procedure was adopted in a similar way as explained for compound **1**. Infrared (KBr, cm^{-1}): 1070 (s), 970 (vs), 895 (vs), 820 (vs, bread), 750 (w, shoulder).

Analysis calculated for $C_{64}H_{146}N_4FeO_{40}PW_{11}$: C, 20.64; H, 3.95; N, 1.51; Fe, 1.50; P, 0.83; W, 54.35. Found: C, 20.54; H, 3.87; N, 147; Fe, 1.35; p. 0.77; W, 53.14.

TGA (weight loss at 500°C under N_2). Calculated for 4 n-Bu_4N^+: 26.04%. Found: 26.73%.

5.2.2.3 Synthesis of $(n\text{-}Bu_4N)_4H_2[BFe(H_2O)W_{11}O_{39}]$

The starting material $BW_{11}O_{39}^{9-}$ was prepared in situ by the following procedures: $Na_2WO_4.2H_2O$ (18.2 G, 0.11 mol) was dissovled in 75 mL of deionized H_2O and its pH adjusted to 6.0•H_3BO_3 (1.25 g, 20.0 mmol) was added and with the addition of 4M HCl, the pH was readjusted to 6.0. $Fe(NO_3)_3$ $9H_2O$ (4.2 g, 10.0 mmol) was dissolved in 50 mL of deionized H_2O and solution was heated to 90-95°C. To this hot solution, the $BW_{11}O_{39}$ solution was added immediately to get a yellow solution and stirred for five minutes. The insoluble material [hydrolyzed excess Fe(III) and paradodecatungstate, a common impurity of $BW_{11}O_{39}^{9-}$] was removed after rapidly cooling the filtrate. The yellow solution was treated with solid n-Bu_4NBr(16.0 g, 50.0 mmol) under vigorous stirring to get pale-yellow precipitate. The precipitate was washed with CH_3OH (30 mL) followed by ether and air dried. The precipitate as placed in a vacuum oven and dried overnight at room temperature, to get 5.2 g of microcrystalline product. Recrystallization was unsuccessful due to some decomposition to a white powder. Infrared (KBr, cm^{-1}): 955 (vs), 880 (s), 810 (vs), 760 (br, should).

Analysis calculated for $C_{64}H_{148}N_4BFeO_{40}W_{11}$ = C, 20.75; H, 4.03; N, 1.51; Fe, 1.51; W, 54.61. Found = C, 18.21; H, 3.61; N, 1.39; Fe, 1.44; W, 44.21.

TGA (wt. loss at 150-500°C under N_2). Calculated for 4 n-Bu_4N^+: 25.3%. Found: 26.0%.

Analysis calculated for $C_{64}H_{146}N_4FeO_{40}PW_{11}$: C, 20.64; H, 3.95; N, 1.51; Fe, 1.50; P, 0.83; W, 54.35. Found: C, 20.54; H, 3.87; N, 147; Fe, 1.35; p. 0.77; W, 53.14.

TGA (weight loss at 500°C under N_2). Calculated for 4 n-Bu_4N^+: 26.04%. Found: 26.73%.

5.2.2.3 Synthesis of $(n\text{-}Bu_4N)_4H_2[BFe(H_2O)W_{11}O_{39}]$

The starting material $BW_{11}O_{39}^{9-}$ was prepared in situ by the following procedures: $Na_2WO_4.2H_2O$ (18.2 G, 0.11 mol) was dissovled in 75 mL of deionized H_2O and its pH adjusted to 6.0•H_3BO_3 (1.25 g, 20.0 mmol) was added and with the addition of 4M HCl, the pH was readjusted to 6.0. $Fe(NO_3)_3$ $9H_2O$ (4.2 g, 10.0 mmol) was dissolved in 50 mL of deionized H_2O and solution was heated to 90-95°C. To this hot solution, the $BW_{11}O_{39}$ solution was added immediately to get a yellow solution and stirred for five minutes. The insoluble material [hydrolyzed excess Fe(III) and paradodecatungstate, a common impurity of $BW_{11}O_{39}^{9-}$] was removed after rapidly cooling the filtrate. The yellow solution was treated with solid n-Bu_4NBr(16.0 g, 50.0 mmol) under vigorous stirring to get pale-yellow precipitate. The precipitate was washed with CH_3OH (30 mL) followed by ether and air dried. The precipitate as placed in a vacuum oven and dried overnight at room temperature, to get 5.2 g of microcrystalline product. Recrystallization was unsuccessful due to some decomposition to a white powder. Infrared (KBr, cm^{-1}): 955 (vs), 880 (s), 810 (vs), 760 (br, should).

Analysis calculated for $C_{64}H_{148}N_4BFeO_{40}W_{11}$ = C, 20.75; H, 4.03; N, 1.51; Fe, 1.51; W, 54.61. Found = C, 18.21; H, 3.61; N, 1.39; Fe, 1.44; W, 44.21.

TGA (wt. loss at 150-500°C under N_2). Calculated for 4 n-Bu_4N^+: 25.3%. Found: 26.0%.

at intermittent interval until pH of solution became 4.3. This pH was maintained for 15 minutes, and then $Fe(NO_3)_3.9H_2O$ (3.0 g, 7.4 mmol) was added in small portions keeping the temperature constant at 80-5°C to get yellow solution. The mixture was cooled down to room temperature, filtered to remove excess hydrolyzed $Fe(NO_3)_3$ and then n-Bu_4NBr was added (12.0 g, 37.2 mmol) to the above filtrate under vigorous stirring to obtain a yellow precipitate. The solid was filtered, washed with water (2 x 50 mL), EtOH (2 x 50 mL), Et_2O (2 x 50 mL), aspirated to dryness and allowed to air dry overnight to get 22.5 g of product. Recrystallization was carried out in an analogous manner as described for compound **1**. Infrared (KBr, cm^{-1}): 1068(s), 955 (vs), 880 (s), 815 (vs), 755 (w, shoulder).

Analysis calculated for $C_{64}H_{146}N_4FeMo_{11}O_{40}P$: C,, 27.91; H, 5.34: N, 2.03; Fe, 2.03; Mo, 38.32; P, 1.12. Found: C, 26.82; H, 5.07; N, 1.95; Fe, 1.66; Mo 38.85; P, 1.09.

TGA (wt. loss at 550°C under N_2). Calculated for 4 n-Bu_4N+: 35.2%. Found: 33.22%.

5.2.2.6 $(n\text{-}Bu_4N)_4H[SiFe(H_2OMo_{11}O_{39}]$

The starting material, $SiMo_{11}O_{39}^{8-}$, was prepared insitu by following the literature preparation: $Na_2SiO_3.5H_2O$ (4.25 g, 20 mmol) was dissolved in 275 mL deionized water and brought to boiling on a heating mantle in 500 mL, 3-N flask fitted with condenser. In a single addition, MoO_3 (23.03 g, 160 mmol) was added and the mixture was kept stirring at 72-3°C for 3 days to obtain a clear yellowish-green solution. A 100 mL solution of $Na_2MoO_4.2H_2O$ (14.5 g, 60 mmol) was then added drop-wise to the above solution and heated at 72-3°C for an additional day without stirring. The yellowish-green solution was cooled down to room temperature and filtered to remove silicic acid impurity. Took 92.5 mL of above yellowish-green solution and added dropwise to 2.02 g $Fe(NO_3)_3.9H_2O$ dissolved in 50 mL of deionized H_2O at 90°C. During addition of $SiMo_{11}O_{39}^{8-}$, the color of the solution became orange-brown with suspended brown precipitate. Heated at 90°C for an additional five minutes. Cooled down the solution to

room temperature, filtered to remove brown suspension and then added n-Bu_4NBr (7.0 g, 20.0 mmol) under vigorous stirring to get greenish-yellow precipitate. This product was washed with 50°C H_2O until washings were free of Br^- ions ($AgNO_3$ test), EtOH (2 x 50 mL) followed by Et_2O (2 x 50 mL) and aspirated to dryness to obtain 3.6 g of product. Recrystallization was done in an analogous manner as described for compound 1.Yield 70%. Infrared (KBr, cm^{-1}): 955 (s), 930 (w, shoulder), 910 (vs), 860 (w, shoulder), 810 (vs), 740, (s, shoulder), 675 (m).

5.2.2.7 $(nBu_4N)_4H_3[SiW_9\{Fe(H_2O)\}_3O_{37}]$

The sodium salt of $[SiW_9\{Fe(H_2O)_3\}_3O_{37}]^{7-}$ was prepared according to a literature procedure. In a 500 mL round bottom Flask, β-$Na_9SiW_9O_{34}H.23H_2O$ (8.54 g, 3.0 mmol) was dissolved in 200 mL solution of sodium acetate-acetic acid buffer of pH 6. This colorless solution was then treated with $[Fe_3O(OAc)_6(H_2O)_3]Cl$ (1.38 g, 3.0 mmol) suspended in 25 mL of deionized water. Not all of the iron complex was dissolved. The mixture was warmed to 50°C in an oil-bath for 15 minutes. The iron complex dissolved and gave a light greenish brown solution. At room temperature, 0.5 g KCl was added and stirred to dissolve. The mixture was cooled down to 14°C in an ice-bath, filtered to remove a rusty brown precipitate and then added n-Bu_4NBr (10.28 g, 42.4 mmol) under vigorous stirring to get a yellow-green precipitate. The precipitate was washed with water, EtOH, Et_2O and aspirated to dryness to get 1.7 gm of product. Recrystallized according to the procedure as mentioned for compound 1. Yield: 50% Infrared (KBr, cm^{-1}): 100 (w), 955 (s), (905 (vs), 810 (vs), 775 (s, shoulder).

Analysis calculated for $C_{64}H_{153}N_4Fe_3O_{40}SiW_9$: C, 22.26: H, 4.45; N, 1.6l; Fe, 4.83; Si, 0.81; W, 47.7. Found: C, 21.85; H, 4.21; N, 1.54; Fe, 4.36; Si, 0.67; W, 45.4.

TGA (wt. loss at 550 C under N_2). Calculated for 4 n-Bu_4N^+L 27.96%. Found: 28.22%.

5.2.3 Ethane Oxidations Catalyzed by Polyoxoanions

In past reports, we have noted that polyoxoanions having the Keggin structure into which has been incorporated one or more oxidation-active first or second row transition metals have been active high temperature catalysts for oxidizing isobutane and propane. These catalysts did not have the low temperature catalytic activity that the metalloporphyrins exhibited nor did they give alcohols in as high selectivity. Ethane and methane can also be oxidized with the polyoxoanion catalysts since they are more robust at the higher temperatures (>200°C) than the porphyrin catalysts. Although methanol selectivity was not high, interesting selectivity was noted in the case of ethane oxidation, Table 3-5. Ethane can be oxidized using cobalt salts or other conventional catalysts or initiators used in high concentration at temperatures in the neighborhood of 200°C. Selectivity to ethanol (5%) is extremely low in these cases however. The majority of the products are C_1 comounds formed from cleavage of intermediate C_2 radicals. Thus, methanol, formaldehyde, formates, CO and CO_2 are formed with very low yields of methanol or acetaldehyde. We have found, Table 3-5, however, that when tetrabutyl ammonium salts of iron substituted Keggin complexes are used under the same conditions, ethanol is the predominant oxidation product. Investigations of light alkane oxidations using these complexes continues.

5.3 METALS IN REGULAR OXIDIC MATRICES

MnAPO molecular sieves are a member of the AlPO4-based materials patented by Union Carbide (UOP). They are synthesized from gels containing the transition metal ions such as Mn+2, and it is assumed that the cations are incorporated into tetrahedrally coordinated lattice positions during hydrothermal crystallization of the molecular sieves. There has also been evidence to suggest that some of the manganese cations exist in extraframework sites to balance the negative charge formed by the incorporation of the manganese into the neutral AlPO4 framework.

MnAPO-5 is a large pore material (0.8nm) with a novel structure that is templated by a number of different organics, including diethylethanolamine. MnAPO-5 has excellent thermal and hydrothermal stability. MnAPO-47 has the same topology as the zeolite

chabazite and is a small pore material (0.43nm); diethylethanolamine in high gel concentrations is the most common templating agent for the 47 structure type. MnAPO-47 is not thermally stable when calcined in air to remove the organic template, and calcination is generally done in an inert atmosphere.

The tested sample was prepared following USP 4,567,029 Ex. 66. The starting gel ratio was:

2.0 DEEA : 0.167 MnO : 0.917 Al_2O_3 : 1 P_2O_5 : 45 H_2O

The synthesis was done at 200°C for one day, quiescently under autogeneous pressure. The final product was white. Under the microscope, the sample contained two distinct morphologies: cubes and six-sided rods. The six-sided rod morphology is typical of the 5 structure, and the cubes are typical of the 47 structure.

X-ray diffraction pattern of the as-synthesized material was consistent with that of a mixture of 5 and 47 with the predominant phase being 5 (Figure 5-30). Calcination at 600°C in air for three hours yielded a lavender/gray material. The X-ray diffraction pattern of the calcined material showed that the 47 structure type had completely collapsed and that the 5 structure type was still present (Figure 5-31).

The calcined material was sent for chemical analysis and the final product oxide ratio was:

Al_2O_3	0.40
P_2O_5	0.49
MnO	0.11

It can be seen that the divalent manganese substitutes for the trivalent aluminum and not for the phosphorus, and this is consistent with the MeAPO materials and results in a net negative framework charge.

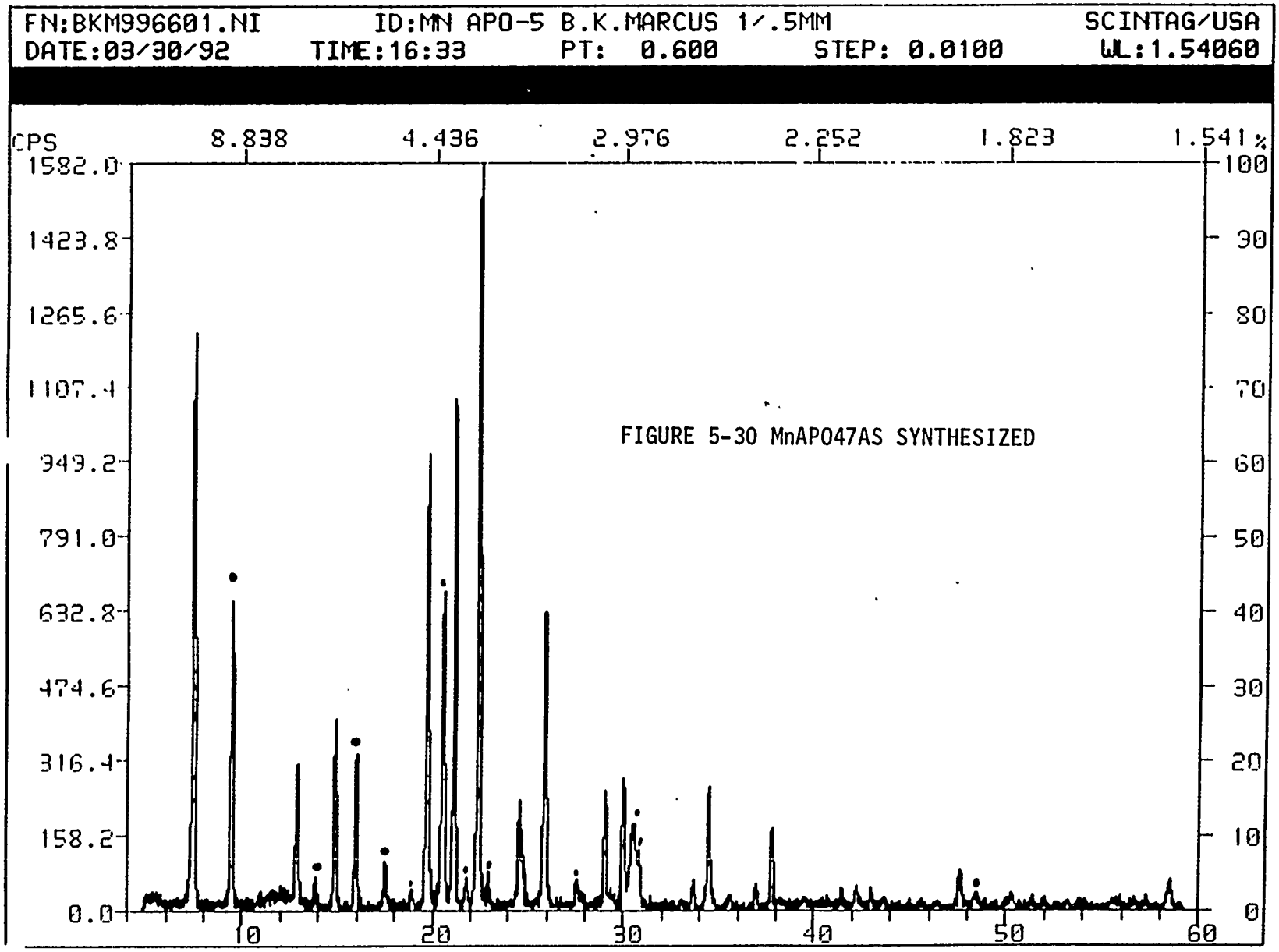

FIGURE 5-30 MnAPO47AS SYNTHESIZED

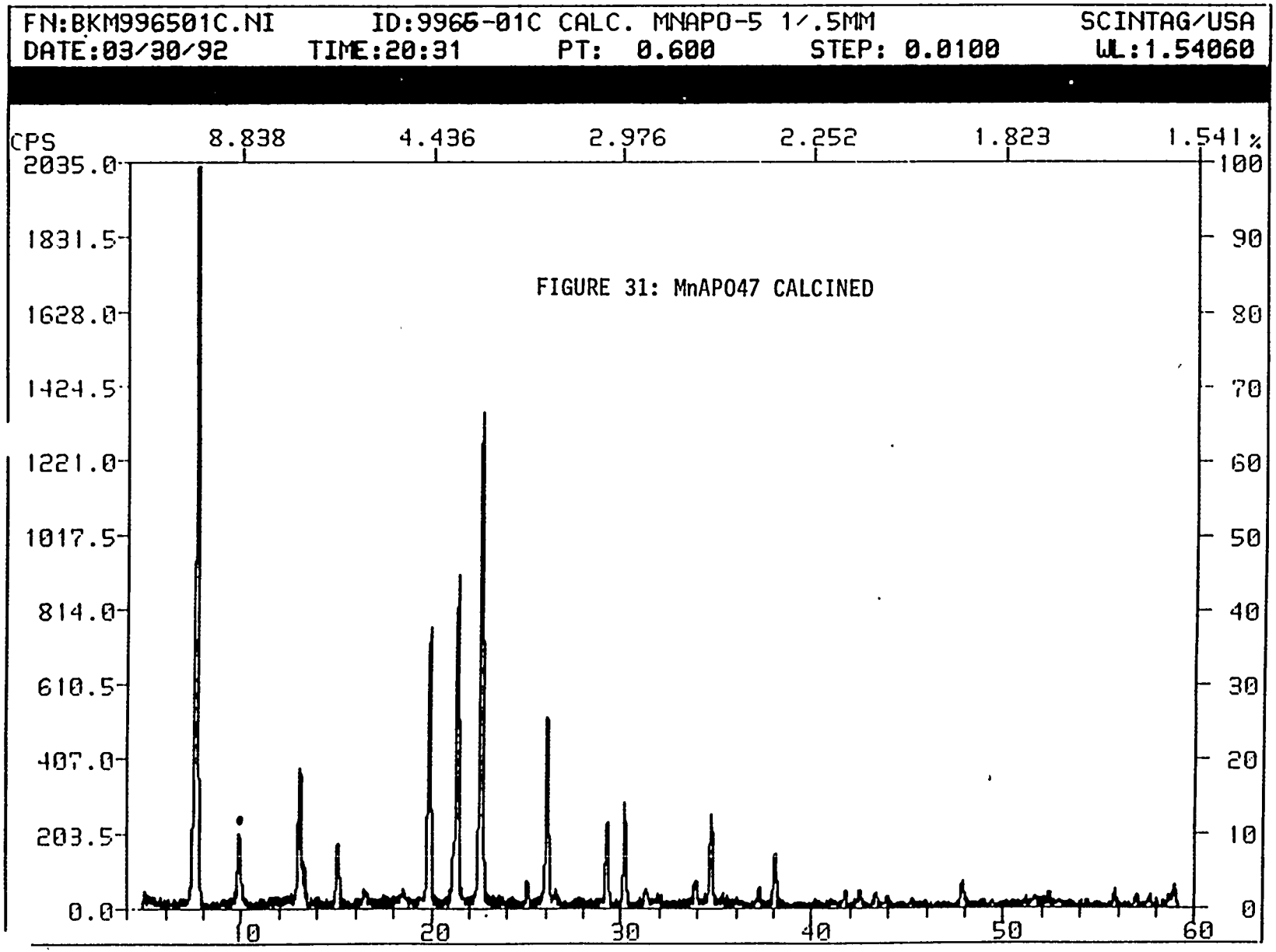

FIGURE 31: MnAPO47 CALCINED

The collapse of the 47 framework structure type would lead to the presence of amorphous managanese in addition to the manganese in the framework. E.S.R. studies have been requested to determine if octahedral manganese is present.

Samples of MnAPO-5 and 47 materials with higher manganese concentrations will be synthesized, as well as other structure types containing manganese.

5.3.2 Methane and Ethane Oxidations Over MnAPO-5

We have prepared the known manganese substituted aluminophosphate MnAPO-5 and used it as a catalyst for the vapor phase oxidation of methane, Table 5-7, and ethane, Table 5-8. Reactions were conducted in a reactor in which the top third was packed with catalyst and the bottom two thirds was void space. We hoped to generate methyl radicals over the catalyst and allow them to be converted in the void space under conditions in which catalytic decomposition of methanol would be reduced. Methane can be converted to methanol in roughly 50% selectivity at elevated temperatures over an iron exchanged, iron framework substituted sodalite catalyst, Fe_x[Fe]SOD, in this reactor configuration. We have found that methane activation occurs at temperatures about 35°C lower with the MnAPO-5 than over Fe_x[Fe]SOD. Although selectivity is not improved, the finding that the manganese catalyst activates the difficult C-H bond of methane more easily than our iron sodalite system is an exciting and potentially important one. We have not yet done the appropriate comparisons between the two catalysts to determine whether the same C-H bond activation relationship holds for ethane as well. Data available to date, however, has shown that ethanol yields are higher and CO make lower over the manganese catalyst. We are continuing to work on the manganese and other aluminophosphate derived catalysts.

TABLE 5-7

METHANE OXIDATIONS OVER MnAPO-5 AND Fex[Fe]SOD[a]

CATALYST	T_b, C	FLOW MS/MIN	PRODUCTS, MMOLE/HR. CH_3OH	CH_2O	CO	CO_2	O_2 CONV.,%	CH_4 CONV.,%	CH_3OH SEL.,%
MnAPO-5	375	55	2.20	0.04	2.24	0.99	86	4.7	40
		98	4.60	0.13	4.94	1.36	93	5.2	42
		377	15.20	1.14	22.00	5.05	99	5.4	35
Fe_x[Fe]SOD	410	50	2.22	NA	2.84	0.66	91	5.4	<39
		92	4.02	NA	5.32	0.96	93	5.3	<39
		378	20.96	NA	19.74	3.14	90	5.5	<48
MnAPO-5	365	55	1.59	0.08	1.47	0.41	58	3.1	45
Fe_x[Fe]SOD	390	50	0.70	NA	1.33	0.32	49	2.3	<33

[a] A 3/1 methane/air mixture was continuously passed over a 1.5 cc bed of catalyst top-loaded into a 5 mL fully heated quartz-lined reactor operated at a pressure of 800 psig.

[b] Applied external temperature (to reactor skin)

TABLE 5-8

ETHANE OXIDATIONS CATALYZED BY Fe_x[Fe]SOD OR MnAPO-5

Catalyst	T_b, C	Flow Ms/Min	C2's, mmoles/hr.			C1's mmoles/hr.					Others mmoles/hr.	O_2 Used %	C_2H_5 Conv., %
			CH_3CH_2OH	CH3CHO	$CH_2=CH_2$	CH_4	CH_3OH	CH_2O	CO	CO_2			
Fe_x[Fe]SOD	290	165	0.1	0.1	c	c	0.4	tr	0.2	0.2	c	10	0.2
MnAPO-5	290	92	1.4	0.3	0.1	1.3	4.0	1.0	3.6	0.6	0.3	94	2.9
Fe_x[Fe]SOD	300	161	2.6	0.8	0	2.9	8.9	3.0	8.4	1.4	0.2	99	3.7
MnAPO-5	300	190	3.3	0.8	0.3	2.7	11.1	3.4	2.1	1.1	0.4	97	3.5
Fe_x[Fe]SOD	315	386	3.0	1.9	4.1	10.0	18.1	14.0	25.1	3.3	0.5	93	3.7
MnAPO-5	300	406	6.2	1.7	1.0	9.1	24.9	8.3	10.5	3.3	0.8	98	4.2

a) Continuous Oxidation of a 3/1 CH_4/air stream at 800 psig over a 1.5 mL bed of catalyst top loaded into a heated 5 mL reactor.

b) Temperature applied to the reactor skin.

c) Less then 0.5 mmoles/hr.

6.0 CONCLUSIONS

Now that we have established structure-reactivity relationships which correlate both the Fe(III)/Fe(II) reduction potential and the steric environment about the metal center with catalytic activity we are beginning to design ligand systems which have electronic and steric properties that will produce superior catalysts. Paramount among the considerations now being employed in addition to chemical characteristics are economic characterisitcs as well. For instance, the cost of raw materials and the molecular weight of the macrocycle are two factors which will be critical in the design of inexpensive catalysts for commercial production of fuels. We are indeed fortunate that iron provides the most active catalyst rather than a costly noble metal.

We are now positioned to ascertain whether the same electronic factors which produce an active metalloporphyrin complex will produce an active iron substituted Keggin ion. We have synthesized polyoxoanions having a range of Fe(III)/Fe(II) reduction potentials and will test these for ethane and propane oxidations in the comming months. The Keggin ions have promise as more robust catalysts for higher temperature reactions provided their activity can be improved.

We have made substantial progress in the area of increasing the activity of heterogeneous catalysts for methane and ethane oxidations. In our laboratories we have recently overcome the structural limitations that some zeolites impose on M(III)/M(II) transformations by incorporating large metal concentrations in aluminophosphates. A manganese aluminophosphate in which both Mn(III) and Mn(II) can be incorporated allows us to activate methane for catalytic conversion to methanol at temperatures fully 35°C lower than are required for Fex[Fe]SOD and over 50°C lower than is necessary for thermal oxidation. Other catalysts of this type have been prepared and will be screened in the near future.